



Norwegian University of  
Science and Technology

# Freeze out in natural gas systems

Utfrysning i naturgass-systemer

**Vegard Førde Lavik**

Master of Science in Product Design and Manufacturing

Submission date: June 2009

Supervisor: Jostein Pettersen, EPT

Co-supervisor: Arne Olav Fredheim, EPT

Jacob Stang, SINTEF

Even Solbraa, StatoilHydro

Norwegian University of Science and Technology  
Department of Energy and Process Engineering



# Problem Description

Målet med Masteroppgaven er å forbedre kunnskap om utfrysning og avsetnings/fjerningsmekanismer. Oppgaven vil fokusere på modellering og prediksjon av utfrysingsparametre.

Assignment given: 15. January 2009  
Supervisor: Jostein Pettersen, EPT





## MASTEROPPGAVE

for

Stud.techn. Vegard Førde Lavik

Våren 2009

### Utfrysing i naturgass-systemer

*Freeze out in natural gas systems*

#### ***Bakgrunn***

Kandidaten har i sin prosjektoppgave høsten 2008 undersøkt problemer knyttet til frysepunkt og utfrysning av kritiske komponenter ved naturgasskondensering. Utfrysing og plugging av rør og varmevekslere er en alvorlig utfordring for kryogene prosessanlegg i drift. På grunn av høye trippelpunktstemperatur og relativ høy konsentrasjon i forhold til løselighetsgrensen i naturgass legges det vekt på de kritiske komponentene CO<sub>2</sub>, benzen og vann.

Den teoretiske delen av prosjektoppgaven innbefattet en oversikt over basisen for termodynamisk likevekt og en kortfattet oppsummering av tidligere relevant arbeid med CO<sub>2</sub>, benzen og vann innenfor utfrysning. Oppgaven fokuserte på utfrysning av rene komponenter og ikke på hydratdannelse.

En forsøksrigg for utfrysing er etablert hos StatoilHydro i Trondheim (PVT-80/170 LT). Denne riggen skal kunne undersøke frysepunktstemperaturer og utfrysningsforhold til blandinger hvor hydrokarbonkomponenter er de dominerende. Etter at det ble oppdaget lekkasje i prøvetakingssystemet har riggen blitt modifisert. Det ble i prosjektoppgaven tatt opp flere forhold som forårsaker disse lekkasjene og det ble identifisert tiltak for å utbedre den eksisterende løsningen.

Ut fra deltagelse ved driften av riggen er det også utarbeidet forslag til generelle tiltak som kan implementeres for å øke driftsmulighetene og påliteligheten til riggen.

Den eksperimentelle delen av prosjektoppgaven ble endret på underveis som følge av problemer knyttet til riggen og omfatter kun ett eksperiment. Den 5. desember 2008 var riggen tilsynelatende i operativt modus slik at vi kunne gjennomføre et forsøk med ren CO<sub>2</sub>. Ved gjennomføring av eksperimentet ble det avdekket forhold som må utbedres. Ved videreføring av arbeidet er det foreslått å rette det eksperimentelle fokuset mot binære blandinger som kan sammenlignes og diskuteres opp mot teori..

## *Mål*

Målet med Masteroppgaven er å forbedre kunnskap om utfrysning og avsetnings/fjerningsmekanismer. Oppgaven vil fokusere på modellering og prediksjon av utfrysingsparametre.

## *Oppgaven bearbeides ut fra følgende punkter:*

1. Kortfattet oppsummering av relevante tidligere arbeider innen utfrysning.
2. Deltakelse i forsøkgjennomføring og analyse av forsøksresultater
3. Sammenligning av eksperimentelle resultater med modeller for utfrysingsmessige forhold
4. Forslag til videreføring av arbeidet

-- ” --

Senest 14 dager etter utlevering av oppgaven skal kandidaten levere/sende instituttet en detaljert fremdrift- og evt. forsøksplan for oppgaven til evaluering og evt. diskusjon med faglig ansvarlig/veiledere. Detaljer ved evt. utførelse av dataprogrammer skal avtales nærmere i samråd med faglig ansvarlig.

Besvarelsen redigeres mest mulig som en forskningsrapport med et sammendrag både på norsk og engelsk, konklusjon, litteraturliste, innholdsfortegnelse etc. Ved utarbeidelsen av teksten skal kandidaten legge vekt på å gjøre teksten oversiktlig og velskrevet. Med henblikk på lesning av besvarelsen er det viktig at de nødvendige henvisninger for korresponderende steder i tekst, tabeller og figurer anføres på begge steder. Ved bedømmelsen legges det stor vekt på at resultatene er grundig bearbeidet, at de oppstilles tabellarisk og/eller grafisk på en oversiktlig måte, og at de er diskutert utførlig.

Alle benyttede kilder, også muntlige opplysninger, skal oppgis på fullstendig måte. (For tidsskrifter og bøker oppgis forfatter, tittel, årgang, sidetall og evt. figurnummer.)

Det forutsettes at kandidaten tar initiativ til og holder nødvendig kontakt med faglærer og veileder(e). Kandidaten skal rette seg etter de reglementer og retningslinjer som gjelder i StatoilHydro og alle (andre) fagmiljøer som kandidaten har kontakt med gjennom sin utførelse av oppgaven, samt etter eventuelle pålegg fra Institutt for energi- og prosessteknikk.

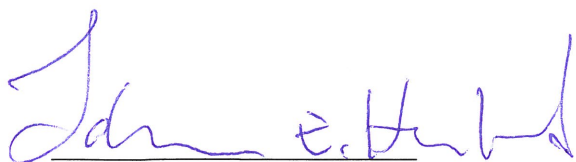
I henhold til ”Utfyllende regler til studieforskriften for teknologistudiet/sivilingeniørstudiet” ved NTNU § 20, forbeholder instituttet seg retten til å benytte alle resultater i undervisnings- og forskningsformål, samt til publikasjoner.

Ett -1 komplett eksemplar av originalbesvarelsen av oppgaven skal innleveres til samme adressat som den ble utlevert fra. (Det skal medfølge et konsentrert sammendrag på maks. en maskinskrevet side med dobbel linjeavstand med forfatternavn og oppgavetittel for evt. referering i tidsskrifter).


Til Instituttet innleveres to - 2 komplette, kopier av besvarelsen. Ytterligere kopier til evt. medveiledere/oppgavegivere skal avtales med, og evt. leveres direkte til, de respektive.

Til instituttet innleveres også en komplett kopi (inkl. konsentrerte sammendrag) på CD-ROM i Word-format eller tilsvarende.

Institutt for energi og prosessteknikk, 12. januar 2009



Johan Hustad  
Instituttleder



Jostein Pettersen  
Faglig ansvarlig/veileder

Kontaktperson(er)/medveileder(e):

Arne Olav Fredheim StatoilHydro  
Even Solbraa StatoilHydro  
Jacob Stang, SINTEF Energiforskning





## **Preface**

This thesis is carried through as part of the Master program at the Faculty of Engineering Science and Technology, at the Department of Energy and Process Engineering at the Norwegian University of Science and Technology.

The project is in collaboration with StatoilHydro's Research Center at Rotvoll, and in relation to the startup of a freeze out rig. The object of this thesis is to increase the knowledge concerning freeze out and precipitate mechanism in natural gas systems, in addition to the thermodynamic models used to describe such systems.

I want to give thanks to the persons who have been contributing with good advices, and helped me in my work:

- Jostein Pettersen, Professor II at NTNU
- Even Solbraa, Doctor Engineer at StatoilHydro
- Jacob Stang, Researcher at SINTEF Energy research
- Andrea Carolina Machado Miguens, Researcher at StatoilHydro
- Longman Zhang, PhD student at NTNU
- Stian Amble, Master student at NTNU

Department of Energy and Process Engineering, NTNU



---

Vegard Førde Lavik, Trondheim 15/06-2009



## Sammendrag

Hensikten med arbeidet har vært å øke kunnskapen om termodynamiske modeller som beskriver utfrysningsforhold i naturgassystemer, samt forståelsen av faseoppførselen til naturgassblandinger hvor en faststoff-fase er inkludert. Dette er viktig fordi utfrysning av kritiske komponenter i naturgassblandingen kan føre til at prosessutstyr og varmevekslere blir plagget, noe som er en alvorlig utfordring i prosessanlegg. Det er derfor interessant å undersøke metanrike binære blandinger som inneholder komponenter med høy risiko for utfrysning. På grunn av høye trippelpunktstemperaturer er karbondioksid, benzen og syklohexan regnet som de mest kritiske komponentene.

Metoden som er undersøkt i denne rapporten for å beskrive faststoff – fluid systemer er tilstandsligningsmetoden. Det benyttes en tradisjonell tilstandsligning for å beskrive fluidfasene, i kombinasjon med et generelt uttrykk for faststoff-fasen som er basert på smelte- og trippelpunktsegenskaper til komponentene. Metoden er basert på antagelsen om at fast stoff-fasen består av en ren komponent. Denne antagelsen gjelder ikke alltid for reelle naturgassblandinger, men den representerer den høyeste risikoen for utfrysninger ved en gitt temperatur.

Ved å benytte simuleringsprogrammet NeqSim har det vært mulig å studere funksjonaliteten til denne metoden. Tilstandsligningsmetoden er implementert i NeqSim, basert på algoritmene som Michelsen og Mollerup har utviklet. For å undersøke nøyaktigheten og påliteligheten til denne termodynamiske modellen er det brukt eksperimentell data fra litteratur og andre eksisterende simuleringsprogram for sammenligning. Blant annet GPA, som er basert på aktivitetskoeffisient metoden og HYSYS, som er en kommersiell prosess-simulator.

Den tradisjonelle Soave-Redlich-Kwong tilstandsligningen er blitt benyttet sammen med klassiske blandingsregler inkludert interaksjonsparametre. Det viste seg at de binære interaksjonsparametrene hadde stor betydning for nøyaktigheten til beregningene, både for metanrike binære blandinger med tunge hydrokarboner og blandinger med karbondioksid. Metoden implementert i NeqSim viste gode resultater for de binære blandinger med karbondioksid og metan, etter at de binære interaksjonsparametrene var optimalisert. Det ble også avdekket at fast stoff – gass systemer var mindre avhengig av interaksjonsparametrene enn fast stoff – væske systemer. Beregningene som involverte metanrike binære blandinger med de tunge hydrokarbonene viste seg å være mer utfordrende, på grunn av numeriske problemer og lite eksperimentell data tilgjengelig.

En av hovedutfordringene ved å utvikle termodynamiske modeller for fast stoff – fluid systemer, er mangelen på eksperimentell data som kan validere modellene. Det eksperimentelle arbeidet ved utfrysningsriggen har hovedsakelig bestått av feilsøking og eksperimenter for å undersøke oppførselen til riggen. Det har blitt fokusert på kartlegging av driftserfaringer, samt identifisering av muligheter og begrensninger ved riggen. Det er også blitt gjennomført en fasestudie av ren karbondioksid, hvor faststoff – væske likevekt og trippelpunktet har blitt eksperimentelt bestemt. For at riggen skal kunne opereres med kjente binære blandinger, må varmetapet fra lavtemperaturcellen reduseres. Dette vil føre til at temperaturdifferansen mellom fluidet og det indre systemet blir lavere, slik at fluider vil fryse ut i safircellen hvor det kan detekteres. Når det gjelder multikomponentblandinger, hvor komposisjonen av de fluide fasene og fast stoff-fasen er ukjent, er det nødvendig å utvikle et prøvetakningssystem som kan bestemme komposisjonene til de ulike fasene.



## Summary

The motivation of the work is to increase the knowledge about thermodynamic modeling of freeze outs in natural gas systems and a deeper understanding of the phase behavior of natural gas mixtures, due to the problems experienced in cryogenic natural gas process-plants. Critical components in natural gas mixtures introduce a risk of forming a solid coating and plugging the process equipment. Hence, it is relevant to examine methane rich binary mixtures containing components with high risk of freezing. Due to their high triple point temperatures, carbon dioxide, benzene and cyclohexane are regarded as the most critical components.

The preferred thermodynamic method for modeling the solid – fluid system is by describing the fluid phases with a traditionally equation of state in combination with an expression for the solid phase based on melting and triple point properties. This method is based on the assumption of a pure component solid phase, which does not always represent the precipitated substances in natural gas systems. However, it is the situation which represents the highest risk of crystallization at a given temperature.

This study was carried out by applying a simulation tool called NeqSim, where the equation of state method is implemented based on the computational algorithms provided by Michelsen and Mollerup. To investigate the reliability and accuracy of the equation of state method, it is used experimental data from the literature as a foundation and further compared against two existing simulation tools for freezing point predictions of natural gas mixtures, GPA and HYSYS.

The Soave-Redlich-Kwong equation was selected together with classical mixing rules and the use of binary interaction parameters. The binary interaction parameters were discovered to be of crucial importance to the accuracy of the predictions, both for the binary mixtures containing carbon dioxide and the heavy hydrocarbons. The model showed promising results for carbon dioxide in methane rich binary mixtures, after the binary interaction parameter had been optimized. However, the interaction parameter dependency for solid-vapor equilibrium systems was discovered to be less than in solid-liquid equilibrium systems. Predictions of freeze outs of heavy hydrocarbons were discovered to be more challenging, due to numerical problems and a scarce experimental database.

One of the main issues concerning the development of reliable thermodynamic models for solid-fluid systems is the lack of experimental data, which prevents extensive validation of the proposed models. The experimental work related to the freeze out rig has mainly involved trouble-shooting and experiments for determining the behavior of the rig. Hence, the experimental focuses were on the gathering operational experience by running these experiments, and identify the main challenges and the potential areas for improvement. Including a phase study of pure carbon dioxide where the solid-liquid equilibrium and three-phase point was determined.

In order to investigate the binary mixtures of interest, where the composition and the component exposed to freeze outs is known, the heat loss from the Dewar container and the temperature difference between the air bath and the fluid has to be reduced. Hence, the solids will form in the sapphire cell, where the freeze outs can be visually detected. Further, for studying multi-component mixtures similar to real natural gas mixtures where the composition of the precipitating substance is unknown; a solution for the sampling of the different phases has to be developed, including extensively testing and validation.



# Table of Contents

1	Introduction .....	1
1.1	Background.....	3
1.2	Object and limitations.....	3
1.3	Report outline .....	4
	Part 1: Literature review of freeze out in natural gas systems.....	5
2	Article review in relation to prediction of freeze outs in natural gas systems .....	5
3	Phase Equilibrium.....	9
3.1	Thermodynamic Equilibrium.....	9
3.1.1	Gibbs Free Energy.....	9
3.1.2	Chemical Potential and Phase Equilibrium .....	10
3.1.3	Gibbs Phase Rule .....	10
3.1.4	Fugacity .....	11
3.1.5	Fugacity Coefficient.....	11
3.2	Calculating Fugacities.....	12
3.2.1	Fugacities of Fluids in Mixture .....	12
3.2.2	Fugacity of Solids.....	12
3.3	Activity coefficient used to describe real solutions .....	13
3.4	Equation of State.....	14
3.4.1	Van der Waals equation of state (vdW).....	15
3.4.2	Redlich-Kwong equation of state (RK).....	15
3.4.3	Soave-Redlich-Kwong equation of state (SRK).....	16
3.4.4	Peng-Robinson equation of state (PR) .....	16
3.5	Mixing rules.....	17
3.5.1	The van der Waals mixing rules .....	17
3.6	Flash calculations and freezing point calculations.....	18
3.6.1	Two phase TP-flash.....	18
3.6.2	Multiphase TPflash.....	21
3.6.3	Algorithm for freezing point predictions.....	22
4	Modeling solid precipitation in natural gas systems.....	25
4.1	NeqSim .....	25
4.1.1	Thermodynamic operations .....	26
4.2	GPA.....	29

4.2.1	The thermodynamic problem.....	29
4.3	HYSYS.....	31
4.3.1	CO2 Freeze out Utility.....	31
4.4	Discussion.....	32
5	Experimental equilibrium data from literature and model evaluation.....	33
5.1	Thermodynamic models used in simulations.....	34
5.2	Comparison of experimental data and different simulation models.....	36
5.2.1	Binary systems containing methane and carbon dioxide.....	37
5.2.2	Binary systems containing methane and heavy hydrocarbons.....	48
5.3	Discussion.....	59
Part 2	Experimental work and evaluation of the freeze out rig.....	61
6	Presentation of the experimental equipment - Freeze out rig.....	61
6.1	Modifications.....	62
6.2	The exterior system.....	63
6.2.1	Mechanical cooling.....	64
6.2.2	Liquid nitrogen cooling.....	64
6.3	The interior system.....	65
6.3.1	Sapphire cell.....	65
6.3.2	Blind cell.....	65
6.3.3	Cold finger.....	65
6.3.4	Temperature and pressure gauges.....	66
6.3.5	Circulation fan.....	66
7	Experiences and limitations of the rig which affect the experimental work.....	67
7.1	Temperature control in the interior system.....	68
7.1.1	Placement of the temperature sensors.....	68
7.1.2	Heat leakage from the Dewar container.....	68
7.1.3	Temperature regulation.....	70
7.1.4	Experimental determination by secondary detection.....	71
7.2	Freeze out on surfaces.....	72
7.3	Sampling of different phases.....	73
7.3.1	Sampling of solids.....	73
7.3.2	Sampling of liquid and vapor phase.....	74
7.4	Detection of phase transitions.....	75
7.4.1	Visual detection in the Sapphire cell.....	75



7.4.2	Infrared detector in the cold finger.....	75
7.4.3	Secondary detection .....	75
8	Experimental results and model evaluation .....	77
8.1	Pure carbon dioxide experiment.....	78
8.1.1	Experimental method.....	78
8.1.2	Results .....	79
8.2	Discussion of the results and model evaluations.....	86
9	Conclusion .....	89
10	Further work.....	91
	References.....	93
	Appendix .....	97



## List of figures

Figure 3-1 Equation-of-state tree showing the interrelationship between various equations of state [22] .....	14
Figure 3-2 Schematic diagram of a VLE flash chamber, made in HYSYS .....	18
Figure 3-3 Flow sheet of the TP-flash calculation procedure [24] .....	20
Figure 4-1 Object-oriented design of NeqSim [5] .....	25
Figure 4-2 Fugacity handling in freezing point calculations .....	27
Figure 5-1 Qualitative Pressure-Temperature Diagram for the Methane-Carbon Dioxide Binary System [12] .....	37
Figure 5-2 Binary interaction parameter dependency in NeqSim model (SLE: CO <sub>2</sub> -CH <sub>4</sub> binary systems) .....	39
Figure 5-3 Binary interaction parameter dependency in NeqSim model (SVE: CO <sub>2</sub> -CH <sub>4</sub> binary systems) .....	39
Figure 5-4 Calculated binary interaction parameter in low temperature CO <sub>2</sub> -CH <sub>4</sub> binary mixture based on ZareNezhad's temperature dependent semi-empirical correlation [10] .....	40
Figure 5-5 Solubility of CO <sub>2</sub> in liquid CH <sub>4</sub> : Predictions and experimental points from Kurata [1] .....	41
Figure 5-6 Solubility of CO <sub>2</sub> in liquid CH <sub>4</sub> : Predictions and experimental points from Davis [13] .....	42
Figure 5-7 Solubility of CO <sub>2</sub> in liquid CH <sub>4</sub> : Predictions and experimental points from Cheung and Zander [33] .....	43
Figure 5-8 Solubility of CO <sub>2</sub> in CH <sub>4</sub> : Predictions and experimental points from Agrawal [36] .....	44
Figure 5-9 Solubility of CO <sub>2</sub> in CH <sub>4</sub> : Predictions and experimental points from Le et al. [37] .....	45
Figure 5-10 Solubility of CO <sub>2</sub> in CH <sub>4</sub> : Predictions and experimental points from Davis [13] .....	46
Figure 5-11 Solubility of CO <sub>2</sub> in liquid CH <sub>4</sub> : Predictions and experimental points from Kurata [1] .....	47
Figure 5-12 Sketch of the phase diagram for binary mixtures consisting of hydrocarbons [2] .....	48
Figure 5-13 Binary Temperature-Concentration diagram of CH <sub>4</sub> – C <sub>6</sub> H <sub>6</sub> system [2] .....	49
Figure 5-14 Average BIAS for NeqSim calculations with different interactions parameters, compared to experimental data from Kurata [34] and Neumann [19] .....	51
Figure 5-15 Solubility of C <sub>6</sub> H <sub>6</sub> in CH <sub>4</sub> : Predictions and experimental data from Kurata [34] .....	53
Figure 5-16 Solubility of low concentrations C <sub>6</sub> H <sub>6</sub> in CH <sub>4</sub> : Predictions and experimental data from Kurata [34] .....	53
Figure 5-17 Solubility of C <sub>6</sub> H <sub>6</sub> in CH <sub>4</sub> : Predictions and experimental data from Neumann [19] .....	54
Figure 5-18 Solubility of low concentrations C <sub>6</sub> H <sub>6</sub> in CH <sub>4</sub> : Predictions and experimental data from Neumann [19] .....	54
Figure 5-19 Experimental three-phase locus of binary C <sub>6</sub> H <sub>6</sub> -CH <sub>4</sub> mixture [17] .....	55
Figure 5-20 Solubility of low concentrations C <sub>6</sub> H <sub>6</sub> in CH <sub>4</sub> : Predictions and experimental data from Luks [17] .....	56
Figure 5-21 Solubility of low concentrations C <sub>6</sub> H <sub>12</sub> in CH <sub>4</sub> : Predictions and experimental data from Kohn [35] .....	57
Figure 5-22 Experimental three-phase locus of binary C <sub>6</sub> H <sub>12</sub> -CH <sub>4</sub> mixture [35] .....	58
Figure 6-1 3D model of the freeze out rig .....	61
Figure 6-2 Flow sheet over freeze out rig: Short time modifications [43] .....	62
Figure 6-3 Circulation system [44] .....	63
Figure 7-1 Heat loss due to radiation in the Dewar container at different temperatures .....	68
Figure 7-2 Effect of gas pressure on thermal conductivity of multilayer insulation (MLI) [45] .....	69
Figure 8-1 Phase diagram of pure carbon dioxide; indicating experiment procedure .....	78

Figure 8-2 Pressure – Temperature diagram: Freezing point measurements [8632-8838].....	80
Figure 8-3 Pressure-Volume diagram: Pressure regulation measurements [8631-8969] .....	81
Figure 8-4 Pressure – Volume diagram: Solid-Liquid equilibrium measurements [8854-8988] .....	82
Figure 8-5 Pressure – Temperature diagram: Triple point measurements [10008-10068] .....	83
Figure 8-6 IR-signal during phase transitions [8632-10068] .....	84
Figure 8-7 Temperature variations in the air bath: Solid-Liquid equilibrium [8854-8988] .....	86

## List of tables

Table 4-1 Component properties used in phase equilibrium calculations .....	28
Table 5-1 Solid-Liquid experiments: Y solubility in liquid Methane (binary systems) .....	33
Table 5-2 Solid-Vapor experiments: Y solubility in methane (binary systems).....	33
Table 5-3 Comparison of EOS model used in different simulation tools to predict freezing point temperature in carbon dioxide – methane mixtures.....	34
Table 5-4 Solid-Liquid experiments: Y solubility in liquid Methane (binary systems) .....	36
Table 5-5 Solid-Vapor experiments: Y solubility in methane (binary systems).....	36
Table 5-6 Comparison of interaction parameters used with SRK in NeqSim (SLE: CO <sub>2</sub> -CH <sub>4</sub> binary systems).....	38
Table 5-7 Comparison of interaction parameters used with SRK in NeqSim (VSE -binary systems) ....	39
Table 5-8 Accuracy of different simulation tools compared with GPA RR 10 [1] .....	47
Table 5-9 Freezing point predictions with different interaction parameters for benzene – methane binary system (SLE) .....	50
Table 8-1 Experimental Test Matrix .....	77
Table 8-2 Calculated experimental sublimation conditions for pure CO <sub>2</sub> .....	81
Table 8-3 Calculations of experimental triple point conditions for pure CO <sub>2</sub> .....	83
Table 8-4 Experimental results and data from literature .....	86



# 1 Introduction

In the recent decades the use of cryogenic processes are expanding, due to the advances in process and material technology which make these solutions economical feasible. When processing natural gas, the liquefied natural gas (LNG) solution is compared to the traditional piping solution, and due to the worlds need for fossil fuel the marked for oil and gas are changing to a more global marked. Where all the producers want to do business in the area they can sell with the highest profit. Thus are the LNG (liquid natural gas) and LPG (liquid petroleum gas) interesting concepts when considering the transport distance to different markets.

The main advantage with the LNG concept is the energy density, which leads to minimal storage requirements; the volume of 1 m<sup>3</sup> LNG at atmospheric pressure equals about 614 m<sup>3</sup> of natural gas at the same pressure. The natural gas with a satisfactory composition is liquefied at a temperature about -162°C, and consists mainly of methane (85-95%) in addition to some fractions of other hydrocarbons and traces of nitrogen and carbon dioxide.

The LNG concept is considered to be an optimal solution for smaller field development; where the gas fields explored are not economical feasible with a traditional offshore development. Several of these gas fields are relevant application areas for an FPSO vessel (floating-production-storage-offloading) solution with LNG production facilities on the topside. This is considered to be the most important solution when extracting oil and gas from the fields in more remote areas in the future.

There are also being done research and development of different concepts regarding transport solutions of liquefied natural gas. In which requires minimal processing before transport and distribution, for example the Heavy Liquefied Gas (HLG) and Liquefied Unprocessed Well Stream (LUWS). The LUWS idea is based on condensing untreated well flow, in contrast to conventional LNG processes, where the well stream is treated before it is chilled and liquefied. While the HLG concept involves liquefaction of the gas at a higher pressure which results in a higher liquefaction temperature, thus the energy requirement in the cooling process will be reduced. The condensed natural gas under pressure at a higher temperature can dissolve more carbon dioxide and heavier hydrocarbons than liquefied natural gas at atmospheric pressure; it is therefore possible to reduce the amount of refinement to a minimum.

These solutions require new processes and equipment developed, for mixtures in which the behavior is unknown. However, the most important part of these concepts, both LNG and the developing solutions are the liquefaction process, where the natural gas gets cooled down. The only difference is the temperature, at which the different petroleum gases are liquefied, and the extent of the separation process, in which for LNG involves separation of methane from heavier alkenes. This is the main process which requires the low operating temperatures, when refining LNG.

In regards to these low temperature processes of natural gas there is a serious issue when the components in the feed stream precipitates. This is especially critical for carbon dioxide and various hydrocarbons components, due to their high triple point temperature. These components introduce a risk of forming a solid coating on heat exchangers, process piping and valves, in which can lead to blockage and further an expensive shutdown of the production.

Freeze out of carbon dioxide, which has the highest triple point temperature of the critical components, can in addition occur on the turbo-expansion outlet. The design practice of the gas expansion process requires that the expansion is to be stopped right before the freezing point condition for carbon dioxide. [1]

Among the critical heavy hydrocarbons are benzene and cyclohexane, components which creates a great risk of freeze outs. Considering the chemical properties they are both likely candidates for freezing, however, the solubility of cyclohexane in binary methane mixture is higher than benzene; at a given concentration the freezing temperature for benzene is higher, thus there is a higher risk of solid formation of benzene. For heavier hydrocarbons than benzene and cyclohexane the freezing risk are neglected, since the molar fraction of these components generally are very small in natural gas streams. [2]

The way to deal with these problems is to better understand the phase behavior of these components in natural gas mixtures. This can be done by reviewing experimental work on the subject, like solubility of the relevant hydrocarbons and carbon dioxide in methane rich binary mixtures. Both solid-liquid equilibrium (SLE) and solid-vapor equilibrium (SVE) systems, unfortunately there is very few SVE data available, especially of hydrocarbons in natural gas mixtures.

Another source of information is computer simulations of natural gas systems. However, it have been experienced unreliable predictions by several commercial simulators, and a substantial disagreement between the different freezing point predictions [3]. In order to overcome the operational challenges and to be able to conduct good design practice, the thermodynamic models involved in the different processes need to be optimized.

The simulations models can reduce the number of experimental data points for a particular design problem; still there is a need for experimental equilibrium data to adjust the different parameters in the models. In this regard, the experimental freezing point data in cryogenic processes are interesting for two reasons; first it is necessary to increase the knowledge of the solubility of solids in cryogenic fluids for design of cryogenic processes. Next, it is important to investigate and validate the thermodynamic models against experimental data.



## **1.1 Background**

At StatoilHydro's research center at Rotvoll, there is installed an experimental freeze out rig. The intentions of acquiring this freeze out rig are to extend the experimental database in literature, due to experienced problems with freeze outs in natural gas process plants. Based on the previous work and participation at the experimental work in relation to the freeze out rig [4], there is recognized a need of more knowledge concerning the phase behavior of natural gas systems. More specific, information about binary methane rich mixtures and freezing points of mixtures containing critical components are necessary; for validating the freeze out rig, and as a foundation for further experimental work. This includes a comprehensive literature study and generation of experimental results at the freeze out rig.

In addition, as mentioned introductorily, a useful source of information is the thermodynamic models and it is recognized that more knowledge is needed in order to optimize these. The previous work of Even Solbraa, part of his PhD thesis [5], resulted in a simulation tool called NeqSim (Non-Equilibrium Simulator) based on the thermodynamic computation algorithms of Michelsen and Mollerup [6]. This computer program is capable of predicting freezing points of different natural gas related mixtures and are a possible source of valuable information of the phase behavior of the different mixtures investigated in the freeze out rig. This simulation tool can be used to understand unexpected phase behavior and support the experimental work in addition to the literature available on the subject. However, there is a need for validating and testing this simulation tool against literature and other thermodynamic models available.

## **1.2 Object and limitations**

The overall object of this thesis is to improve and extend the knowledge about freeze outs with the focus on modeling and predictions of freeze out parameters.

Thus the scope of the systems investigated is limited to solid-fluid equilibrium and solubility of the critical components in binary methane rich mixtures, due to the composition of natural gas systems. Issues regarding water and hydrate formations are excluded, respectively since the subject are covered elsewhere [7, 8] and outside the scope of this thesis.

The preferred method for describing the solid-fluid systems and predict freeze out parameters; is by using an equation of state for describing the fluid phases and a general expression for describing the solid phase, for investigating the functionality of this method is the NeqSim simulator used and compared to the GPA and HYSYS simulators.

Since the experimental work at the rig mostly have included trouble-shooting and experiments for determining the behavior of the rig, while the phase behavior studies of mixtures relevant to freeze outs have been postponed, the experimental part of this report will focus on the experience obtained and the challenges and limitations discovered by running these experiments.

The vision and motivation of this work is; the report shall found the basis for further experimental work on the freeze out rig, and be valuable source of information for the people involved.

### **1.3 Report outline**

The report is divided into two parts; Literature review of freeze out in natural gas systems, and experimental work and evaluation of the freeze out rig.

#### **Literature review of freeze out in natural gas systems**

First, there are presented a short description of the previously work regarding prediction of freeze outs in natural gas systems. Further are the fundamental theory and thermodynamic equations regarding descriptions of phase equilibrium presented, including calculations procedures and introduction of computational simulation tools, respectively, NeqSim, GPA and HYSYS.

Secondly, a literature study of the previous experimental works regarding the solubility's of the critical components in selected binary mixtures is carried through, including review and description of the experimental methods, in appendix C5. The first part of the report is completed with a presentation of the experimental results gathered in the literature and a model evaluation, where the simulations tools are compared to the experimental data; the results are analyzed and discussed. All the raw data from the simulations are presented in appendix C1-C4.

#### **Experimental work and evaluation of the rig**

This section starts with a presentation of the freeze out rig and further states the operation challenges and possibilities regarding the freeze out rig, including the experience gathered from previous experimental work and the discovered limitations which affects the experimental work.

Next is a phase study experiment of pure carbon dioxide presented. Where the freezing point temperature of liquid carbon dioxide, solid-liquid equilibrium and the triple point of carbon dioxide are investigated and the functionality of the rig discussed; before a final conclusion is drawn.

## Part 1: Literature review of freeze out in natural gas systems

### 2 Article review in relation to prediction of freeze outs in natural gas systems

It's done a lot of work to simulate and predict the thermodynamic behavior of mixtures related to the oil and gas industry, on the basis of experimental and analytical data. Mainly is this work related to flow assurance in offshore environments, due to the risks of deposition of fluid hydrocarbon solids (like waxes and hydrates), which is a major concern for the oil and gas industry. Thus the study of liquid-liquid, liquid-liquid-vapor, and liquid-vapor equilibrium constitute a mature research area. This in contrast to the study of solid-liquid (SLE), solid-vapor (SVE), and solid-liquid-vapor equilibrium (SLVE), which are the subject investigated in this report. In order to secure safe handling of natural gas processes, it is necessary to optimize the thermodynamic models used for design and operation of such systems. The papers studied regarding this issue are briefly described beneath, while the different experimental sources will be discussed and evaluated later in the report.

Eggeman, T. and S. Chafin, *Beware the pitfalls of CO<sub>2</sub> freezing prediction*. [3]

Eggeman and Chafin applied a set of thermodynamic models and estimation procedures for the determination of the freezing point of carbon dioxide in vapor and liquid methane, including an activity coefficient model based on the Non-Random-Two-Liquid (NRTL) model for description of the fluid properties, while equation (3.20) was used for the solid phase. In addition they investigated the functionality of the traditional Peng-Robinson equation of state for the same mixture. These predictions have been compared to, among others, experimental data from Kurata [1], and experimental data on the equilibrium between liquid and solid in the binary systems of Knapp et al.[9].

ZareNezhad, B., *Prediction of CO<sub>2</sub> freezing points for the mixtures of CO<sub>2</sub>-CH<sub>4</sub> at cryogenic conditions of NGL extraction plants*. [10]

He has developed a semi-empirical quadratic temperature dependent binary interaction parameter for describing the molecular interactions in mixtures consisting of carbon dioxide and methane at cryogenic conditions in natural gas processes, presented in equation (5.2). The Peng-Robinson equation of state has been used for predicting the carbon dioxide freezing points for vapor and liquid phases in binary mixtures with methane, and classical mixing rules for validating this temperature dependent binary interaction parameter. The results have been compared to high quality experimental sources, the freeze out from vapor phase are compared to the GPSA Data Book [11], while the liquid phase predictions are compared to the work by Kurata [1]. The expression for the fugacity of the solid phase used is the same as Eggeman and Chalfin [3] employed in their work, presented in equation (3.20).

Hlavinka, M.W. and V.N. Hernandez, *Proper Interpretation of Freezing and Hydrate Prediction Results from Process Simulation*. [12]

This paper is focusing on the phase equilibrium that is present in solid formation region of natural gas systems, mainly by studying the binary carbon dioxide-methane system. Where the simulation tool, called ProMax from the Bryan Research & Engineering Inc., are applied for predicting different equilibrium conditions. These results have been compared, among others, to the experimental results from Davis et al.[13] and Kurata [1], in addition to the predictions made by Eggeman [3]. They also discuss the importance of knowing the phase behavior to safely employ computational tools for predictions.

Kohn, J.P. and K.D. Luks, *Solubility of Hydrocarbons in Cryogenic LNG and NGL Mixtures*. Research Report RR-22. [14]

GPA has a number of research reports concerning the solubility of hydrocarbons in cryogenic LNG and NGL mixtures. This report is describing a method to estimate solubility of the heavy hydrocarbons in LNG and cryogenic NGL mixtures. The model is based on the definition of excess Gibbs energy, in which includes empirical correlation, or activity coefficients, that agreed with the experimental data available. In addition, the report present the experimental data used in the model development, including binary hydrocarbon mixtures and a limited number of more complex systems.

Luks, K.D., et al., *Measurement and Prediction of the Solubility of Hydrocarbons in Cryogenic LGN and NGL*. [15]

This article is written as part of the same project as the research reports RR 22 [14], published by the Gas Processors Association (GPA), and concerns the solubility of hydrocarbons in LNG and NGL systems. Where they summarize the research work done, the systematic experimental study of binary and ternary SLV systems, where the solid phase is a hydrocarbon. In addition to evaluate the correlation made for multi component systems, which are based on the activity coefficient model described in the research report RR 22. This model is more thoroughly discussed later in this thesis, and used in simulations.

Carter, K. and K.D. Luks, *Extending a classical EOS correlation to represent solid-fluid phase equilibria*. [16]

They present a method for describing all the solid-fluid phase equilibriums of a binary mixture, similar to the articles by Eggeman and ZareNezhad; involving a traditional equation of state, preferably the Peng-Robinson or the Soave-Redlich-Kwong equation, for describing the fluid phase properties, while equation (3.20) are used to describing the solid phase. Recognizing this method yields a more general approach for describing natural gas systems, and less experimental data needed for correlating the prediction model.

de Hemptinne, J.C., *Benzene crystallization risks in the LIQUEFIN liquefied natural gas process*. [2]

In order to understand the physical phenomenon of crystallization is the phase diagram of the binary benzene - methane system studied thoroughly. In addition have they developed a thermodynamic model to calculate the phase diagram of two typical compositions encountered in the LIQUEFIN process, where they uses the Peng-Robinson equation of state with the Huron-Vidal mixing rule, and equation (3.20) for describing the solid phase. The experimental data evaluated in this study are the work done by Luks [17], Rijkers [18] and Neumann [19].

Solbraa, E., *Equilibrium and Non-Equilibrium Thermodynamics of Natural Gas Processing*, [5]

As mentioned in the introduction, the results of Solbraa's PhD project, was a simulation program based on Michelsen and Mullerup [6] algorithms. In which it can be used for simulating the most common processes related to the oil and gas industry. This thesis gives a thorough description of the possibilities and development of the computational tool.

Solbraa, E., *NeqSim USERS GUIDE*. [20]

Solbraa has also written a user guide for the program he developed, this have been useful for understanding the user interface and the calculation procedure.



### 3 Phase Equilibrium

The equilibrium condition between different phases in a multi-component system are reached when the exchange of substance between the phases have reached a constant value, meaning that the mass transfer from one phase to another is equal in each direction. For a system in a non-equilibrium condition, the mass transfer between the phases will try to establish a new equilibrium condition. This phase equilibrium condition is, dependent on several variables, including temperature, pressure, composition and the chemical nature of the substances. However, the driving force for this mass transfer taking place is dependent on how far the system is from the thermodynamic equilibrium.

Phase equilibrium studies are focusing on the relation between these parameters, in which can be used to describe the systems of interest. The functionality of these models which are used to calculate the thermodynamic and physical properties are crucial to the accuracy of the result.

#### 3.1 Thermodynamic Equilibrium

The freezing phenomena is addressed in the phase changes in a fluid, thus it is important to consider the thermodynamic mechanisms for understanding the freeze out subject complete. The phase equilibrium criteria are developed from the principle of conservation of energy and the second law of thermodynamics. The next subchapters give a short introduction to the properties and parameters used for describe and investigate phase equilibriums in fluids.

##### 3.1.1 Gibbs Free Energy

When investigating phase equilibrium, it is appropriate to use the Gibbs function, which is defined as:

$$G = H - TS = U + pV - TS \quad (3.1)$$

By using the 2. law of thermodynamics and Gibbs in differential form, the following function is derived:

$$dG - Vdp + SdT \leq 0 \quad (3.2)$$

All processes carried through at a specific temperature and pressure ( $dT = 0$  and  $dp = 0$ ), are bounded by:

$$dG]_{T,p} \leq 0 \quad (3.3)$$

This inequality indicates that the Gibbs function of a system, at specific temperature and pressure, decreases through an irreversible process. Each step in such a process results in a reduction of the Gibbs function, and brings the system closer to equilibrium, where equilibrium is achieved at the time the process reach a minimum value of the Gibbs function:

$$dG]_{T,p} = 0 \quad (3.4)$$

Equation (3.4) establishes a relationship between the properties of a system at equilibrium. The way the system has reached the equilibrium condition is not important, but as soon equilibrium condition is achieved, at a specific temperature and pressure, no further spontaneous changes can take place. When we use equation (3.4) we specify the temperature and pressure, but it is not necessary to further specify how the system achieves the equilibrium state.

### 3.1.2 Chemical Potential and Phase Equilibrium

The chemical potential is defined as the partial molar Gibbs energy:

$$\mu = \frac{G}{n} = \bar{g} = \bar{h} - T\bar{s} \quad (3.5)$$

For a system consisting of two components (A and B) in two phases (1 and 2) with the same temperature and pressure, the change in Gibbs function in each phase is described as:

$$\begin{aligned} dG^1 \Big|_{T,p} &= \mu_A^1 dn_A^1 + \mu_B^1 dn_B^1 \\ dG^2 \Big|_{T,p} &= \mu_A^2 dn_A^2 + \mu_B^2 dn_B^2 \end{aligned} \quad (3.6)$$

When mass is transported between the two phases, and no chemical reactions occur, the total mass of the two components is constant. Thus the increase of mass in one of the phases, are followed by reduction of mass in the second phase.

Since  $n_A^1$  and  $n_B^1$  can vary independently of each other, and the system is at equilibrium ( $dG \Big|_{T,p} = 0$ ), the expressions reduce to:

$$\begin{aligned} \mu_A^1 &= \mu_A^2 \\ \mu_B^1 &= \mu_B^2 \end{aligned} \quad (3.7)$$

This shows that the chemical potential for each component is the same in both phases, which is the criterion of two phase equilibrium. It is readily generalized to multiple phases by successive application to pairs of phases. The general result is,

$$\mu^1 = \mu^2 = \mu^3 \quad (3.8)$$

where the superscript notes the different phases. In addition to the equilibrium criterion the Gibbs free energy have to be at a global minimum.

### 3.1.3 Gibbs Phase Rule

The equilibrium criterion of a system consisting of two components and two phases, given by equation(3.7), can be extended with similar reasoning with respect to multi-component, multi-phase and non-reacting systems. At equilibrium the chemical potential must be the same in all phases. For a case with  $N$  components present in the  $P$  phases can be modeled using  $N(P-1)$  equations:

$$N \left\{ \begin{array}{l} \overbrace{\mu_1^1 = \mu_1^2 = \mu_1^3 = \dots = \mu_1^P}^{P-1} \\ \mu_2^1 = \mu_2^2 = \mu_2^3 = \dots = \mu_2^P \\ \cdot \\ \cdot \\ \cdot \\ \mu_N^1 = \mu_N^2 = \mu_N^3 = \dots = \mu_N^P \end{array} \right. \quad (3.9)$$



Here is the term  $\mu_i^j$  describing the chemical potential of the ( $i$ ) component in the ( $j$ ) phase. This set of equations form the basis of the Gibbs phase rule, which makes it possible to determine the various independent intensive properties that can be arbitrarily specified to determine the intensive state of the system. The number of intensive properties is called freedom degrees.

Since the chemical potential is an intensive property it is dependent of the molar composition ratio present and not the amount of components. In other words, in a given phase of  $N$  components at temperature  $T$  and pressure  $p$ , the chemical potential is determined by the mole fraction of the components present and not the respective amounts.

The numbers of intensive properties that are freely variable, or the number of freedom degrees are:

$$F = [P(N-1) + 2] - N(P-1) = 2 + N - P \quad (3.10)$$

### 3.1.4 Fugacity

The use of chemical potential in equilibrium calculations will often lead to computational difficulties, when the chemical potential at some states approach minus infinity. Thus for some systems it may be more convenient to use fugacity instead of chemical potential, the fugacity function behaves in many cases better, and may be evaluated as:

$$\mu = \bar{g} = RT \ln(f) \quad (3.11)$$

Fugacity has the same notation as pressure, and in ideal gas systems it generally plays the same role as the pressure. Since ideal gas behavior is achieved when the pressure goes to zero, the constant term can be determined by the requirement showing that the fugacity of a pure component is equal to the pressure in the limit of zero pressure. Mathematically described:

$$\lim_{p \rightarrow 0} \frac{f}{p} = 1 \quad (3.12)$$

These two equations completely define the fugacity function, and by substituting the fugacity expression into equation (3.7), the phase equilibrium criterion is described as:

$$f_i^1 = f_i^2 \quad (3.13)$$

Thus for a multiphase, multi-component system the fugacity for a component must be the same in all phases in order to achieve equilibrium.

### 3.1.5 Fugacity Coefficient

The fugacity coefficient for a pure component is defined as:

$$\phi = \frac{f}{p} \quad (3.14)$$

where  $p$  is the pressure.

And in a mixture, the fugacity coefficient for component  $i$  is,

$$\begin{aligned}\phi_i^L &= \frac{f_i^L}{x_i P} \\ \phi_i^V &= \frac{f_i^V}{y_i P}\end{aligned}\quad (3.15)$$

depending of the system in consideration, gas ( $V$ ) or liquid phase ( $L$ ). When equilibrium is obtained the fugacity coefficient will be equal in all phases.

$$\phi_i^L = \phi_i^V \quad (3.16)$$

### 3.2 Calculating Fugacities

The equilibrium point between two phases in a mixture with a given composition can be calculated by determining the pressure and temperature that satisfies the equation (3.13) for all components. Fugacities of mixtures are generally not listed in the tables, but must be calculated using the thermodynamic relations from known conditions, or from an equation of state (EOS).

#### 3.2.1 Fugacities of Fluids in Mixture

By assuming incompressible liquid, the fugacity of a component in a mixture may be calculated using the following equation:

$$RT \ln \phi = RT \ln \frac{f_i}{y_i P} = \int \left( v_i - \frac{RT}{P} \right) dP \quad (3.17)$$

#### 3.2.2 Fugacity of Solids

For solid phases, it is assumed that the component with the lowest solubility will freeze out in a pure phase. This simplifies the calculation for the fugacity of solids, since the mole fraction of the freeze out component is equal to one and the fugacity of the solid is not dependent of the mixture composition.

$$f_i^{Solid} = f_i^{SatVapor} e^{\frac{V_i^{Solid} (P - P_i^{SatSolid})}{RT}} = P_i^{SatSolid} \phi_i^{SatVapor} e^{\frac{V_i^{Solid} (P - P_i^{SatSolid})}{RT}} \quad (3.18)$$

For a pure component at the triple point the fugacity is equal in all phases. A pressure increase at constant temperature will change the fugacity of the liquid and solid with the term in the exponent in equation (3.18), referred to as the Poynting Correction Factor (PCF). In this case, the fugacity will only be dependent of the molar volume and can be calculated by:

$$f_i^{T_p, Solid} e^{\frac{V_i^{T_p, Solid} (P - P_p)}{RT}} \approx f_i^{T_p, Liquid} e^{\frac{V_i^{T_p, Liquid} (P - P_p)}{RT}}, T = T_{tp} \quad (3.19)$$

From this equation it can be assumed that the liquid-solid equilibrium line starts at the triple point and goes as a vertical line in the phase diagram with an approximately constant temperature. This is confirmed by the normal melting temperature of most substances vary with only 0.1 K [21].

Another expression for the solid fugacity is recognized in the literature [2, 3, 16], used for studying solid-liquid equilibrium; the equation is directly derived from the partial molar Gibbs energy changes between the solid and liquid phases, described by:

$$\ln\left(\frac{f_{Si}^0}{f_{Li}}\right) = \frac{\Delta H_i^f}{RT} \left(1 - \frac{T}{T_i^f}\right) + \frac{\Delta C_{pi}}{R} \left(1 - \frac{T}{T_i^f} - \ln\left(\frac{T}{T_i^f}\right)\right) + \frac{\Delta v_i (P - P_{atm})}{RT} \quad (3.20)$$

where  $\Delta H_i^f$  is representing the heat of fusion,  $\Delta C_{pi}$  is the heat capacity change, and  $\Delta v_i$  the density change at fusion, or melting conditions. This equation represents a more limiting description of the fugacity of the solid phase, since it is related to the enthalpic and entropic changes between the solid and liquid state.

### 3.3 Activity coefficient used to describe real solutions

Consider a reference state where the component  $i$  of a multi-component system is pure at a temperature  $T$  and a reference pressure  $p_{ref}$ , the difference of chemical potential between a specific state and reference state be given by:

$$\mu_i - \mu_i^0 = \bar{R}T \ln \frac{\bar{f}_i}{f_i^0} \quad (3.21)$$

The superscript <sup>0</sup> states the properties of the reference state. The fugacity ratio in the logarithmic expression is known as the activity  $\gamma_i$ , to the component  $i$  in the mixture.

$$\gamma_i = \frac{\bar{f}_i}{f_i^0} \quad (3.22)$$

For an ideal mixture the activity are defined as:

$$\gamma_i = \frac{y_i f_i}{f_i^0} \quad (3.23)$$

### 3.4 Equation of State

Since the ideal gas law is not applicable on natural gas mixtures, the use of equations of state are necessary for being able to calculate the state of a fluid or fluid mixture at given conditions. The equation of state method is important for designing of processes in chemical engineering, and it is assumed that it will have a growing role in phase equilibrium studies of fluids and fluid mixtures. This chapter will give an introduction of the different equations of state based on the review article of Wei and Sadus [22].

Traditional use of equations of state was mainly for pure components, the development of these models has allowed the equations to describe mixtures as well. At first they were only used for non-polar mixtures, but as the development continued they were able to calculate phase equilibria for both non-polar and polar mixtures. The advantages by using equations of state for calculating phase equilibria are many; they can be used over a wide range of temperature and pressure, applicable for multi-component mixtures, consisting of light gases and heavy liquids.

The progress of the computational power and statistical development has allowed the equations of state to take consideration to molecular behavior that applies for real fluids and mixtures. Thus the accuracy of the underlying model is improved.

For describing natural gas systems are Peng-Robinson (PR) and Soave-Redlich-Kwong (SRK) widely used in the chemical process industry. Figure 3-1 presents the different modified equation of state models and which model or theory they originate from. The focus is on equations of state based on the van der Waals equation of state, on the left hand side.

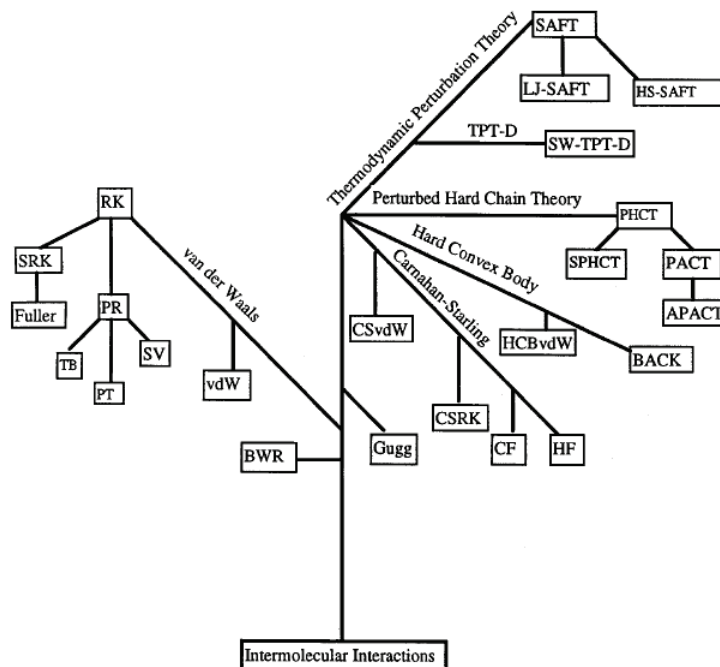


Figure 3-1 Equation-of-state tree showing the interrelationship between various equations of state [22]

All the two-constant equations consist of two constants, in which are calculated in different ways. In order to describe mixtures, the equations of state are modified by using different mixing rules depending on the composition of the appropriate mixture; the relevant mixing rules for this study are presented in chapter 3.5.

### 3.4.1 Van der Waals equation of state (vdW)

The van der Waals equation of state was the first equation capable of representing vapor-liquid coexistence, and it were proposed in 1873. The expression is as followed:

$$Z = \frac{V}{V-b} - \frac{a}{RTV} \quad (3.24)$$

where  $Z$  is indicating the compressibility factor ( $Z = pV/RT$ ). In both expressions is  $T$  the temperature,  $V$  is volume,  $p$  is the pressure, and  $R$  is the molar universal gas constant. The parameter  $a$  is representing the attractive forces between the molecules, and the parameter  $b$  is representing the co-volume occupied by the molecules, thus if the molecules are treated as hard-spheres with a diameter,  $\sigma$ ; the expression for the co-volume are expressed by  $b = 2\pi N\sigma^3/3$ .

The  $a$  and  $b$  parameters is a function of the critical properties of the fluid. Because of the functionality of the van der Waals regarding the description of the contribution of repulsive and attractive intermolecular interactions, it is consider to be an “hard sphere (repulsive) + attractive” term equation of state. It is capable of describing the vapor and liquid phases and phase transitions in a qualitative manner, but is seldom sufficient accurate for phase equilibrium calculations. An example is that the compressibility factor calculated by equation (3.24), which applies for all fluids, are  $Z_c = 0.375$ . In contrast, the real value for various hydrocarbons is in between 0.24 and 0.29. The van der Waals equation of state has been succeeded by several more accurate equations; the equations further presented in this work are regarded as modifications of the van der Waals equation.

### 3.4.2 Redlich-Kwong equation of state (RK)

The modification to the van der Waals equation of state by adding a temperature dependent attractive term is regarded as one of the most important improvements. The Redlich-Kwong equation of state is expressed by:

$$Z = \frac{V}{V-b} - \frac{a}{RT^{1.5}(V+b)} \quad (3.25)$$

For pure substances, the equation parameters  $a$  and  $b$  are usually expressed as,

$$\begin{aligned} a &= 0.4278R^2T_c^{2.5}/p_c \\ b &= 0.0867RT_c/p_c \end{aligned} \quad (3.26)$$

and by applying mixing rules to the equation parameters  $a$  and  $b$ , the Redlich-Kwong equation of state can be used for describing mixtures. It has been showed that by treating the interaction parameters as empirical parameters have led to a substantial improvement of the description of the fugacity in gas mixtures. In addition, the accuracy of the critical properties for binary mixtures can be increased by adjusting the value of the interaction parameter in the mixing rule for the  $a$  term.

### 3.4.3 Soave-Redlich-Kwong equation of state (SRK)

By replacing the temperature dependent attractive term  $(a/T^{1.5})$ , in the Redlich-Kwong equation, with a more general temperature dependent term  $a(T)$ , Soave (1972) made a significant improvement to the Redlich-Kwong equation:

$$Z = \frac{V}{V-b} - \frac{a(T)}{RT(V+b)} \quad (3.27)$$

where,

$$a(T) = 0,4274 \left( \frac{R^2 T_c^2}{p^c} \right) \left\{ 1 + m \left[ 1 - \left( \frac{T}{T_c} \right)^{0,5} \right] \right\}^2$$

$$m = 0,480 + 1,57\omega - 0,176\omega^2 \quad (3.28)$$

$$b = 0,08664 \frac{RT_c}{p^c}$$

and  $\omega$  is the acentric factor. The vapor pressure of several hydrocarbons and binary systems have been calculated and compared to experimental data (Soave, 1972) for investigating the accuracy of the Soave-Redlich-Kwong equation of state. The result showed that the equation of state predictions made a good agreement with the experimental data, and that the Soave-Redlich-Kwong equation of state was capable to accurately describe the phase behavior of mixtures.

### 3.4.4 Peng-Robinson equation of state (PR)

Some years later, Peng and Robinson proposed a new modification to the Redlich-Kwong equation of state where they redefined the temperature dependent attractive term,  $a(T)$ :

$$a(T) = 0,45724 \left( \frac{R^2 T_c^2}{p^c} \right) \left\{ 1 + k \left[ 1 - \frac{T}{T_c} \right] \right\}^2$$

$$k = 0,37464 + 1,5422\omega - 0,26922\omega^2 \quad (3.29)$$

$$b = 0,07780 \frac{RT_c}{p^c}$$

In addition they modified the volume dependence, since the earlier equations were overestimating the critical compressibility factor. Thus the Peng-Robinson equation of state was defined by:

$$Z = \frac{V}{V-b} - \frac{a(T)V}{RT[V(V+b)+b(V-b)]} \quad (3.30)$$

The modification resulted in an improvement of the calculated critical compressibility factor,  $Z_c = 0.307$ . Peng and Robinson also showed that their equation could be applied for accurate prediction of the vapor pressure of pure substances and equilibrium ratios in mixtures.

As mentioned are the Peng-Robinson and Soave-Redlich-Kwong equations of state widely used in the industry, and they have many advantages regarding describing binary and multi component systems. They are accurately representing the correlation between temperature, pressure and phase compositions. The only requirements necessary is the critical properties and acentric factors for the generalized parameters, and little computational time is needed to get accurate phase equilibrium correlations. The restriction of the quality of the result is the estimation of the vapor pressure, since the description of saturated liquid volumes is over predicted compared to experimental data. In chapter 5.1 are the equations of state used in the simulations further discussed.

### 3.5 Mixing rules

The area where equations of states are most beneficially is for calculating phase equilibrium for fluids and fluids mixtures, and in practice it is the same equations of state are used on pure fluids as on fluid mixtures. This is due to the applications of mixing rules, which is a calculation method for obtaining the mixture parameters. The mixing rules relate the pure components properties to the properties of the mixture.

The most basic mixing rule is just a linear average of the equation of state parameters, presented beneath:

$$a = \sum_i x_i a_i \quad (3.31)$$

Equation (3.31) is seldom employed, since it does not account for the unequal interactions in binary fluids.

$$b = \sum_i x_i b_i \quad (3.32)$$

Thus employment of both equation (3.31) and (3.32) will result in large deviations between calculated and experimental data. But equation (3.32) are sometimes used because its simplicity.

#### 3.5.1 The van der Waals mixing rules

The van der Waals mixing rules is the most used mixing rules, called one-fluid mixing rules and often referred to as the classical mixing rules.

$$a = \sum_i \sum_j x_i x_j a_{ij} \quad (3.33)$$

$$b = \sum_i \sum_j x_i x_j b_{ij} \quad (3.34)$$

where  $a_{ii}$  and  $b_{ii}$  are representing the constants for pure component  $i$ , while  $a_{ij}$  and  $b_{ij}$  ( $i \neq j$ ) are cross components parameters which are determined by an appropriate combining rule with or without binary parameters. Section A1, in the appendix, presents an outtake from the review article by Wei and Sadus [22], where the most relevant combining rules are discussed.

### 3.6 Flash calculations and freezing point calculations

For calculating the equilibrium conditions of a fluid mixture at given pressure and temperature is done by applying a TP-flash calculation. The flash procedure is used to determine several mixture properties at phase equilibrium. For example the number of phases, the molar amount of each phase, molar phase composition, phase densities, molar enthalpy and entropy of each phase. This chapter is based on the review of Michelsen and Mollerups work, published by Poling [23].

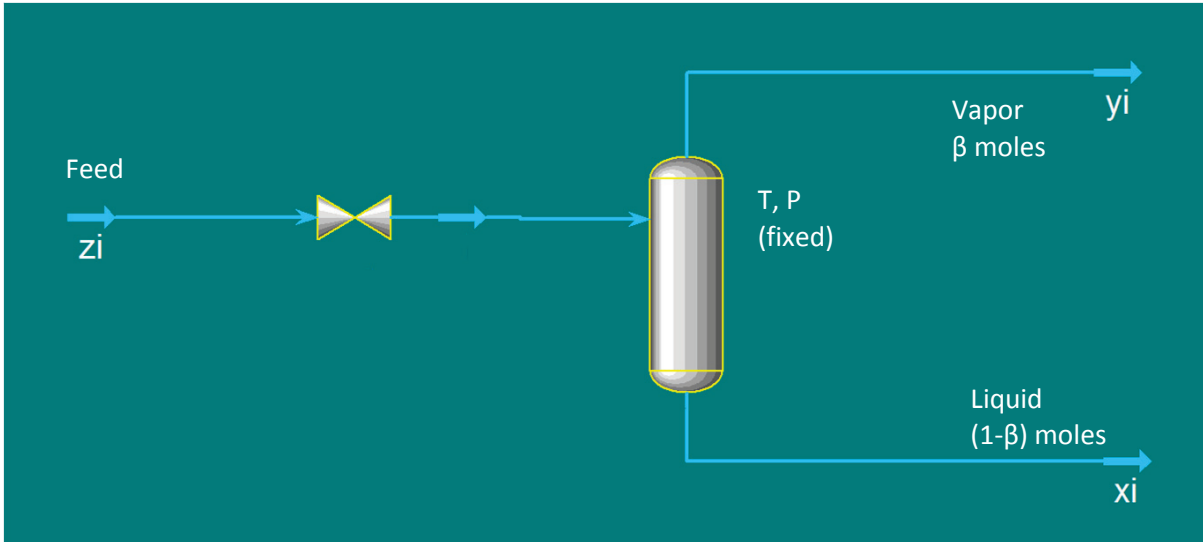


Figure 3-2 Schematic diagram of a VLE flash chamber, made in HYSYS

There are many possibilities for stating other properties instead of temperature and pressure, like PH-flash or PS-flash where the pressure, together with enthalpy and entropy are given, respectively. In figure 3-2 is such a flash process illustrated, where the feed stream consisting of  $N$  components. With the given composition  $z_i$ , where the subscript  $i$  indicates the different components, ( $i = 1, 2, 3, \dots, N$ ). Initially the feed stream is a single phase mixture, which is expanded through the valve into the flash chamber where the temperature and pressure are fixed. The condition in the flash chamber leads to two or more phases, in figure 3-2 it is sketched a vapor phase and a liquid phase. With the notation  $y_i$  and  $x_i$  representing the respectively phase compositions, and  $\beta$  indicating the molar vapor phase fraction. It is assumed an equilibrium condition between the vapor and liquid phase.

#### 3.6.1 Two phase TP-flash

The procedure for determining if a mixture splits into two or more phases, at a given temperature and pressure, is called a stability analysis. The starting point of this stability analysis, is where the Gibbs energy function,  $G_0$ , would have the same value as if there was only one phase present.

$$G_0 = G(n_1, n_2, n_3, \dots, n_N) \quad (3.35)$$

Where  $n_i$  is indicating the number of moles of each component,  $i$ , in the mixture, and  $N$  is the total number of components present. Next, consider the situation when the mixture splits in two different phases ( $I$  and  $II$ ), with the respectively composition  $(n_1 - \varepsilon_1, n_2 - \varepsilon_2, n_3 - \varepsilon_3, \dots, n_N - \varepsilon_N)$  and



$(\varepsilon_1, \varepsilon_2, \varepsilon_3, \dots, \varepsilon_N)$ , where  $\varepsilon_i$  is the composition of the second phase. By applying a simplified Taylor series, the Gibbs energy of phase  $I$  can be estimated:

$$G_I = G_0 - \sum_{i=1}^N \varepsilon_i \left( \frac{\partial G_I}{\partial n_i} \right)_n \quad (3.36)$$

The Gibbs function in phase  $II$  is given by:

$$\Delta G_{II} = G(\varepsilon_1, \varepsilon_2, \varepsilon_3, \dots, \varepsilon_N) \quad (3.37)$$

Thus the change in the Gibbs energy, as a function of the chemical potential the different phases:

$$\Delta G = G_I + G_{II} - G_0 = \sum_{i=1}^N \varepsilon_i ((\mu_i)_{II} - (\mu_i)_0) = \varepsilon \sum_{i=1}^N y_i ((\mu_i)_{II} - (\mu_i)_0) \quad (3.38)$$

This term for the change in Gibbs energy can be expressed as a function of the fugacity coefficients, the procedure is shown in Appendix A2.1, and the result is presented beneath:

$$\frac{\Delta G}{\varepsilon RT} = \sum_{i=1}^N y_i (\ln y_i + \ln(\phi_i)_{II} - \ln z_i - \ln(\phi_i)_0) \quad (3.39)$$

Where the  $\varepsilon = \sum_{i=1}^N \varepsilon_i$ ,  $y_i$  is the mole fraction of component  $i$  in phase  $II$ , and  $z_i$  is the mole fraction of component  $i$  in the total mixture. If the difference between the Gibbs energy in phase  $I$  and  $II$  compared to the initial phase is greater, or equal to zero, for all the possible compositions of phase  $II$ , there exists only one phase. This stability criterion is shown mathematically by:

$$\sum_{i=1}^N y_i (\ln y_i + \ln(\phi_i)_{II} - \ln z_i - \ln(\phi_i)_0) \geq 0 \quad (3.40)$$

The minimum value of the left hand expression, will be a stationary point, in Appendix A2.2 it is shown how to initiate the calculation. Together with the stability criterion, the material balance equation  $(\beta y_i + (1-\beta)x_i = z_i)$ , equilibrium equation  $(y_i \phi_i^V = x_i \phi_i^L)$  and the summation of mole fraction  $\left( \sum_{i=1}^N (y_i - x_i) = 0 \right)$  must be satisfied for two-phase equilibrium. The last three equations can be simplified by introducing the equilibrium ratio  $K_i = y_i/x_i$ , which gives the following expression for  $x_i$  and  $y_i$ :

$$x_i = z_i / (1 + \beta(K_i - 1)) \quad (3.41)$$

$$y_i = K_i x_i \quad (3.42)$$

And for  $K_i$ :

$$K_i = \phi_i^L / \phi_i^V \quad (3.43)$$

Substituting the expressions for  $x_i$ ,  $y_i$  in the equation for material balance, equilibrium and summation of mole fraction, results in the following equations

$$\ln K_i = \ln \phi_i^L - \ln \phi_i^V \quad (3.44)$$

$$(i = 1, 2, 3, \dots, N)$$

$$\sum_{i=1}^N (y_i - x_i) = \sum z_i (K_i - 1) / (1 + \beta (K_i - 1)) = 0 \quad (3.45)$$

Thus the numbers of equations are reduced, and with a given total composition, temperature and pressure all the parameters can be calculated. The  $K_i$  parameter are calculated from the stability criterion, while  $\beta$  are estimated from equation (3.45). This calculation procedure is presented as a flow sheet in figure 3-3 beneath.

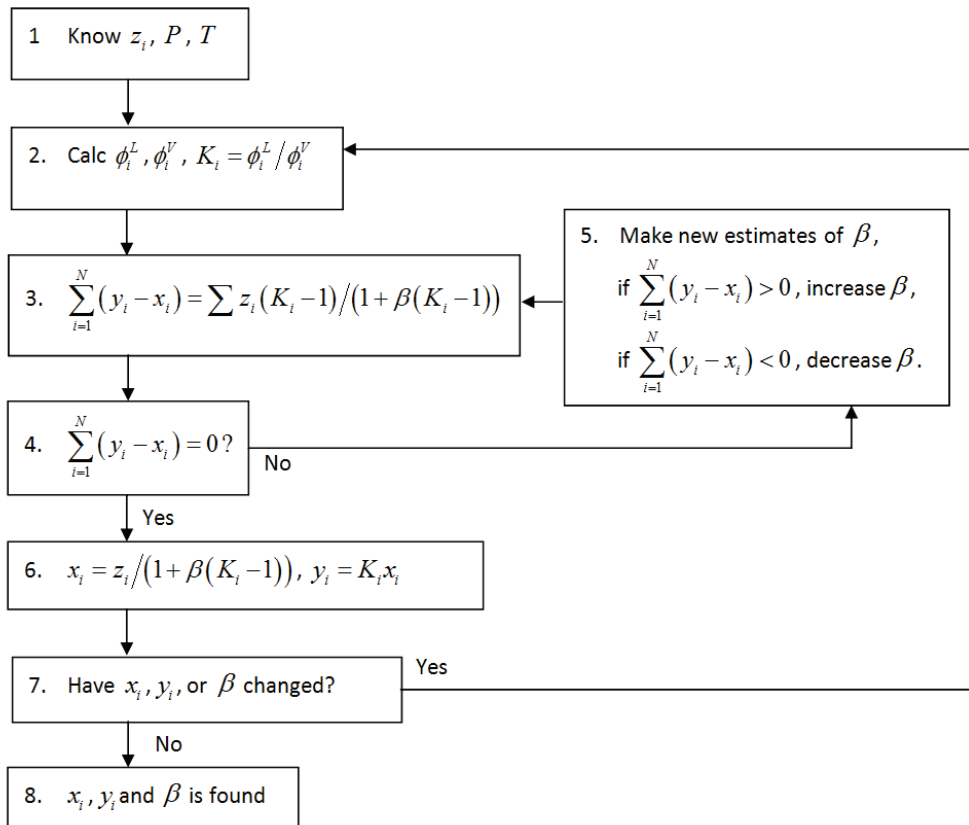


Figure 3-3 Flow sheet of the TP-flash calculation procedure [24]

After the parameters in step number 2 are calculated, by using a stationary point to initiate the calculation (see Appendix A2.2), the  $\beta$  parameter are adjusted to correspond the govern equations, in step number 3 to 5. This is repeated until equation (3.45) are fulfilled, and the vapor and liquid molar fraction parameters are recalculated by applying equation (3.41) and (3.42). This calculation procedure is continued until the solution converges. Thus the  $x_i$ ,  $y_i$  and  $\beta$  have stayed constant during an iteration loop, and the parameters are determined.

### 3.6.2 Multiphase TPflash

By performing a stability analysis on the phases determined in the TP-flash procedure can indicate if the system consists of even more phases. If the stability analysis shows that one or both phases are unstable it is an indication of more than two phases exists. And if this is the case, a three phase TP-flash can be carried out. Similar, if a stability analysis of each of the phases any of the phases present are unstable, a four phase TP-flash can be accomplished. This procedure is completed when all the phases present are stable.

The similar equation of (3.45) for a system consisting of  $J$  phases is expressed by:

$$\sum_{i=1}^N z_i (K_{im} - 1) / H_i = 0 \quad (3.46)$$

$$(m = 1, 2, 3, \dots, J - 1)$$

Where  $K_{im}$  is the ratio of the mole fraction of component  $i$  in phase  $m$ , and the term for the  $H_i$  parameter is:

$$H_i = 1 + \sum_{m=1}^{J-1} \beta_m (K_{im} - 1) \quad (3.47)$$

Similar as for the two-phase TP-flash, are  $\beta_m$  the molar fraction of phase  $m$ . The initial  $K$ -values are determined by the previously preformed stability analysis, for example in the three-phase TP-flash calculations are  $K$ -values from the two-phase TP-flash used. And the  $\beta_m$ -values are calculated by applying a Newton-Raphson iteration method of the equations (3.46) and (3.47). Next, the phase compositions are determined from:

$$y_{im} = z_i K_{im} / H_i \quad (3.48)$$

$$(m = 1, 2, 3, \dots, J - 1)$$

$$y_{iJ} = z_i / H_i \quad (3.49)$$

Where the  $y_{im}$  and  $y_{iJ}$  are, respectively the mole fraction of component  $i$  in phase  $m$  and the mole fraction of  $i$  in phase  $J$ . And by using an equation of state correlation the various fugacity coefficients can be determined, employing the Soave-Redlich-Kwong equation of state the fugacity coefficient is calculated by:

$$\ln \phi_i = (b_i/b)(Z - 1) - \ln Z + \ln [V/(V - b)]$$

$$+ a/bRT \left[ b_i/b - 2 \sum_j z_j (1 - k_{ij}) (a_i a_j)^{0.5} / a \right] \ln [(V + b)/V] \quad (3.50)$$

The different equation of state parameters is described in Chapter 3.4.3. Considering the  $K$ -values it is used an analogue equation of the term presented in (3.44). A problem related to multiphase systems is that a number of these solutions do not converge; the reason for this is the Newton-Raphson method is not suitable for these difficult systems [6].

### 3.6.3 Algorithm for freezing point predictions

The procedure described beneath are applied in multiphase calculations based on composition independent fugacity coefficients, which means that the solid phase present consists of a pure component. This solid forming component has the capability of distributing itself in the fluid phases but the solid phase can only consist of a pure component. The algorithm is based on the method described by Michelsen and Mollerup [6], and the study of the algorithm carried through by Rydberg [25] have been useful in this relation.

The freezing point temperature algorithm is described beneath:

- 1 Initiate the computation with a mixture of known composition, temperature guess and pressure.
- 2 Create a hypothetical solid phase with same composition as the system.
- 3 Determine the fugacity coefficients of the different components in the fluid phases, by solving a TP-flash with an implemented EOS and mixing rules.
- 4 Determine the fugacity coefficient  $\phi_i^{solid}$  for the component under investigation in the hypothetical solid phase using the following equation:

$$\phi_i^{solid} = \frac{P_{sub}}{P_{system}} \phi_i^{P_{subvapor}} e^{\left( V_i^{Solid} \frac{(P - P_i^{SatSolid})}{RT} \right)} \quad (3.51)$$

- 5 Next, calculate the fugacity ratio of the each component in the hypothetical solid phase and the fugacity of the fluid phase.

$$\text{fugacity ratio} = \frac{f_i^{solid}}{f_i^k} \quad (3.52)$$

- 6 The freezing point temperature is determined indirectly from equation (3.52); the temperature which gives a fugacity ratio equal to 1, is the freezing point temperature for the component under investigation.

This algorithm is then solved again for the system, now including a real solid phase. Resulting in a new composition, the stability analysis performed (in step 3) will confirm if the system is at a global minimum of Gibbs energy. And if the fugacity ratio is less than 1, the solid phase is not formed and the component is treated as a fluid phase component.

Equation (3.52) is deduced from the governing equation (3.13) and the expression presented beneath:

$$\beta_{solid} = z_i - \sum_{k=1}^F \beta_k \frac{\phi_i^{solid}}{\phi_i^k} \quad (3.53)$$

Where  $\beta_k$  and  $\beta_{solid}$  are the mole fraction of the total amount of component  $i$  in phase  $k$  and the solid mole fraction, respectively. As before is,  $z_i$  the total amount of  $i$  in phase the system.

Considering equation (3.53), if  $\beta_{solid} > 0$  is true, a solid phase is present. Thus the freezing point got to fulfill the criterion  $\beta_{solid} = 0$ , in which are the conditions the first solid forms.

By applying this freezing point criterion ( $\beta_{solid} = 0$ ) and the equations (3.14) and (3.15), it can be shown that in order to find the freezing point the fugacity ratio got to be equal to 1.

$$\beta_{solid} = z_i - \sum_{k=1}^F \beta_k \frac{\frac{f_i^{solid}}{P}}{\frac{f_i^k}{Px_i^k}} = z_i - \sum_{k=1}^F \beta_k x_i^k \frac{f_i^{solid}}{f_i^k} = 0 \quad (3.54)$$

For this statement to be true, the fugacity of the fluid phases has to be equal to the fugacity of the solid phase, thus the total amount of component  $i$  will be equal to the sum of fraction of all the fluid phases.

The iteration procedure starts at the triple point or a guessed temperature until the equation above are satisfied, due to the fact that the triple point are the highest temperature solids will form. And the outcome of the procedure is temperatures at which the different components will freeze, but only the highest temperature is valid for the mixture, since a solid phase in the mixture will affect the physical properties of the mixture.

The use of this algorithm is further discussed in the NeqSim chapter, where this procedure has been implemented in a Java source code (chapter 4.1.1.1).



## 4 Modeling solid precipitation in natural gas systems

The main challenge when modeling solid precipitation in natural gas systems; is the description of the solid phase in fluid mixtures. As presented in the previous chapter, regarding flash calculations and freezing point calculations, an EOS is typically used for describing the fluid phases. However, these PVT correlations lack the capability of describing the solid phase behavior, more specific the volumetric information of the solid phase. The most common method used is by calculating the fugacity of the solid phase on the basis of melting properties, and using an EOS for calculating the fluid phases.

For efficient calculation and precise prediction of the different thermodynamic values, in this case freezing point calculations, a proper equation of state model is required together with mixing rules. There are a number of equations to choose from, and different methods used to calculate the mixture properties. The following chapter gives a short introduction to the computer programs used to predict freeze out of different components in natural gas mixtures. The results from these calculations are presented in chapter 5.

### 4.1 NeqSim

The NeqSim program was developed by Even Solbraa as part of his Doctoral thesis [5], the object was to be able to simulate the most common processes in the petroleum industry. The simulation model is based on the work by Michelsen and Mollerup [6], which provided the tools to implement algorithms for modeling and calculating phase equilibrium. "This includes a methodology for efficient coding of procedures for calculating of thermodynamic properties, in particular when these properties are derived from an equation of state." [6] In other words, the methodology made it possible to build a thermodynamic library where it is easily to change or implement new thermodynamic models. The source code is programmed in Java, which is an object oriented programming language.

The programs source code is based on six modules, five of these modules are presented in figure 4-1, which shows the relations between the different modules and objects implemented.

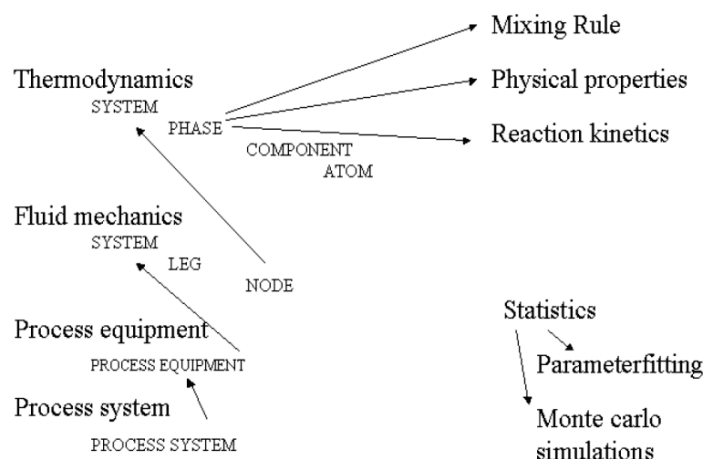


Figure 4-1 Object-oriented design of NeqSim [5]

The sixth module is the graphical user interface (GUI).

The program has a wide range of application and is suitable for producing useful results in many areas within the oil and gas business. Since the calculations related to this project are based on phase equilibrium, the focus is on the thermodynamic module. For more details about the structure and content of the thermodynamic module, and the phase and component objects, see appendix B1.

The thermodynamic system requires a set of input data to calculate the parameters of interest, an equation of state including mixing rules have to be chosen, in addition specify the temperature, pressure and composition. Next the system will be resolved, and there are created a thermodynamic operational object for the specified system. The component object includes all the variables for each component in the mixture, and the data are taken from the thermodynamic library. The method used to reflect the specific variables, or combinations of variables, are determined by the choice of thermodynamic operations.

#### **4.1.1 Thermodynamic operations**

Within the thermodynamic module there are a number of thermodynamic models and algorithms implemented, and the most important calculation procedures are:

- Flash calculations (TP, PH, PS, ...)
- Multiphase flash calculations
- Freezing Point / hydrate calculations
- Dew/bubble point calculations

In addition, one can reproduce thermodynamic diagrams, calculations for reactive compounds, pH-calculations and thermodynamic properties of electrolytic systems. A short introduction to the relevant calculation procedures based on the methodology from Michelsen and Mollerup are presented in chapter 3.6. The most important thermodynamic operation related to this study is the freezing point temperature flash and the usage of this procedure are described beneath.

##### **4.1.1.1 Freezing point temperature flash**

The algorithm implemented in NeqSim is presented in chapter 3.6.3.

##### **LNGFreeze.java**

The calculation are started by specifying the equation of state, mixing rule, composition, temperature and pressure. The equations of states used relevant in this report are the Peng-Robinson and Soave-Redlich-Kwong, with the intentions to base the calculation on traditional, reliable, and well known models. In relation, the calculations are preceded with classical mixing rules for the same reasons.

Next, a hypothetical solid phase is created, where the composition of the solid phase is the same as the initial system. And a thermodynamic operation is called (FreezingPointTemperatureFlash.java), this operation will check if the component under investigation participates and calculate the freezing point temperature in the case of freeze outs in the system.



### FreezingPointTemperatureFlash.java

This algorithm is initiated by the system conditions and the preferred thermodynamic model including mixing rules selected in LNGfreez.java. The computation is an iteration process where the system, consisting of  $k$  components, is checked for any solid phases. In case of solid formation at the specified temperature and pressure, the result is presented in form of the components name and its triple point temperature, which is the highest temperature one can get freeze outs from.

If there is no solid phase detected, a new iteration procedure starts; iterating from the triple point until there is detected a solid phase. Where a TP-flash is initiated for the initial system and returns a value for the fugacity coefficient of the vapor and liquid phases. These values are compared to the solid fugacity coefficient, which are expressed by equation (3.51). This is presented schematic in the figure below:

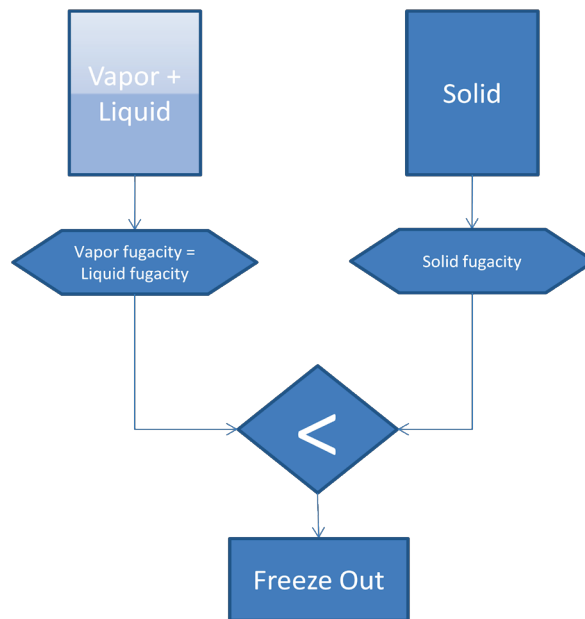


Figure 4-2 Fugacity handling in freezing point calculations

The expression for the solid phase is a quite simple expression, where the sublimation pressure at system temperature is expressed by the Clausius-Clapeyron equation:

$$\ln\left(\frac{P_{sub}}{P_{trp}}\right) = \left(\frac{\Delta H_{sub}}{R}\right) \left(\frac{1}{T_{trp}} - \frac{1}{T_{sys}}\right) \quad (4.1)$$

By using this equation it is guaranteed consistency in the triple point, where the vapor pressure curve and the sublimation curve meet, due to the possibility of using the triple point pressure of the vapor curve as a reference pressure at the triple point temperature. This expression contains three parameters which are based on experimental data and possible sources and of uncertainties for some components; this regards the triple point pressure, temperature and the enthalpy of sublimation. For carbon dioxide the values are well documented, but for the other components of interest; benzene and cyclohexane there are more deviations between the different experimental values. The values used are presented in table 4-1.

Component	Ref	Triple point temperature [K]	Triple point pressure [bars]	Enthalpy of Sublimation [K]/mole]
Carbon dioxide	NIST [26, 27]	216.58	5.185	[26.1-26.3]
Benzene	DIPPR [28]	278.7	0.0476	45.0
Benzene	NIST [27]	278.5 ± 0.6 <sup>(1)</sup>	-	[38.0-53.9 ± 0.8]
Cyclohexane	DIPPR [28]	279.7	0.0536	37.2
Cyclohexane	NIST [27]	279.7 ± 0.4 <sup>(2)</sup>	-	[27.6-46.6]

Table 4-1 Component properties used in phase equilibrium calculations

<sup>(1)</sup> Average of nine values

<sup>(2)</sup> Average of eight values

All these different phase properties are registered in the component library in addition to many others, and it is easy to change or update the values

However, the iteration process continues until the solid formation criterion ( $\beta_{solid} = 0$ ) is satisfied, or in other words until the fugacity ratio between the solid phase and an arbitrary fluid phase is equal to 1, as described by equation (3.52) and step 6 in the freezing point temperature algorithm. This is the temperature at which solids first will form. The result is then displayed, including the different phase fractions and compositions.

## 4.2 GPA

The GPA program is developed as part of the research program the Gas Process Association conducted in the study of solubility of hydrocarbons in cryogenic LNG and NGL mixtures [14], this study also involves the research reports RR 27 [29] and RR 33 [30]; including measuring the necessary data and to develop a model for predicting freeze out of components in natural gas processes. The work is mainly done by Professors Kohn and Luks, which also have published some of the experimental work examined later.

The examined version of the program is GPA 2.0 which was published in 1982 and developed by Kraemer Luks. The program is designed to analyze the feed composition of a natural gas stream and determine if there are possibilities for precipitates at the given temperature, in addition to return the highest temperature at which crystals appear. The input data is the composition of the natural gas mixture, and the temperature of interest. In contrast to other simulation tools, where the system pressure also is a crucial input parameter, but as showed later the pressure is suppressed from the governing equations in the source code. The program can handle feed stream mixtures consisting of a high number of components; N<sub>2</sub>, CH<sub>4</sub>, C<sub>2</sub>H<sub>6</sub>, C<sub>3</sub>H<sub>8</sub>, n-C<sub>4</sub>H<sub>10</sub>, i-C<sub>4</sub>H<sub>10</sub>, n-C<sub>5</sub>H<sub>12</sub>, i-C<sub>5</sub>H<sub>12</sub>, n-hexane, n-heptane, n-octane, n-nonane, n-dacane, benzene, cyclohexane, and CO<sub>2</sub>. However, since the solubility limits of these hydrocarbons solids are generally very low in methane rich mixtures, the focus of experimental and modeling work have been low concentrations of the heavy hydrocarbons.

As indicated there is two different calculation modes; one temperature specified calculation where the SLV equilibrium are computed and determined which component present have sufficient amount to crystallize. The other method calculates the highest temperature at which crystals will appear. In both situations are the bubble point pressure calculated and the different liquid and vapor phase compositions, in addition it is indicated which component that will precipitate. The two calculations can be run separately or simultaneous, depending of the user. The computation of the mentioned parameters is a type of bubble point calculation based on the liquid phase composition and the temperature. This calculation procedure applies the Chueh-Prausnitz version of the Redlich-Kwong equation of state for the gas phase, and the liquid phase activity coefficients are described by a Scatchard-Hildebrand version.

### 4.2.1 The thermodynamic problem

In the User's Guide developed by Keeler [31], the equations used in the computations are described in details, an outtake is presented in section B2 in the appendix; based on the User's Guide and GPAs research report RR 22 [14]. The method used represents another computation method in contrast to the equation of state method described earlier; the calculations are based on binary and ternary activity coefficient model and the parameters are fitted to the early experimental work associated with the GPA. The governing equations are presented beneath:

$$\begin{aligned}\mu_{is}(T, P) &= \mu_{il}(T, P, x_k), \\ i &= 1, 2, \dots, n\end{aligned}\tag{4.2}$$

Here are  $i = 1, 2, \dots, n$  referring to the solutes in the mixture, and the precipitations are assumed to consist of a pure component in the solid phase. This equation states that the chemical potential of the solid component at the given pressure and temperature equals the chemical potential in the liquid phase with the calculated composition and given temperature and pressure, in which leads to

the equilibrium restrictions of the solid phase are only dependent of the liquid phase conditions. Hence, freeze out calculations from the vapor phase cannot be performed.

$$\begin{aligned} \mu_{kl}(T, P, x_k) &= \mu_{kg}(T, P, y_k), \\ k &= 1, 2, \dots, m+n \end{aligned} \tag{4.3}$$

Here are  $k = 1, 2, \dots, m+n$  referring to both the solutes ( $n$ ) and the solvents ( $m$ ). When the composition of the solvents ( $m$ ) in the liquid phase is given in addition to the temperature, the problem will be completely defined.

Further on, they are suppressing the pressure dependency from equation (4.2) which allows equation (4.2) to be solved independently from equation (4.3). Thus the two equilibrium restrictions can be solved by first employing equation (4.2), where the liquid composition  $x_k$  are calculated and then get the vapor phase composition  $y_k$  and pressure  $P$  as an result of solving equation (4.3) with an bubble point calculation.

Assuming a pressure independency is reasonable, since the algorithm only predicts freezing point temperatures from the liquid phase. However, the model is based on the definition of excess Gibbs energy and thus the activity coefficients empirical correlations are tuned to give results which have a good agreement with experimental data. Some of the experimental sources used in this study are from Luks et al. early work. It is also recognized by Luks that the freezing point predictions did not account for the phenomenon of super-cooling. But since the model's use is related to the design issues in natural gas processing it is accepted with an over prediction of the freezing temperature. The main goal of developing this simulation tool was to get useful predictions for realistic natural gas streams due to the problem of a limited database of experimental work.

## 4.3 HYSYS

*“HYSYS is a process simulation environment designed to serve many processing industries especially Oil & Gas and Refining. With HYSYS you can create rigorous steady state and dynamic models for plant design, performance monitoring, troubleshooting, operational improvement, business planning, and asset management. Through the completely interactive HYSYS interface, you can easily manipulate process variables and unit operation topology, as well as fully customize your simulation using its customization and extensibility capabilities.” [32]*

### 4.3.1 CO<sub>2</sub> Freeze out Utility

*“An equation-of-state based approach is used to calculate the incipient solid formation point for mixtures containing Carbon Dioxide (CO<sub>2</sub>). The model can be used for predicting the initial solid formation point in equilibrium with either vapors or liquids. The fugacity of the resultant solid is obtained from the known vapor pressure of solid CO<sub>2</sub>. The fugacity of the corresponding phase (in equilibrium with the solid) is calculated from the equation of state.*

*CO<sub>2</sub> Solids prediction is restricted to the Peng Robinson (PR) and Soave Redlich Kwong (SRK) equations of state.” [32]*

Since this is a commercial simulation program, it is difficult to obtain detailed information about the calculation procedure of the fugacity of the solid phase and the data used for carbon dioxide. The information gathered is from the Aspen Plus 11.1 User Guide [32].

#### 4.4 Discussion of the simulations models

As described the NeqSim simulator have a various numbers of thermodynamic models implemented, while the HYSYS simulator offers the traditional Peng-Robinson and Soave-Redlich-Kwong equations of state. It is also recognized from previously work, that these equations of state are widely used for describing the fluid phases in solid-fluid equilibrium calculations and the prediction of freezing point temperatures, and are representing a more general correlation of phase equilibrium calculations when combined with equation (3.51) for description of the solid phase.

NeqSim represent a flexible environment which are well suited for testing and validation of such methods; in form of the advantage by programming in the object oriented language Java, and the methods of Michelsen and Mollerup which made it possible to build a thermodynamic library where thermodynamic models easily can be changed or implemented. Considering HYSYS which is a major commercial process simulator, in contrast to NeqSim which is an open source development, the level of complexity is much lower in NeqSim.

These two simulators represent the equation of state method of calculating the solid-liquid equilibrium, in contrasts to the GPA simulator which are based on empirical correlated activity coefficients, where the parameters have been fitted to the experimental data available. This involves a crucial dependency on experimental data, and the model may not be able to predict freezing conditions of system outside the experimental database. The model has previously demonstrated that the performance is higher at low temperatures and low solute concentrations, due to the correlations mentioned above. However, the purpose with this model developing was to predict for realistic natural gas streams where little or no data exists, and the parameters are to some limit based on interpolations and extrapolations. In many ways is the model representing great limitations, including the pressure independency and the fact that it only can describe freezing conditions in the liquid phase.

However, the interaction parameters in the equation of state model have to be determined, and this is done by parameter fitting to the experimental data. In addition are the expression which describes the solid phase fugacities, dependent on experimental component data, as the enthalpy of sublimation, and the triple point condition, for the carbon dioxide component the experimental values are well documented, hence the model are able to predict temperatures both for freeze out from vapor and liquid phases. The need of experimental data in these models is still crucial for the accuracy of the predictions, but the amount of data needed in the equation of stat model is still smaller than the amount needed to correlate the activity coefficient based model (GPA).

Regarding the binary methane rich systems including heavier hydrocarbon are the experimental documentation more scarcely, and the component properties more uncertain (referring to table 4-1), which introduces a higher uncertainty when predicting the freezing point temperatures. The optimization of these values is a relevant area of further research.

## 5 Experimental equilibrium data from literature and model evaluation

The experimental studies on the subject of phase equilibrium including a solid phase in light hydrocarbon systems were mainly done between the 50th-70th decades. However, the current understanding of solid-fluid equilibrium in hydrocarbon dominant mixtures is limited to a number of binary and ternary systems. A selection of these experimental sources are further investigated and evaluated, exclusively the binary systems including methane as the dominant component. The most important selection criterion for this type of experimental data, are the concentration of the solute component, in which should represent the concentration in real natural gas. Thus it has been focused on low solute concentration, especially of the critical hydrocarbons in methane binary mixtures.

The experimental data evaluated in this study are presented in table 5-1 and 5-2, and this forms the foundation of the investigation related to the accuracy and behavior of the different simulation tools, in which represent different thermodynamic models.

As stated earlier, this study focuses on the following three components; carbon dioxide (CO<sub>2</sub>), benzene (C<sub>6</sub>H<sub>6</sub>) and cyclohexane (C<sub>6</sub>H<sub>12</sub>). However, the amount of experimental data on methane rich binary mixtures including benzene and cyclohexane are scarce compared to the studies including carbon dioxide. Hence, it was only discovered one experimental article concerning the freeze out of hydrocarbons from vapor phase, refereeing to Rijkers [18] study.

Table 5-1 includes the sources of experimental data regarding solid formation of the selected components in liquid methane.

Comp. Y	Ref.	Mole fraction		Temp [K]		Press [bars]		NP	Author	Exp. Meth.
		Min	Max	Min	Max	Min	Max			
CO2	[1]	0.0016	0.90	129.6	214.16	3.57	48.18	20	Kurata	Spec
CO2	[13]	0.0016	0.205	129.65	201.26	3.62	48.18	11	Davis	Spec/SynVis
CO2	[33]	0.0003	0.126	110.7	194.6	-	-	9	Cheung	Spec
Benzene	[34]	3.9E-7	0.0014	99.4	199.8	-	-	38	Kurata	Spec
Benzene	[19]	6E-6	4.83E-4	103.8	185.4	-	-	12	Neumann	-
Benzene	[17]	0.00011	0.9815	165	277.7	10.13	172.25	23	Luks	SynVis/Syn-Mass
Benzene	[18]	0.08	1.00	264.59	278.45	5E-4	5.39	15	Rijkers	SynVis/Syn-Mass
Cyclo-hexane	[35]	0.0031	1.00	154	279.83	9.42	75.99	38	Kohn	SynVis/Syn-Mass

Table 5-1 Solid-Liquid experiments: Y solubility in liquid Methane (binary systems)

Table 5-2 present the experimental data evaluated in relation with solid formation of the components in gaseous methane.

Comp. Y	Ref	Mole fraction		Temp [K]		Press [bars]		NP	Author	Exp. Meth.
		Min	Max	Min	Max	Min	Max			
CO2	[36]	0.0012	0.1067	137.5	198.1	1.72	27.85	42	Agrawal	SynVis
CO2	[37]	0.01	0.0293	168.6	187.7	9.62	30.08	55	Le	SynVis
CO2	[13]	0.0012	0.1173	140.93	205.7	6.85	48.39	8	Davis	Spec
Benzene	[18]	0.080	0.236	264.95	266.30	4.2	5.39	4	Rijkers	SynVis/SynMass

Table 5-2 Solid-Vapor experiments: Y solubility in methane (binary systems)

All the pressure and temperature conversions of the experimental data are based on factors from Perrys’s Chemical Engineers Handbook [21].

For information about the experimental data gathered, table 5-1 and 5-2 are presenting the composition, temperature and pressure range for the experimental data and the total number of data points. As mentioned, the sources of highest interest are low concentration data of the critical components, due to the natural gas composition. There are some points that have been rejected, due to difficult data points where the computation fails to describe the phase behavior. This will be stated later on, and discussed thoroughly. The different experimental methods used in the research are indicated on the right hand side in the table, further description and study of the experimental methods is presented in appendix C5.

The following chapters will investigate each of the mentioned components and discuss the different aspects related to the specific component, with respect to freeze out in natural gas systems. In addition there are some other interesting experimental sources, listed in appendix C6, which are not evaluated in this work; since these sources unfortunately were hard to acquire.

## 5.1 Thermodynamic models used in simulations

The method by using a cubic equation of state are evaluated by others as an promising correlation tool for freezing point predictions in natural gas systems, including a variety of different processes within the oil and gas industry. However, there are still some challenges related to this approach, among other factors, the proper mixing rule and values for the binary interactions parameters applied.

An advantage with this approach is that the framework provided can easily be extended to new situations; for example by changing the equation of state parameters, the area of application changes, from light gases to heavy liquids. The method represent a more generally correlation of the solid-fluid equilibrium in which are less dependent on experimental data. It is known that Peng-Robinson and Soave-Redlich-Kwong are highly capable of describing fluid phase equilibrium mixtures containing relatively non-polar components, hence natural gas and petroleum mixtures. The applicability in freezing point calculations has been shown elsewhere [2, 3, 10], where they provide results with sufficient accuracy. These equations of state are widely used in both academic environments as well as the industry, and without exceptions implemented in process design software, e.g. HYSYS.

In relation to this objective it is interesting to compare the two classical equations of state; Peng-Robinson and Soave-Redlich-Kwong, as done in table 5-3, where the predictions have been compared to the experimental data from Agrawal. This dataset consist of solubility of carbon dioxide solids in gaseous methane (SVE), and are evaluated later in chapter 5.2.1.4.

Simulation tool	Comp. Y	Ref	Author	PR		SRK		System	Appendix
				BIAS [K]	AAD [K]	BIAS [K]	AAD [K]		
NeqSim	CO2	[36]	Agrawal	0.59	1.57	0.67	1.60	SVE	C1.1
HYSYS	CO2	[36]	Agrawal	0.84	1.67	0.89	1.69	SVE	C1.2

Table 5-3 Comparison of EOS model used in different simulation tools to predict freezing point temperature in carbon dioxide – methane mixtures



From table 5-3, it is confirmed that both the equation of state predicts the freezing points with a satisfying degree of accuracy, but more importantly a similar degree of accuracy. It is also worth mentioning that the calculation done with the NeqSim simulator, in this section, is performed with classical mixing rules without the use of binary interaction parameters, which also is the situation for the calculations in HYSYS.

The GPA simulator is, as mentioned, an activity coefficient based model, and in this relation it is meaningless include the GPA model in the comparison of the simulation tools and the models used. For assuming the scope the equations of state models affects the calculation, in relation to the parameterization of the activity coefficients, is it necessary to carry through a more comprehensive study.

However, after Carter and Luks developed the GPA model they indicated that an equation of state model together with the solid description provided by equation (3.20) would provide a more general correlation of the freezing point predictions than the activity coefficient based method. In their latest work [16], they are using the Soave-Redlich-Kwong equation for calculating the fluid fugacities when they are studying the methane – carbon dioxide binary system.

In the study of Eggeman et al. [3] and ZareNezhad [10], a traditionally form of the Peng-Robinson equation of state was used for describing the fluid phases in the binary mixture of carbon dioxide in liquid methane. The result of their studies are presented and compared to the simulation tools used in this study in table 5-8, where the experimental reference data used are the GPA RR 10 [1].

For freezing point predictions of binary systems consisting of benzene, de Hemptine discussed the feasibility of basing the modeling in a similar manner, by employing the Peng-Robinson equation of state, and equation (3.20) for describing the solid fugacity. Further he recognized the use of a Huron-Vidal mixing rule would improve the description of the non-idealities of the benzene component compared to the classical mixing rule.

A decision is made to base the further calculations in NeqSim and HYSYS, on the Soave-Redlich-Kwong equation. Considering the results presented in table 5-3, the different equations performed with a similar accuracy. This correlation for the fluid phases are widely used to model to describe the fluid behavior in natural gas processing systems and central in the solid-fluid equilibrium research. Regarding the NeqSim simulations, the intension is to further investigate the scope of using binary interaction parameters in order to optimize the accuracy of the predictions, thus it is decided to use classical mixing rules with interaction parameters.

## 5.2 Comparison of experimental data and different simulation models

When analyzing the results, the emphasis is first of all, the accuracy of the results. Next, in which temperature interval the deviations are highest and if there are any conditions where the simulations fails to describe the system of interest. This is done with the intentions to investigate whether it is the experimental results or the calculation methods used which are causing deviations, and further discuss the reasons. The method used for comparison of predicted and experimental freezing points is average absolute deviation and BIAS, described beneath.

$$\text{AAD} = \text{average of ABS} (T_{\text{calc}} - T_{\text{exp}}) \quad (5.1)$$

$$\text{BIAS} = \text{average of} (T_{\text{calc}} - T_{\text{exp}})$$

Where a negative BIAS value indicates the calculated results predicts in average a lower freezing point temperature than the experimental dataset. For predictions where the BIAS and AAD values are equal, the entire predicted dataset are either, over or under predicting the freezing point temperatures. Regarding the accuracy of the predictions, there are both insecurity related to the experimental results and in the thermodynamic models, in form of component properties and the description of the vapor pressure.

The information presented in table 5-4 and 5-5, forms the foundation of the discussion in the next chapters. The table's shows an overview over the accuracy of the results generated regarding freezing point temperatures of the methane rich binary mixtures investigated. All the raw data are presented in table form in the appendix, and the column on the right hand side specify the appendix number.

Comp. Y	Ref	Author	NeqSim			GPA			HYSYS			App
			BIAS [K]	AAD [K]	NP	BIAS [K]	AAD [K]	NP	BIAS [K]	AAD [K]	NP	
CO2	[1]	Kurata	-0.71	1.38	20/20	0.21	1.21	20/20	-3.51	3.51	20/20	C2.1
CO2	[13]	Davis	-0.12	1.13	11/11	-0.71	1.10	11/11	-4.80	4.80	11/11	C2.2
CO2	[33]	Cheung	0.68	3.00	9/9	-0.51	2.07	9/9	-4.37	4.69	9/9	C2.3
Benzene	[34]	Kurata	-2.94	3.84	18/38	4.74	6.66	38/38				C3.1
Benzene	[19]	Neumann	0.23	3.52	7/12	5.18	5.18	12/12				C3.2
Benzene	[17]	Luks	-	-	-	-3.34	3.34	5/23				C3.3
Benzene	[18]	Rijkers	-	-	-	-	-	-				C3.4
Cyclohexane	[35]	Kohn	0.79	1.07	19/39	-1.28	1.68	15/39				C4.1

Table 5-4 Solid-Liquid experiments: Y solubility in liquid Methane (binary systems)

Comp. Y	Ref	Author	NeqSim			GPA			HYSYS			App
			BIAS [K]	AAD [K]	NP	BIAS [K]	AAD [K]	NP	BIAS [K]	AAD [K]	NP	
CO2	[36]	Agrawal	1.08	1.83	42/42	35.68	35.68	42/42	0.89	1.69	42/42	C2.4
CO2	[37]	Le	-0.25	2.10	55/55	-	-	-	-0.73	2.13	52/55	C2.5
CO2	[13]	Davis	1.17	1.84	8/8	16.38	16.38	8/8	1.29	1.92	8	C2.6
Benzene	[18]	Rijkers	-	-	-	-	-	-	-	-	-	-

Table 5-5 Solid-Vapor experiments: Y solubility in methane (binary systems)

As described earlier, the HYSYS model only is capable of predicting carbon dioxide freeze outs. However, it seems to predict crystallization from the vapor phase better than from the liquid phase, and may be caused by the use of mixing rules without interaction parameters; this is further discussed later. Opposite for the GPA activity coefficient based model, which only can predict freeze outs from the liquid phase; this is confirmed by the simulations done for the SVE systems.

### 5.2.1 Binary systems containing methane and carbon dioxide

The component which represents the highest risk of precipitation in natural gas systems is definitely carbon dioxide, both due to the high triple point and the concentrations of carbon dioxide in natural gas. Hence, it is regarded as a critical component in many cryogenic processes in the industry and there exist several studies concerning both freeze outs from vapor and liquid phase in binary mixtures with methane.

#### 5.2.1.1 Phase behavior

In order to handle and discuss both the experimental data and the results from the simulations it is necessary to have good understanding of the phase behavior for the mixtures under investigation. For the binary system consisting of carbon dioxide and methane, a qualitative phase diagram is presented in figure 5-1. From the Gibbs phase rule it is indicated that in a two phase binary system, the degrees of freedom is two; thus the two phase locus is shown by an area in the phase diagram. Similar are the degree of freedom one in a three-phase binary system, and the three-phase locus is indicated with a line in the phase diagram.

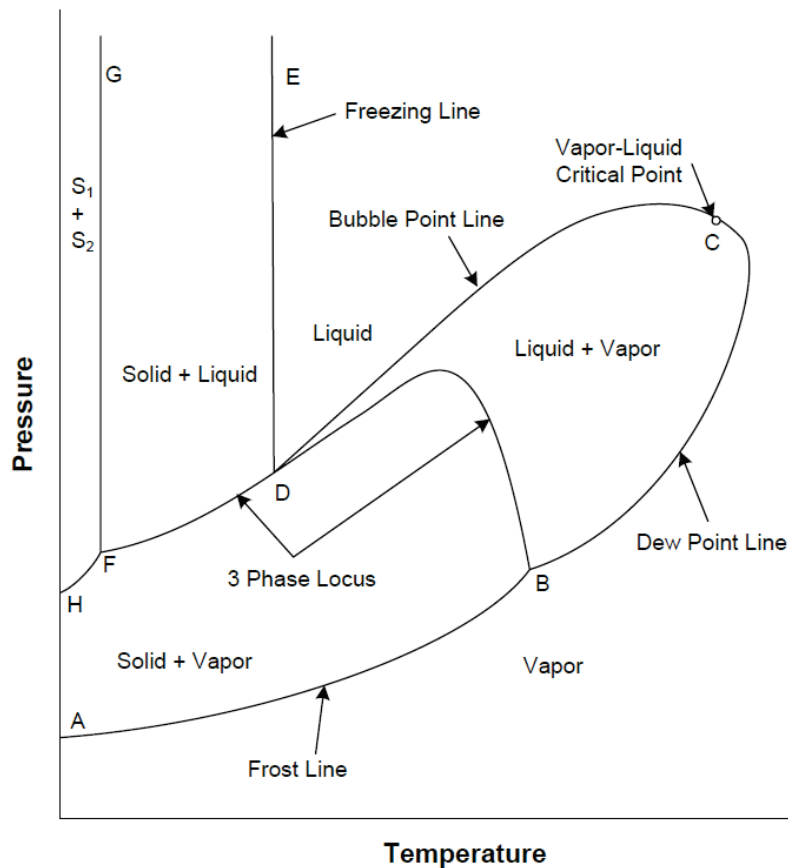


Figure 5-1 Qualitative Pressure-Temperature Diagram for the Methane-Carbon Dioxide Binary System [12]

There are two basic methods for precipitation of solid carbon dioxide in the methane binary system. First, when the carbon dioxide content in a liquid exceeds the solubility limit of the liquid phase, this is indicated by the freezing line (DE) in figure 5-1 and described by Solid-Liquid equilibrium. A phenomenon that can affect this precipitation method is super-cooling of the liquid phase, which occurs when the precipitation of the solute happens at a lower temperature than the true thermodynamic Solid-Liquid equilibrium point.

Next method of solid deposition is if the carbon dioxide content exceeds the solubility limit of the gas phase. Hence, the solid formation is described by the solid-vapor equilibrium, this is indicated by the frost line (AB) in the phase diagram.

Most of the experimental data gathered are based on three-phase experiments, where the solubility of carbon dioxide in the three-phase locus, indicated by the line (BDF). However, the lines FH and FG are also indicating three-phase lines, but at these conditions there will be a solid methane phase present, thus it is an irrelevant temperature area in the scope of natural gas processing.

Solid carbon dioxide formed between the three-phase locus (BDF) and the frost line (AB) will be dissolved in the liquid phase until the temperatures drops to below the freezing line (DE). The interesting areas regarding freeze out of carbon dioxide in natural gas system is at low carbon dioxide concentrations, and considering that the point (B) is the triple point for pure carbon dioxide and the point (F) is the triple point for pure methane, is the DF line the most interesting of the three-phase locus. A change in the overall composition will not affect these lines, BD and DF, due to degrees of freedom these are fixed in a pressure temperature diagram. However, the lines AB, BC, CD, DE, and point C will be affected by an overall change in composition.

### 5.2.1.2 Binary interaction parameter

When calculating the fluid mixture parameters, appropriate values for the binary interaction parameters should be selected. In table 5-6 and 5-7, the Soave-Redlich-Kwong equation of state is used to predict the freezing point, of carbon dioxide in binary mixtures with methane, for different interactions parameters, both for solid-liquid and solid-vapor equilibrium systems. The calculations in NeqSim are executed with classical mixing rules as stated in chapter 5.1, by applying equation (3.33) and (3.34).

Comp. Y	Ref	Author	$k_{ij} = 0.09$		$k_{ij} = 0.11$		$k_{ij} = 0.12$		$k_{ij} = 0.13$		$k_{ij} = 0.15$		Appendix
			BIAS [K]	AAD [K]	BIAS [K]	AAD [K]	BIAS [K]	AAD [K]	BIAS [K]	AAD [K]	BIAS [K]	AAD [K]	
CO2	[1]	Kurata	3.78	3.78	-1.69	1.93	-0.71	1.38	1.31	2.56	-	-	C2.7
CO2	[13]	Davis	-4.77	4.77	-1.55	2.01	-0.12	1.13	-	-	6.75	6.75	C2.8

Table 5-6 Comparison of interaction parameters used with SRK in NeqSim (SLE: CO<sub>2</sub>-CH<sub>4</sub> binary systems)

The Solid-Liquid equilibrium calculations are compared, with data from Kurata [1] and Davis [13]. These experimental source is considered as one of the most reliable experimental freezing points sources [10], for the system investigated. The sources are discussed more thoroughly in the next section.

Selection of the different binary interaction parameters are based on the trial and error method, and initiated with the existing value for the interaction parameter, gathered from the simulation program PVTsim® 13, where the vapor-liquid interaction parameter for the Soave-Redlich-Kwong equation have a value of 0.12. A difference of 0.03 was chosen, in order to investigate how this change would affect the freezing point predictions. The results are presented in figure 5-2, where it is recognized for solid-liquid equilibrium calculation, for a methane-carbon dioxide mixture, is optimal with an interaction parameter close to 0.12, which is the identical to the vapor-liquid equilibrium value.

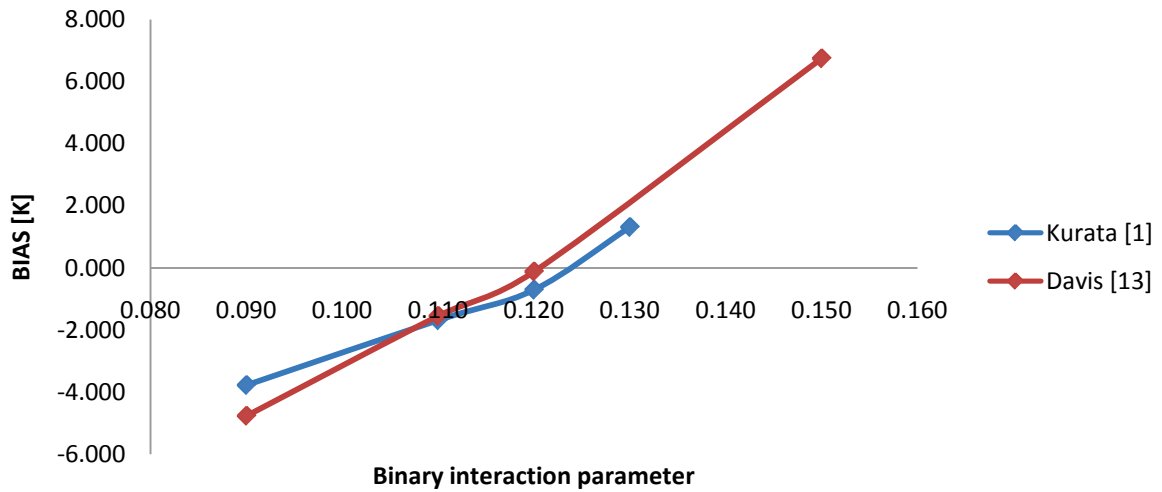


Figure 5-2 Binary interaction parameter dependency in NeqSim model (SLE: CO<sub>2</sub>-CH<sub>4</sub> binary systems)

Next, the same procedure was carried through for the solid-vapor equilibrium, presented in table 5-7. However, the selection of interaction parameters was extended, and calculations without interaction parameters was performed.

Comp. Y	Ref	Author	k <sub>ij</sub> =0		k <sub>ij</sub> =0.09		k <sub>ij</sub> =0.12		k <sub>ij</sub> =0.13		k <sub>ij</sub> =0.15		Appendix
			BIAS [K]	AAD [K]	BIAS [K]	AAD [K]	BIAS [K]	AAD [K]	BIAS [K]	AAD [K]	BIAS [K]	AAD [K]	
CO <sub>2</sub>	[13]	Davis	-0.09	2.10	1.17	1.84	1.54	2.00	-	-	2.14	2.48	C2.9
CO <sub>2</sub>	[36]	Agrawal	0.67	1.60	0.98	1.77	1.08	1.83	-	-	1.19	1.90	C2.10

Table 5-7 Comparison of interaction parameters used with SRK in NeqSim (VSE -binary systems)

For the methane-carbon dioxide solid-vapor equilibrium systems, the binary interaction parameter seems to have less affection on the freezing point predictions, compared to the solid-liquid system. In this case a parameter value zero seems to give the best results compared to experimental data from Agrawal and Davis. Considering the fact that the predictions with HYSYS are done without the use of interaction parameters; the results in table 5-4 and 5-5 are confirming this hypothesis, where the accuracy are better for SVE systems.

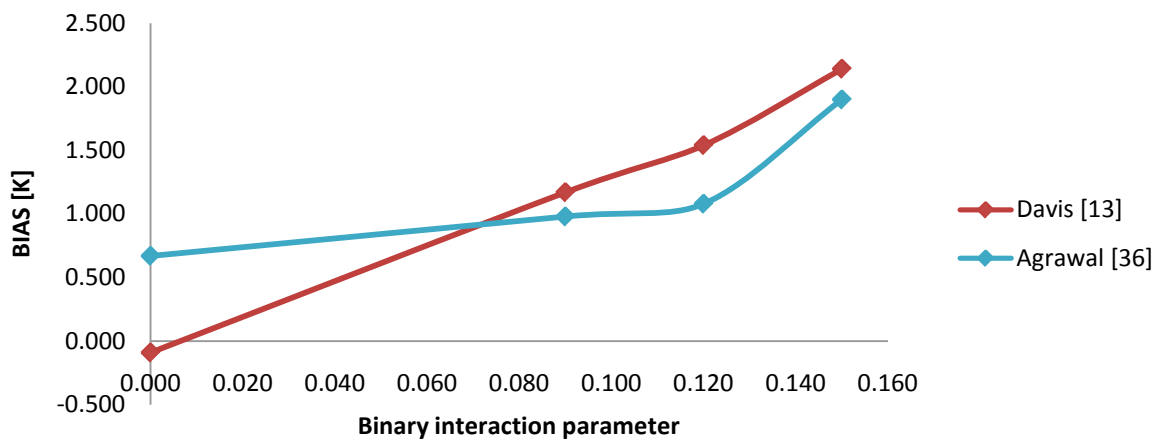


Figure 5-3 Binary interaction parameter dependency in NeqSim model (SVE: CO<sub>2</sub>-CH<sub>4</sub> binary systems)

However, the SVE systems seem to be less dependent of the binary interaction parameter compared to the SLE system. Hence, it is chosen to simplify the calculations procedure by executing further calculations with a parameter value of 0.12 for both the SLE and SVE systems.

This value can be compared with the study of ZareNezhad [10], where the Peng-Robinson equation of state was used for predicting the carbon dioxide freezing points for vapor and liquid mixtures of the methane-carbon dioxide binary system, and he introduced a semi-empirical temperature dependent  $k_{ij}$ . The results generated in his study are compared to different simulation tools including NeqSim, HYSYS and the GPA model in chapter 5.2.1.5, where the experimental data from Kurata [1] are used as a reference. However, this semi-empirical temperature dependent interaction parameter applied by ZareNezhad is presented beneath.

$$k_{ij} = -36.134 \frac{1}{T^2} + 5.4835 \frac{1}{T} + 0.09980 \quad (5.2)$$

This expression is used to calculate the binary interaction parameter for a temperature interval from 130 K to 210 K; the result is presented in figure 5-4.

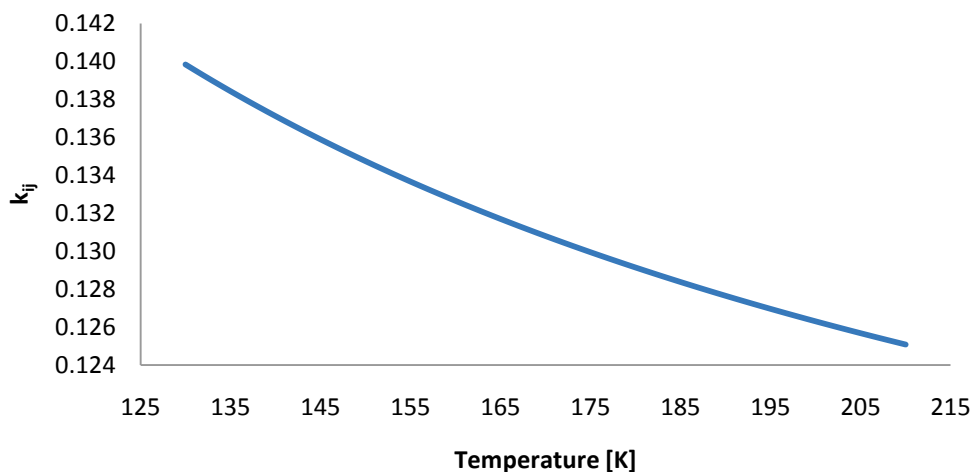


**Figure 5-4 Calculated binary interaction parameter in low temperature CO<sub>2</sub>-CH<sub>4</sub> binary mixture based on ZareNezhad's temperature dependent semi-empirical correlation [10]**

From the result presented in figure 5-4, it is reasonable to believe an interaction parameter of 0.12 is too low; however, it is hard to determine how the application of different equations of state affect the result, but it is known that these equations have quite the same values for the interaction parameters.

Note that NeqSim with the Soave-Redlich-Kwong equation of state, and classical mixing rules; uses a fixed binary interaction parameter, in contrast to ZareNezhad's semi-empirical temperature dependent interaction parameter. The interaction parameter used in other works [2, 3, 10, 16] are typically the fitted to experimental vapor-liquid equilibrium data. However, they also acknowledge the serious impact this value has on the predictions.

### 5.2.1.3 Solid-Liquid equilibrium for binary $CH_4$ and $CO_2$ systems

The experimental data used as references for the binary interaction parameter study for the solid-liquid system are the high quality experimental data from the work done by Kurata [1] and Davis [13]. These data are presented in the GPAs research report RR10 [1], which is a collection of experimental work on solubility of carbon dioxide in light hydrocarbons. This was published in 1974 by Dr. Fred Kurata, which got the task to present all available information about the solubility of carbon dioxide in light hydrocarbons in one publication, and it is regarded as one of the most reliable low temperature sources. The research report from GPA includes the low concentration solubility limits Davis et al. [13] produced, together with higher concentration data from Brewer & Kurata [38], and Donnelly & Katz [39]. Another collection of experimental data of the methane-carbon dioxide system is the presented in the work of Knapp et al., however, the publication where not available. Hence, the SLE calculation will be compared against the sources available, which constitute a comprehensive selection of experimental data. Cheung [33] have also produced quality experimental data of solubility of carbon dioxide in liquid hydrocarbons at cryogenic temperatures.

Figure 5-5 and 5-6 are presenting the experimental data gathered from the research report RR 10, including the data from Kurata [1] and Davis [13], and the simulations carried through with NeqSim, GPA and HYSYS. Regarding the accuracy of the NeqSim predictions compared to the whole dataset from Kurata, which consists of freezing point temperatures for carbon dioxide concentrations from 0.16 to 90 mole %, the consistency are quite decent; the predicted temperatures are overall a little lower than the experimental results, except for the carbon dioxide concentrations of 10-40 mole %. This results in an average deviation of -0.71 K, and an average absolute deviation of 1.38. The raw data, in which the BIAS and AAD are calculated from, are presented in the appendix; see table 5-4 and 5-5 for the section specification.

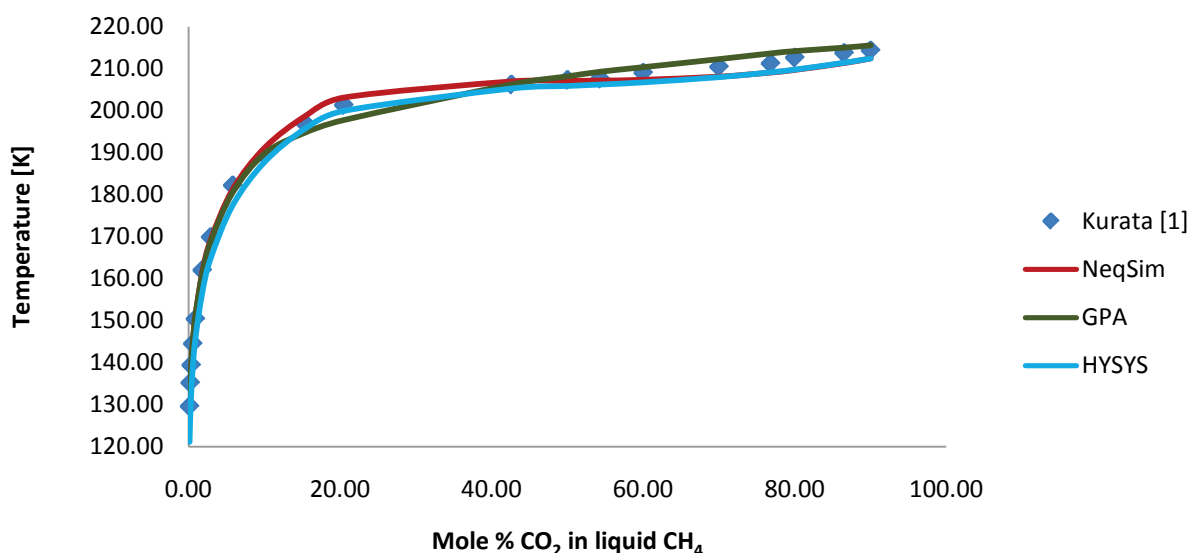


Figure 5-5 Solubility of  $CO_2$  in liquid  $CH_4$ : Predictions and experimental points from Kurata [1]

Considering the low concentration data from Davis, in which consists of concentrations from 0.16 to 20.5 mole % of carbon dioxide, presented in figure 5-6. As mentioned these experimental data are also included in the dataset from Kurata, presented in figure 5-5.

However, the NeqSim have a better consistency when only considering the low temperature points; the results were within an absolute average deviation of -1.13 K and a max absolute deviation of 1.82 K.

Regarding the activity coefficient based GPA model, it has a very good agreement to both the data from Kurata [1] and Davis [13], with an average absolute deviation calculated to 1.21 K and 1.10 K, respectively. Both the datasets are consistent in the whole temperature interval. The maximum absolute deviation of 3.56 K, when comparing to Kurata, is located at 201.3 K (sample number 10 in appendix C2.1). Similar to the results compared to Davis, this is also located in the same temperature area, more precisely at 197.74 K and has the value of 3.52 K.

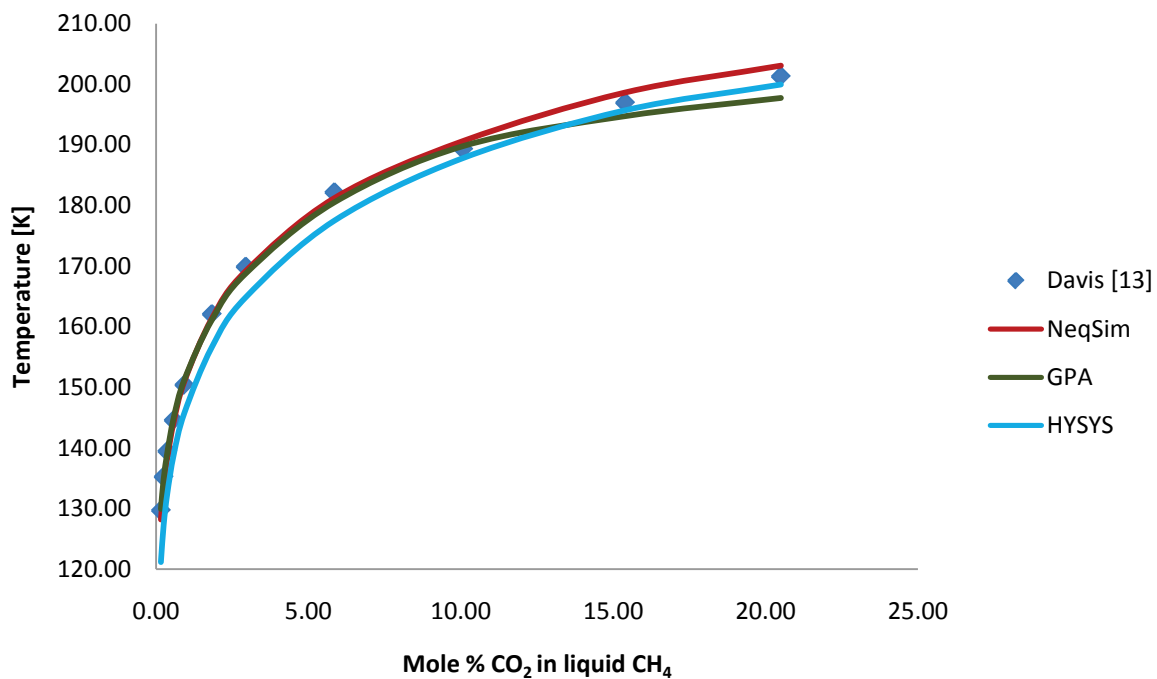


Figure 5-6 Solubility of CO<sub>2</sub> in liquid CH<sub>4</sub>: Predictions and experimental points from Davis [13]

The review of the HYSYS model regards to solubility of carbon dioxide in liquid methane shows slightly poorer results than the two other models. Compared to the experimental dataset from Kurata, the average absolute deviation is calculated to 3.51 K, and a maximum absolute deviation of 8.45 K. The deviation tends to increase in the low temperature area; from a temperature of 180 K to 130 K (referring to the sample numbers 13-20 in appendix C2.1) it predicts a temperature at least 4 K lower than the reference temperature, thus the large absolute deviation.



From figure 5-7 it is quite clear that the GPA calculation is the most precise, NeqSim predicts a higher temperature in average, while HYSYS is under predicting the freezing point temperatures. Especially in the upper temperature range, however, all the simulations give good results in the lower temperature range. Considering the average absolute deviation, the outcome is the same; GPA gives the best AAD of 2.07 K, while NeqSim and HYSYS gives respectively 3.00 K and 4.69 K.

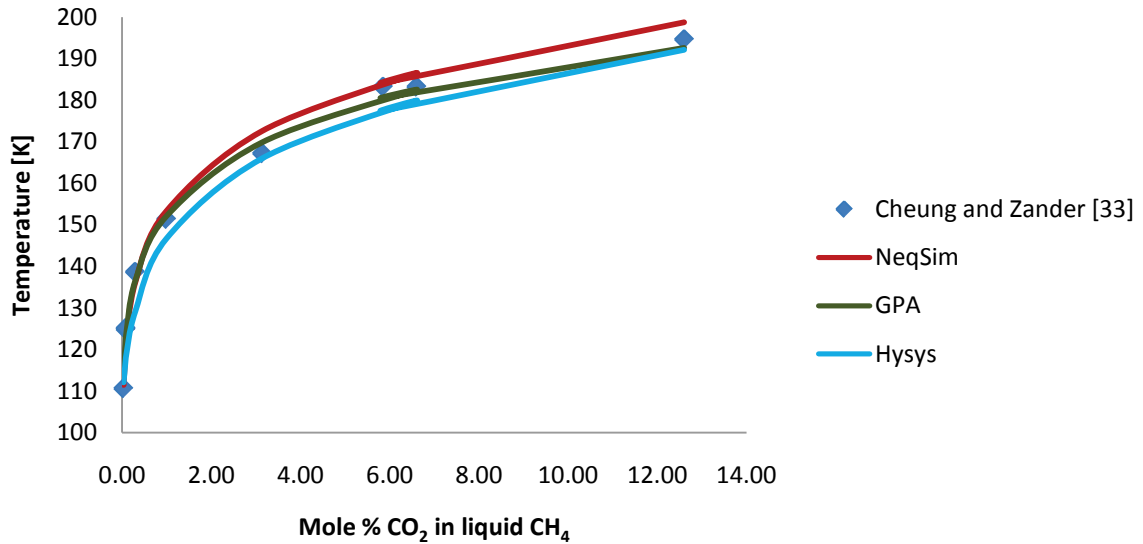


Figure 5-7 Solubility of CO<sub>2</sub> in liquid CH<sub>4</sub>: Predictions and experimental points from Cheung and Zander [33]

One observation made when studying the tabulated values, sample number 1 in appendix C2.3, which is hard to observe from the figure is that the maximum absolute deviation (3.65 K) in the results from GPA is at the lowest carbon dioxide content. At this condition, both NeqSim and HYSYS predict a temperature which is closer to the experimental point.

#### 5.2.1.4 Solid-Vapor equilibrium for binary CH<sub>4</sub> and CO<sub>2</sub> systems

For solid-vapor equilibrium (SVE) systems, it is harder to obtain experimental data; freeze out of carbon dioxide in SVE systems has not been studied as much as SLE systems. Pikaar [40] have in his work generated SVE data for the binary system consisting of methane-carbon dioxide, and is often cited in the literature. Pikaar used two different methods for producing experimental SVE data. However, there were discrepancies between the two datasets, especially for mixtures containing small amounts of carbon dioxide. Along with Pikaar, the work of Agrawal and Laverman [36] are the only significant work carried through related to SVE systems, there are also discrepancies between these datasets at high pressures. Since natural gas is normally processed at high pressures, Le et al. [37] in their work from 2007 attempted to verify the validity of these datasets. The data from the study of Le et al. had a better agreement with the datasets to Pikaar than the corresponding data sets to Agrawal and Laverman [36]. For freezing points study in vapor-solid systems has the sources of Agrawal, Le et al. and Davis been chosen.

Considering figure 5-8, both NeqSim and HYSYS calculate in general temperatures above the experimental points from Agrawal, except for the data series including a carbon dioxide content of 10.7 mole %. The dataset exists of methane-carbon dioxide compositions at different pressures, and has a carbon dioxide content of respectively (from right to left), 0.12%, 0.97%, 1.8%, 3.07% and 10.7%.

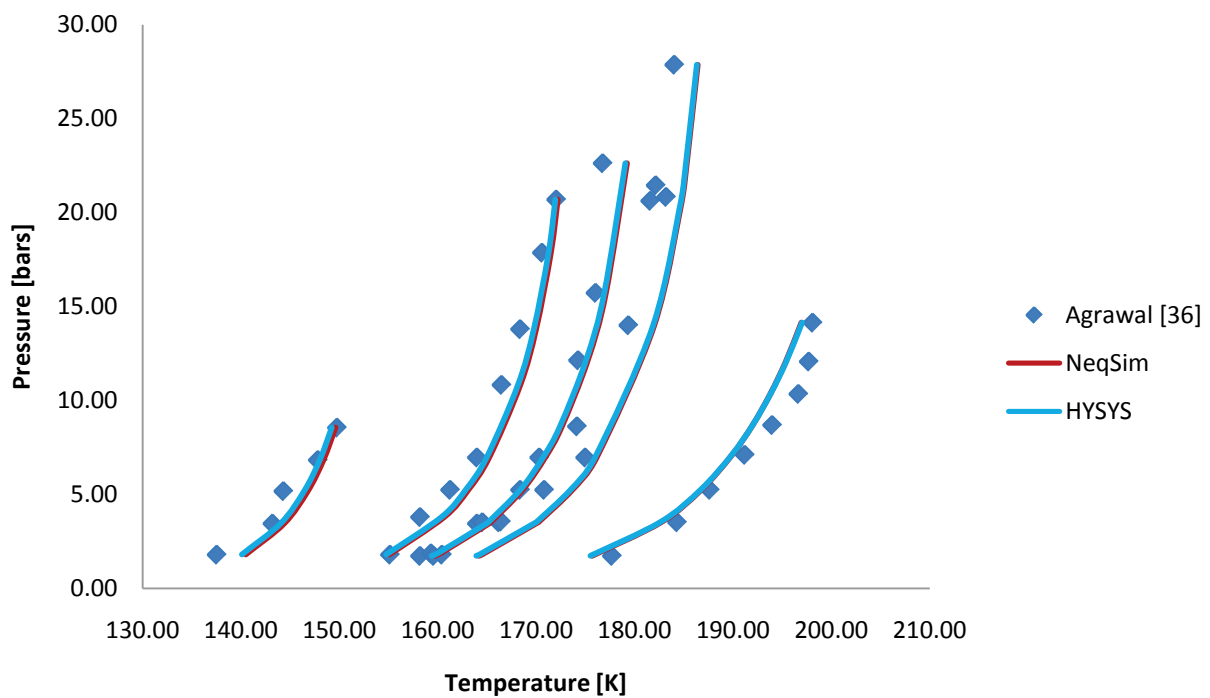


Figure 5-8 Solubility of CO<sub>2</sub> in CH<sub>4</sub>: Predictions and experimental points from Agrawal [36]

The two simulation tools predict more or less the same temperatures, thus the two curves are overlapping in the figure. However, the NeqSim results give an average absolute deviation of 1.83 K compared to the experimental points from Agrawal, and a max absolute deviation of 4.59 K. Similar are the predictions from the HYSYS simulator, which gives an average absolute deviation of 1.69 K and a max absolute average of 4.34 K.

However, it is worth mentioning that the data from Agrawal was used in the optimization of the binary interaction parameter in NeqSim, and the study showed better consistency to the experimental data with a binary interaction parameter equal to zero, presented in table 5-7. For the simplicity it has been decided to use a binary interaction parameter of 0.12, this is also based on the small widespread of average absolute deviation calculated for different interaction parameters in vapor-solid systems.

The experimental dataset from Le et al. includes freezing point temperatures for three different compositions of the binary mixture consisting of methane-carbon dioxide, respectively (from left to right in figure 5-9) with 1.0, 1.91 and 2.93 mole % carbon dioxide content.

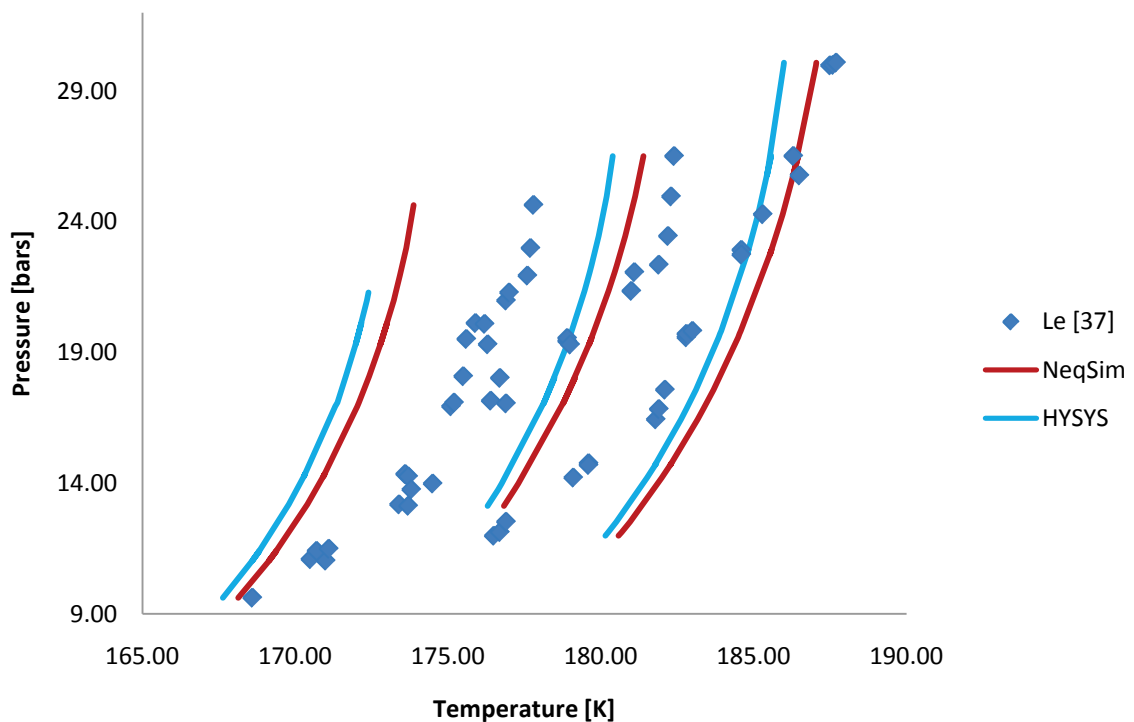
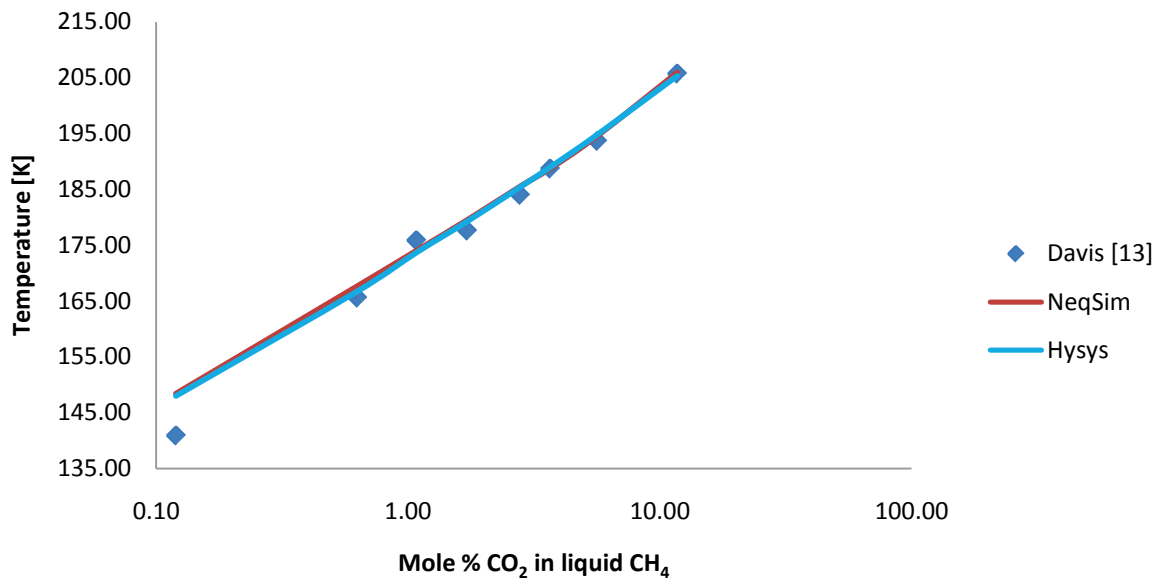


Figure 5-9 Solubility of CO<sub>2</sub> in CH<sub>4</sub>: Predictions and experimental points from Le et al. [37]

The agreement between predicted and experimental data from this dataset is about the same as the data from Agrawal. From studying figure 5-9 it looks like the deviation is much larger than the deviation in figure 5-8, but considering the different temperature intervals the result is more or less similar. The average absolute deviation calculated for the tree data sets are for NeqSim valued at 2.10 K, and a maximum absolute deviation of 4.18 K. As seen in figure 5-9 the data set with the largest deviation is for a carbon dioxide content of 1.0 mole %, the predicted values from NeqSim in with these conditions gives an average absolute deviation of 2.82 K and a maximum absolute deviation of 4.18 K.

Considering the result produced with HYSYS; the deviation are higher, compared to the NeqSim result, for the data set with 1 mole % carbon dioxide content. In addition HYSYS were unable to reproduce three high pressure data points in this data set, thus the highest pressure simulated with HYSYS in this data set was 21.29 bars. In the two other datasets, consisting of 1.91 and 2.93 mole % carbon dioxide content, are HYSYS predicting slightly more precise temperatures.

As mentioned, Davis carried through three-phase experiments where he sampled both the liquid and vapor phase, thus the similar figure as the liquid-solid studies where the axes represent temperature and carbon dioxide content.



**Figure 5-10 Solubility of CO<sub>2</sub> in CH<sub>4</sub>: Predictions and experimental points from Davis [13]**

As seen in figure 5-10, the two simulations overlap through the whole temperature interval, thus a more or less similar average absolute deviation. The NeqSim results achieved an average absolute deviation of 2.0 K, while HYSYS performed slightly better; AAD of 1.92 K. However, for a mixture consisting of 0.12 mole % carbon dioxide the deviations were more severe (referring to sample number 1 in appendix C2.6). The measured freezing conditions were at a temperature of 140.08 K and a pressure equal to 6.85 bars; both NeqSim and HYSYS fails to predict this temperature with the given carbon dioxide composition. Hence, a maximum absolute deviation of 7.48 K for the calculations with NeqSim, while the HYSYS prediction performed slightly better with a maximum absolute deviation of 7.12 K.

It is difficult to make any conclusions about the reliability of this data point, but from studying the results by Agrawal there is reasons to believe that this temperature should be higher. Agrawal measured several points with a carbon dioxide content of 0.12 mole %, and one point is measured with approximately the same pressure (6.83 bars), referring to sample number 4 in appendix C2.4. He measured the temperature to be 147.2 K, which is a more reasonable result compared to the predicted temperatures. This temperature difference from the two sources could be a result of different experimental methods, but without a comprehensive study of the possible sources of uncertainties and evaluating the experimental methods in more depth it is difficult to make any conclusions.

### 5.2.1.5 Other thermodynamic models for the binary carbon dioxide – methane system

The three simulation tools used in this study, respectively, NeqSim, GPA and the HYSYS simulator, is compared to predictions made by other simulation tools and models; in which are used in literature when discussing the accuracy of the thermodynamic modeling of freezing point predictions in natural gas systems. The experimental data used for comparison to all these simulation tools are the quality experimental data gathered in the GPA report RR 10 [1]. Except from the predictions done by Eggeman and ZareNezhad, where only the low composition data are considered; are all the experimental data used in the verification of the simulation tools. The raw data from this study are presented in the table C2.11 in the appendix, in addition to figure 5-11.

Simulation tool	Ref	BIAS	AAD	NP
NeqSim		-0.71	1.38	20/20
GPA	This work	0.21	1.21	20/20
HYSYS		-3.51	3.51	20/20
Eggeman	[3]	-0.08	0.62	11/20
ZareNezhad	[10]	-0.03	0.69	11/20
ProMax	[12]	-0.82	1.01	20/20
PROSIM	[12]	-1.55	2.67	20/20

Table 5-8 Accuracy of different simulation tools compared with GPA RR 10 [1]

Considering the quality of the predictions and the utility value, the GPA is the only who predicts an average freezing point temperature above the experimental value. This is an important quality when using the simulation tool in design of natural gas processes. However, it is necessary to have a safety margin when dealing with such design issues. The HYSYS simulator has the most inaccurate overall performance, where all the predictions are below the real freezing temperature. Opposite are the predictions by Eggeman and ZareNezhad the most precise, partially due to the number of data points included. But the use of semi-empirical temperature-dependent interaction parameter, in ZareNezhad’s study, introduces a considerable improvement. And similar, by applying an activity coefficient model based on the Non-Random-Two-Liquid (NRTL) theory in Eggeman’s study.

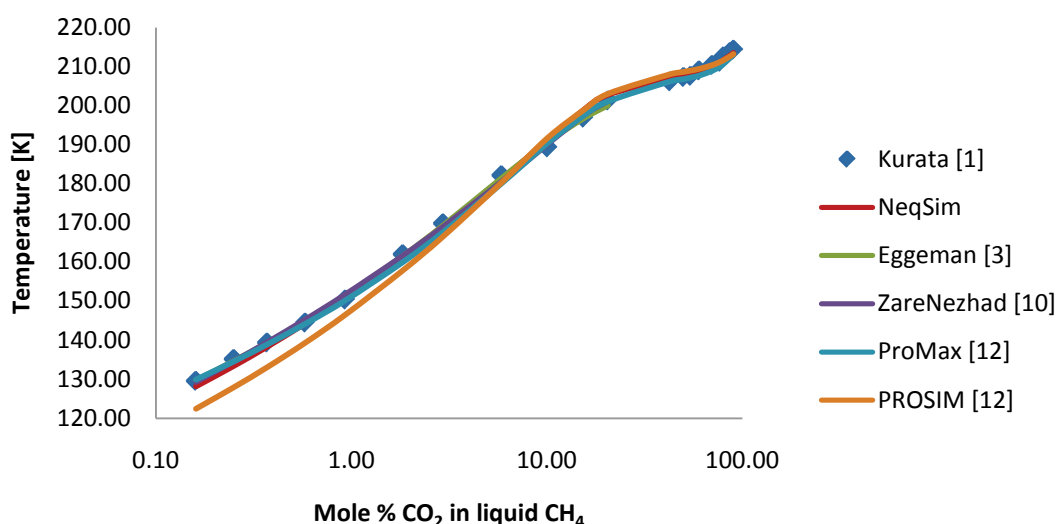


Figure 5-11 Solubility of CO<sub>2</sub> in liquid CH<sub>4</sub>: Predictions and experimental points from Kurata [1]

From figure 5-11, it can be concluded that the PROSIM predictions, from the study of Hlavinka [12], are the ones with the lowest accuracy in the low temperature interval, while all the others performs with sufficient deviation in this temperature interval.

## 5.2.2 Binary systems containing methane and heavy hydrocarbons

As mentioned in the introduction of this report, there is a risk of precipitation of heavy hydrocarbons in methane rich mixtures, mainly benzene and cyclohexane, due to their high triple point temperature. In de Hemptine's work [2] it is showed, when considering small concentration of the heavy component in binary mixtures with methane, that benzene have a higher freezing temperature compared to cyclohexane, based on experimental SLE data from Neumann [19].

### 5.2.2.1 Phase behavior

When investigating the experimental results and the simulated results it is important to fully understand the phase behavior of the mixture studied. Figure 5-12 is based on the work of Kohn and Luks [41], which have classified the SLV equilibrium in to four types of phase diagrams. The one which applies for the methane-benzene mixture is presented beneath.

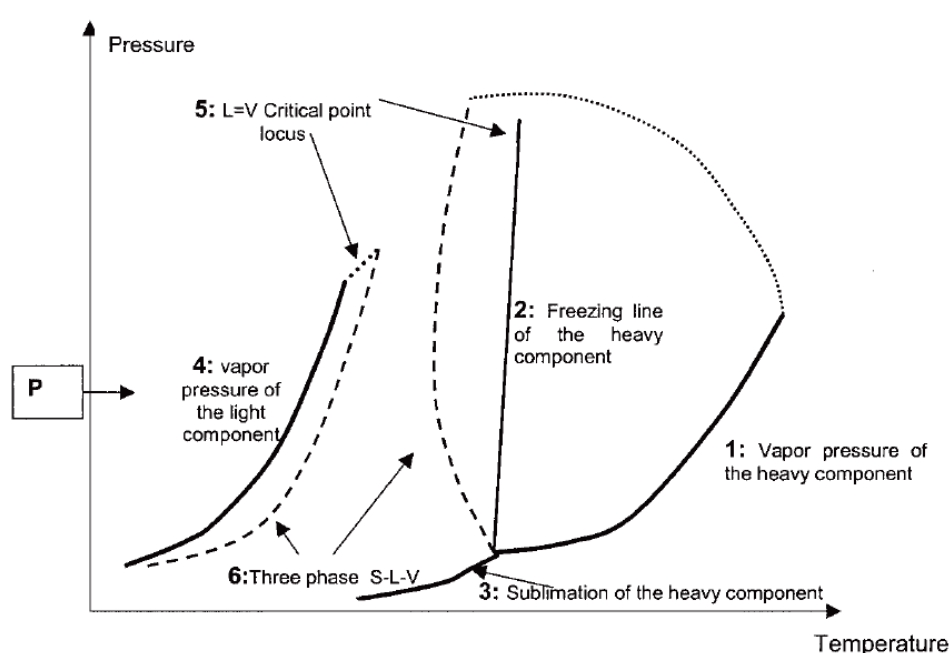


Figure 5-12 Sketch of the phase diagram for binary mixtures consisting of hydrocarbons [2]

From figure 5-12, the phase behavior of the heavy component is recognized on the right side of the diagram, where the vapor-liquid line (1), liquid-solid line (2) and vapor-solid line (3) of the heavy component is sketched. For the light component, in this case methane, it is only the vapor-liquid line (4) which is relevant when investigating freezing of heavy hydrocarbons. The stippled lines (6) represent the three phase solid-liquid-vapor equilibrium. And the critical points (5) are presented in the pressure-temperature diagram by dotted lines which connect the vapor pressure lines and the three phase locus of each component.

Description of the phase transitions in these binary mixtures of hydrocarbons is easier to understand when considering a temperature-composition diagram, presented in figure 5-13. The diagram is showing the different equilibrium conditions in a benzene-methane binary system at constant pressure, indicated in figure 5-12. The pressure applied is higher than both of the triple point pressures of the hydrocarbon components, and lower than the critical pressures. Regarding the composition of the mixture, the concentration is going from pure methane at the left hand side to pure benzene at the right. It is anticipated that the cyclohexane component will have a similar phase

behavior, except some small differences in temperature. Considering figure 5-13, the mixture will always be in a vapor phase at high temperatures (1). Lowering the temperature in benzene rich mixtures will result in a vapor-liquid equilibrium (2), the liquid phase created in this case will have a higher benzene concentration than the vapor phase. Thus mixtures with an even higher benzene concentration will fully condensate to liquid (3), and exposed to further cooling will result in freeze outs from the liquid (4). This liquid-solid equilibrium (4) represents the highest temperature condition at which a solid phase will occur.

Next phase transition is the high temperature solid-liquid-vapor equilibrium (5), due to an unstable liquid phase (2) at these temperatures; a pure benzene solid phase precipitates. The liquid phase will continue solidifying as the temperature is lowered, until the system consists only of the vapor and solid phase (6).

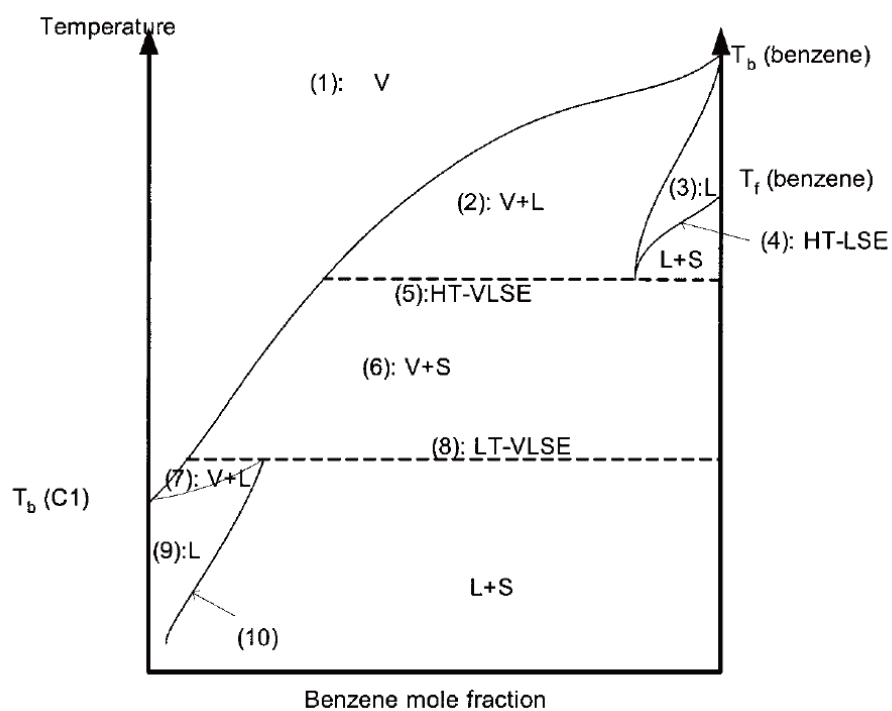


Figure 5-13 Binary Temperature-Concentration diagram of  $\text{CH}_4 - \text{C}_6\text{H}_6$  system [2]

Considering the composition of a natural gas stream, which involves a small concentration of heavier components and a high methane fraction, the precipitation will occur directly from the vapor phase as the temperature is lowered in the vapor-solid area (6). However, regarding the number of components in a natural gas mixture; three phases may exist simultaneous in this temperature region.

As the temperature reaches the boiling temperature of methane an additional solid-liquid-vapor equilibrium occurs (8). At these conditions the liquid phase consists mainly of methane, which is a result of dissolution of the solid benzene phase in the liquid methane rich phase. And if the benzene fraction is small enough a solid-vapor system (6) may experience a melting of the solid benzene phase as the temperature are lowered, this is indicated in the figure 5-13 by the vapor-liquid area (7). Further cooling will create a single liquid phase (9) or a solid-liquid phase (10) depending of the composition of the binary methane-benzene system.

### 5.2.2.2 Binary interaction parameter

The simulation work, including the components benzene and cyclohexane, got postponed due to an error in the freezing point temperature flash algorithm. The error search was done by Even Solbraa, due to the extent of this source code. However, he managed to solve this challenge and made the simulations of these critical components possible.

Since the solid phase expression, equation (3.51), includes the sublimation pressure, which further involves the triple point pressure, temperature and the enthalpy of sublimation through the Clausius-Clapeyron equation (4.1), there are some uncertainties related to these results. As mentioned in the chapter where the freezing point temperature flash is discussed, the experimental values of these parameters vary over a relatively large interval, especially the enthalpy of sublimation values. Thus the intention was to carry through a parameter fitting, optimizing both the enthalpy value and the binary interaction parameter, against the experimental data available. Unfortunately, these calculations were highly unstable, which ruled out the option of a parameter fitting procedure.

This problem has also affected the simulations which have been carried through, first by limiting the simulations to a benzene composition lower than 0.01 mole %. Secondly, the investigation of the enthalpy of sublimation values was difficult to carry through, due to the stability of the calculations. Hence, the existing values for enthalpy of sublimation and the triple point conditions in NeqSim were used to determine an optimal binary interaction parameter. The values used corresponds to the values listed in the DIPPR database [28], see figure 4-1. The result of the investigation of the interaction parameters for benzene in methane rich mixtures is presented in table 5-9.

Regarding cyclohexane, the obtained experimental data included only compositions for the heavy hydrocarbon of interest over 0.01 mole%, and the simulations had problem with converging even though different enthalpy of sublimation and interaction parameters was used, without resulting in any significant logical pattern. The enthalpy values used was within the experimental determined values listed in the NIST chemical web book [27], referring to figure 4-1. The freezing point predictions at increasing mole fraction of cyclohexane lead to a decrease in freezing temperature in some cases and the calculation failed to reach the stability criterion, equation (3.54), for several of the conditions simulated. Thus the calculations including cyclohexane in binary methane rich mixtures is carried out without the use of binary interaction parameters, since these calculations were highly unstable.

Comp. Y	Ref	Author	$k_{ij}=0.0209$		$k_{ij}=0.0509$		$k_{ij}=0.0809$		$k_{ij}=0.0909$		$k_{ij}=0.1109$		App
			BIAS [K]	AAD [K]	BIAS [K]	AAD [K]	BIAS [K]	AAD [K]	BIAS [K]	AAD [K]	BIAS [K]	AAD [K]	
Benzene	[34]	Kurata	-45.60	45.60	-24.69	24.69	-8.01	8.01	-2.94	3.84	6.68	6.73	C3.5
Benzene	[19]	Neumann	-42.69	42.69	-21.74	21.74	-4.90	6.48	0.23	3.52	10.00	10.00	C3.6

Table 5-9 Freezing point predictions with different interaction parameters for benzene – methane binary system (SLE)

The procedure used for determine the interaction parameter is based on the vapor-liquid interaction parameter from the NeqSim library of 0.209, corresponding to the value used in PVTsim® for vapor-liquid systems with the Soave-Redlich-Kwong equation of state. However, this value under-predicted the freezing point temperature with crucial deviations, as seen in table 5-9. Further was the same difference between the interaction parameters, as tried with the carbon dioxide-methane system (0.03), used for the benzene-methane system, resulting in the values presented above. In addition, while simulating, an interaction parameter of 0.0809 showed promising results, thus an interaction



parameter of 0.0909 was selected. As mentioned, the calculations were highly affected by the enthalpy of sublimation parameter, where low parameter values resulting in three-phase equilibrium over a large pressure interval, whereas the calculation collapses for low enthalpy of sublimation values.

When simulating the binary benzene-methane system the initial temperature dictated the system pressure necessary for describing the liquid phase, however, the freezing point temperature was not affected. In other words the freezing point temperature was equal for different initial temperatures and pressures, in addition did the simulations converge and reached the minimum Gibbs energy stability criterion, which indicate that the simulations were performing well. However, this concerns the low concentration of benzene, in the area of the sublimation line (3) in figure 5-12.

From figure 5-14, an interaction parameter in the area between 0.09 and 0.10 could possibly be an optimal interaction parameter value for solid-liquid equilibrium including binary mixtures of benzene and liquid methane.

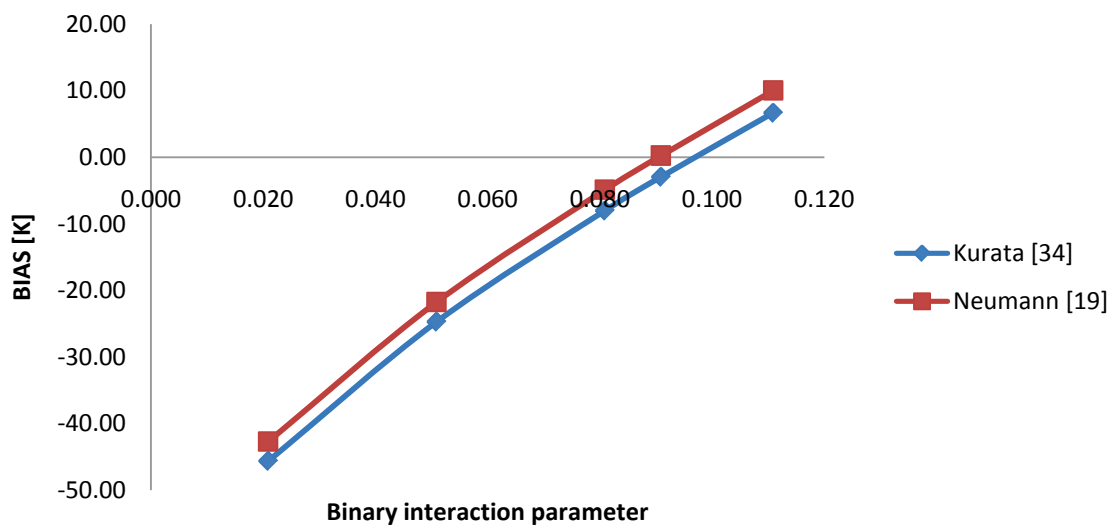


**Figure 5-14 Average BIAS for NeqSim calculations with different interactions parameters, compared to experimental data from Kurata [34] and Neumann [19]**

However, for low concentration freezing points predictions of benzene, there is reason to believe there is a measure for improving, as the proposal from ZareNezhad [10]; by implementing a semi-empirical temperature dependent binary interaction parameter. For more precisely determination it is necessary with a larger database of predictions, and preferably more experimental data points. For the further calculations regarding mixtures including benzene, an interaction parameter of 0.0909 are used.

### 5.2.2.3 *Low temperature Solid-Liquid-Vapor equilibrium (SLVE) for binary CH<sub>4</sub> and C<sub>6</sub>H<sub>6</sub> systems*

There are two interesting conditions for this system, first where the heavy hydrocarbon freezes out from vapor, as described by the phase behavior (solid-vapor area (6) in figure 5-13). In natural gas liquefaction, this freeze out method is the most likely to happen. Unfortunately these types of data are quite rare and the only source of solid-vapor systems found is from the work of Rijkers, which involves high benzene concentrations. Second, where the precipitation of benzene occurs in the liquid phase, indicated by the solubility line of solid benzene in liquid methane (line 10 in figure 5-13).

Since the literature regarding the solid-vapor systems is scarce, the literature studied is mainly freeze outs from liquids. The experimental data gathered in GPAs research report RR 14 [34], are one of the sources for such systems. This is an compilation of data gathered from different published articles and works, and the data regarding the solubility of benzene are from a study Kuebler and McKinley [42] published. The reason for importing these data was; *"... since the solubility of this component in liquid methane was so low, even near the critical temperature of methane, the analytical equipment available at the time of the study was unable to measure the solubility. However, the data taken from the literature subsequent to our study include data on the benzene solubility..."* [34]

The publication from Kuebler and McKinley were unfortunately unavailable, and thus not evaluated in this study. However, the data gathered from the GPA report are further used to determine the accuracy of the simulations tools, in figure 5-15 and 5-16. Kohn and Luks have previously evaluated this article in their study of three-phase solid-liquid-vapor equilibrium of binary hydrocarbon systems; *"..The best existing data on the solubility of hydrocarbons in liquefied methane are those of Kuebler and McKinley, which includes n-alkanes up through n-heptane and also benzene and toluene.."* [35].

Both NeqSim and GPA have problems of describe the phase behavior in mixtures of methane and benzene with a larger content of benzene. However, the GPA simulator is at least able to predict a consistent set of temperatures, the reason for these errors is not fully understood. In contrast are the relevant mixtures for this study; low concentrations of the heavy hydrocarbon in methane rich binary mixtures.

The simulation done with the GPA model shows a reasonable agreement with the experimental data. Compared to the data in research report RR 14 by Kurata, the average absolute deviation is 6.66 K. Where a benzene concentrations above 0.01 to 0.0363 are representing the highest deviation, leading to a maximum deviation of 17.40 K. The first point in this dataset excluded, since it represents pure methane. The results are shown in figure 5-15, where the predictions from NeqSim are also presented; however, the NeqSim simulator had problems describing the benzene-methane system for benzene concentration greater than 0.01 mole %. The predicted results had an average absolute deviation of 3.84 and a maximum deviation of 8.47, which is considerably better than the GPA predictions.

However, when comparing the NeqSim and GPA predictions within the same temperature interval, the GPA simulator performs better; in contrasts when considering the whole dataset. For the sample numbers 2-19 in appendix C3.1, the GPA predictions result in an average deviation of 2.12 K and an average absolute deviation of 4.72 K, this is more consistent to the accuracy of the NeqSim predictions. From the raw data presented in appendix C3.1 it can be observed that the NeqSim

predictions are performing poor in the low temperature area, while the GPA have the biggest deviation located for benzene concentrations about 0.01-0.03 mole %, as seen in the figure.

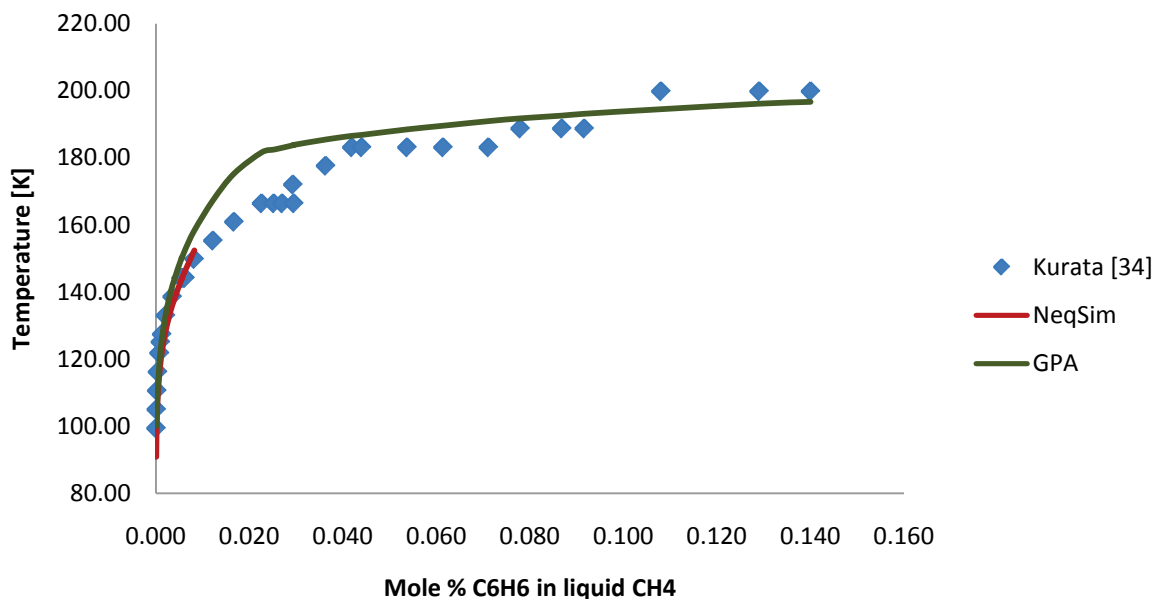


Figure 5-15 Solubility of  $C_6H_6$  in  $CH_4$ : Predictions and experimental data from Kurata [34]

The low concentration points are presented in figure 5-16. Considering the simulations, the GPA simulator corresponds better to the experimental data than the NeqSim predictions, especially for the concentration of benzene is bellow 0.002 mole %.

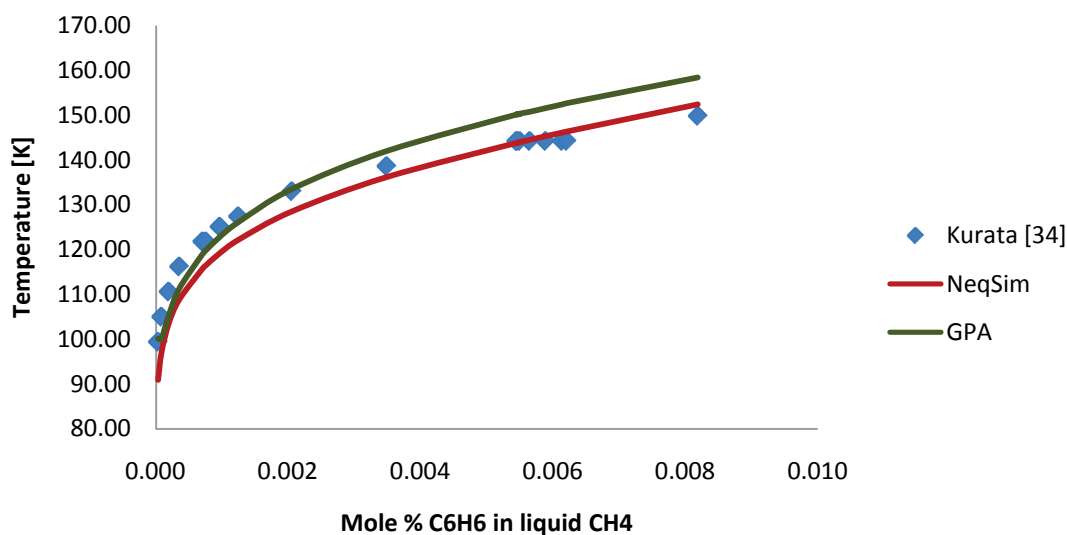


Figure 5-16 Solubility of low concentrations  $C_6H_6$  in  $CH_4$ : Predictions and experimental data from Kurata [34]

Whereas the NeqSim performs better in the area above a benzene concentration of 0.002 mole %, the average deviation of the predictions presented in figure 5-16 are -2.94 K, which also indicating that the overall temperature predictions are too low, resulting in a maximum deviation of -8.47 K at the lowest temperature (sample no. 2 in appendix C3.1). Considering the average absolute average deviation it performs better than the GPA simulator with a value of 3.84 K.

Another source is the experimental work by Neumann [19], however, the paper is written in his mother tongue, German. Thus the experimental details are not fully understood and the article not reviewed in the same extent as the rest of the experimental sources. Anyhow, the experimental data are presented in figure 5-17. Compared to the data from the GPA report RR 14, the predictions are more consistent to the experimental data from Neumann. For the GPA simulator are the average deviation compared to these data equal to 5.18 K, and since all the temperature predictions are higher than the experimental data the average absolute deviation also equals to 5.18 K.

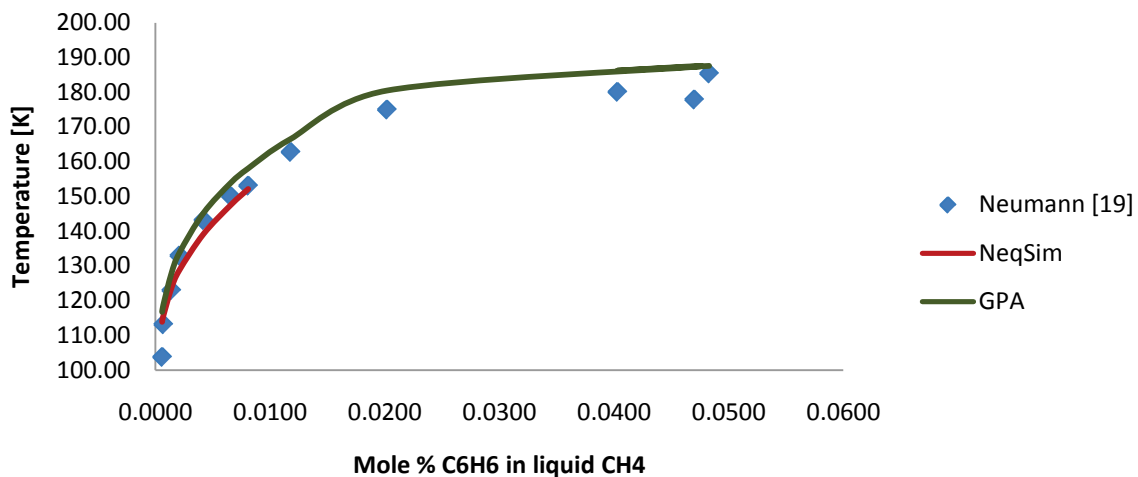


Figure 5-17 Solubility of C<sub>6</sub>H<sub>6</sub> in CH<sub>4</sub>: Predictions and experimental data from Neumann [19]

As shown in figure 5-17, NeqSim had trouble with predicting freezing points temperatures for mixtures containing more than 0.01 mole % benzene; for the lower benzene concentrations NeqSim was able to predict freezing point temperatures with a good accuracy. These data points are presented in figure 5-18.

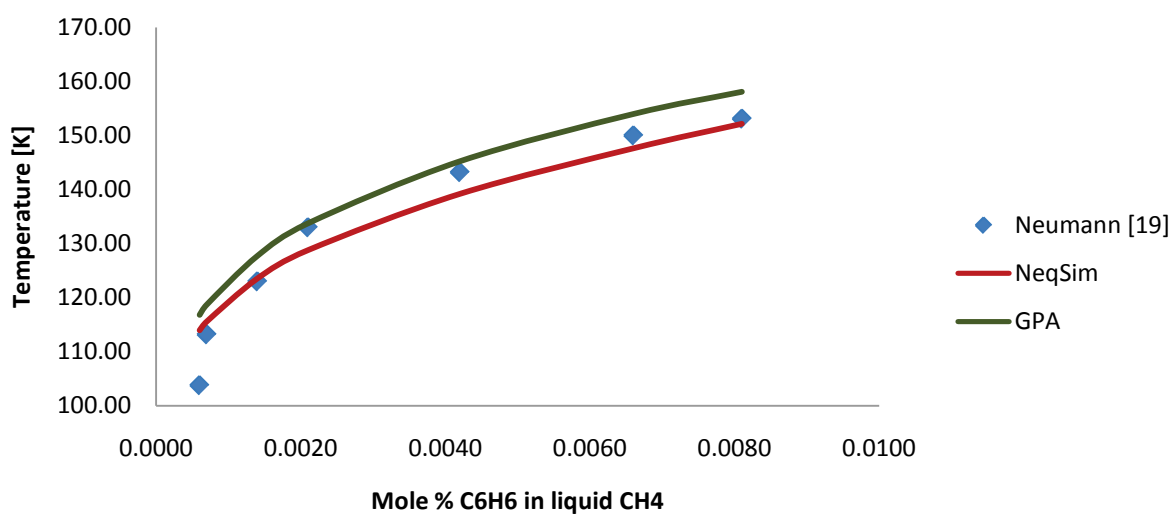


Figure 5-18 Solubility of low concentrations C<sub>6</sub>H<sub>6</sub> in CH<sub>4</sub>: Predictions and experimental data from Neumann [19]

The average deviation compared to the sample numbers 1-7 (presented in table C3.2 in the appendix) is equal to 0.23 K, whereas the average absolute deviation is 3.53 K. The reason for this positive average deviation is the over predicted temperature of 10.18 K at the lowest temperature; this is also the maximum deviation compared to this data set. The GPA simulator has an even higher predicted temperature at this composition, respectively a maximum deviation of 13.01 K.

#### 5.2.2.4 Solid-Liquid-Vapor equilibrium (SLVE) for binary $CH_4$ and $C_6H_6$ systems

The three phase locus is studied by Luks et al. [17] and an extract of his work is presented in figure 5-19. The figure shows both the low and high temperature three phase locus of the benzene-methane mixture. The two lines presented here can be recognized in figure 5-12, as the three phase locus indicated by the stippled lines (6). The figure beneath shows clearly how the three phase lines change with pressures and the ending point of the low temperature three-phase line (left hand side in figure 5-19) is the critical point of methane. The high temperature three-phase location extends since benzene-methane mixture have a critical point at a much higher pressures, than pure methane.

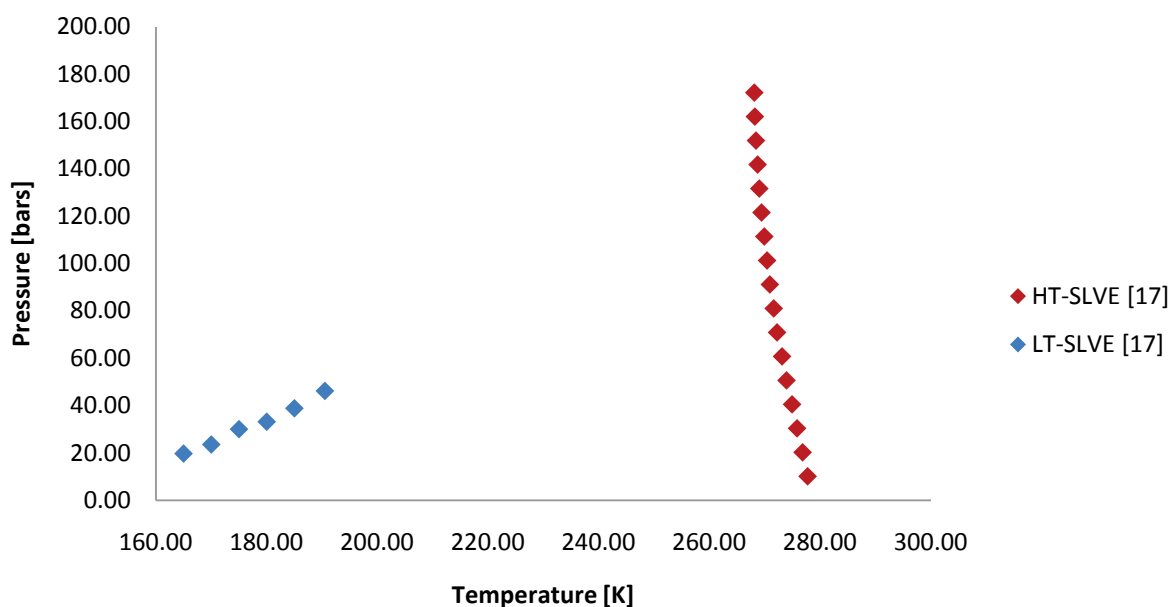


Figure 5-19 Experimental three-phase locus of binary  $C_6H_6$ - $CH_4$  mixture [17]

These data represent a wide range of benzene compositions, the high temperature three-phase line include the concentrations from 98.15 mole % benzene at low pressure to 72.46 mole % at high pressure. The simulations tools used in this study were unable to predict freezing temperatures at these benzene concentrations. However, for the low temperature data, consisting of benzene concentrations from 0.011 mole % to 0.0170 mole % (respectively from low to high pressures), the GPA simulator where able to predict freeze out from the liquid phase. And since the vapor phase at these low temperatures are assumed to be virtual pure methane, the predictions preformed with a sufficient accuracy. This is shown in figure 5-20, while the raw data is available in appendix C3.3.

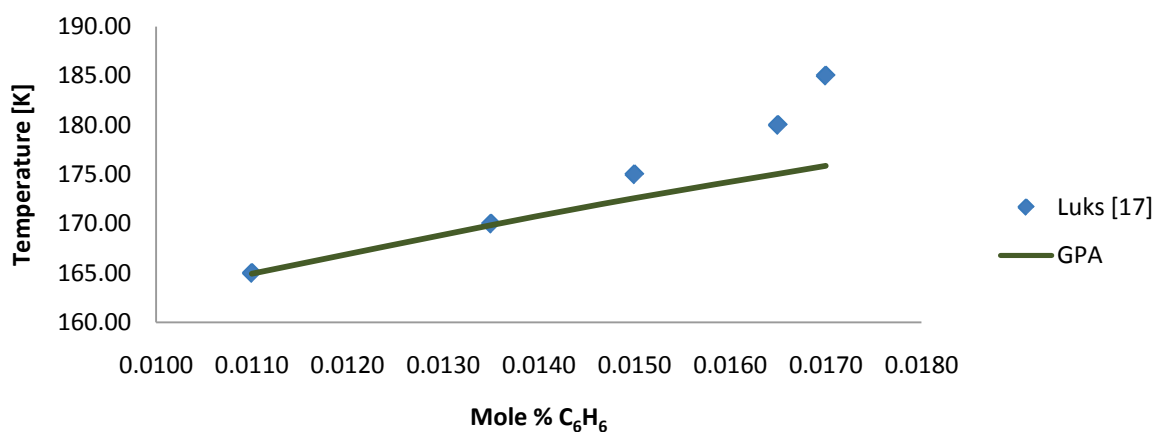


Figure 5-20 Solubility of low concentrations C<sub>6</sub>H<sub>6</sub> in CH<sub>4</sub>: Predictions and experimental data from Luks [17]

Considering the accuracy, the deviations are increasing with increasing benzene composition; the freezing point temperature predictions at these conditions seem to be a linear function of the molar benzene concentration.

As mentioned previously, the simulation tools have problems with increasing benzene compositions in binary mixtures with methane. For the NeqSim simulator the limit is experienced to be at 0.01 mole % while the GPA simulator seems to manage to describe systems including 0.14 mole % in the data compared to the experimental work in RR 14. However, for the data from Rijkers [18] in which involves compositions from 8.04 mole % and up to 89.83 mole %, the GPA simulations failed. The fact that this dataset represent freeze out experimental data from the vapor phase is the reason for including this dataset in the appendix.

#### 5.2.2.5 Low temperature Solid-Liquid-Vapor equilibrium (SLE) for binary CH<sub>4</sub> and C<sub>6</sub>H<sub>12</sub> systems

The only source of experimental data obtained for the binary system consisting of cyclohexane and methane, are the work done by Kohn and Luks [35]. In the published article they recognize a phenomenon that, to Kohn and Luks's knowledge, never has been reported for a system where methane is the solute. The behavior observed occurred when the molar volume of the liquid phase in a solid-liquid-vapor system is increasing, the composition is decreasing. This phenomenon has the opposite behavior as to what is expected in low temperature systems. The raw data are presented in appendix C4.1, the sample numbers 20a to 24, where it can be observed that the liquid volume are decreasing and at the same time the benzene composition are increasing. As mentioned this is a behavior never reported before, and request a more thoroughly phase behavior investigation. Kohn and Luks also recognized that the experimental work of Kuebler and McKinley [42] was carried out at over pressures, "which procedure in effect creates a solid-liquid system substantially removed from the critical region (no vapor phase present), which would mask the phenomenon reported here"[17].

However, the experimental data involving lower compositions (sample numbers 25-39 in appendix C4.1) was used to compare the simulation tools, and the result is presented in figure 5-21.

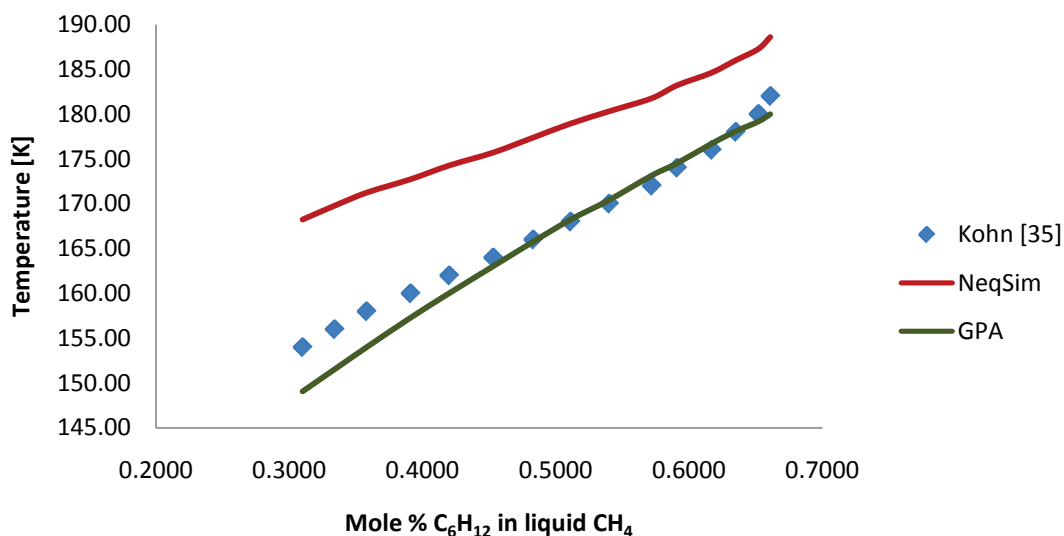


**Figure 5-21 Solubility of low concentrations C<sub>6</sub>H<sub>12</sub> in CH<sub>4</sub>: Predictions and experimental data from Kohn [35]**

As shown in the figure the predictions done by the GPA simulator represent a good correlation to the experimental data, this is again supported by an average deviation of -1.28 K and an average absolute deviation of 1.68 K. However, for higher cyclohexane composition; the simulations performed with severe deviations, and for concentrations above 1 mole % the calculations failed.

Regarding the freezing point predictions done by NeqSim the deviation where considerable higher; BIAS and AAD values of 10.67 K, note that the sample numbers from 20a to 24 (in appendix C4.1) are excluded in the accuracy calculations. Even though the deviation is higher, the NeqSim curve has a more similar shape compared to the experimental data than the GPA predicted curve. As mentioned in the chapter regarding binary interaction parameters, it was not possible to determine the optimal interaction parameter or enthalpy of sublimation; hence, the calculations are carried out without the use of interaction parameters. This would be a relevant issue for further investigation, with an optimal interaction parameter the deviations are reduced to an acceptable level.

### 5.2.2.6 Solid-Liquid-Vapor equilibrium (SLVE) for binary $CH_4$ and $C_6H_{12}$ systems

Considering the whole experimental dataset from Luks, which include both the high temperature and low temperature solid-liquid-vapor systems, presented in figure 5-22. The high temperature three-phase locus includes compositions from 56.22 mole % to 96.32 mole %, while the low temperature three-phase locus includes compositions from 0.310 mole % to 0.651 mole %.

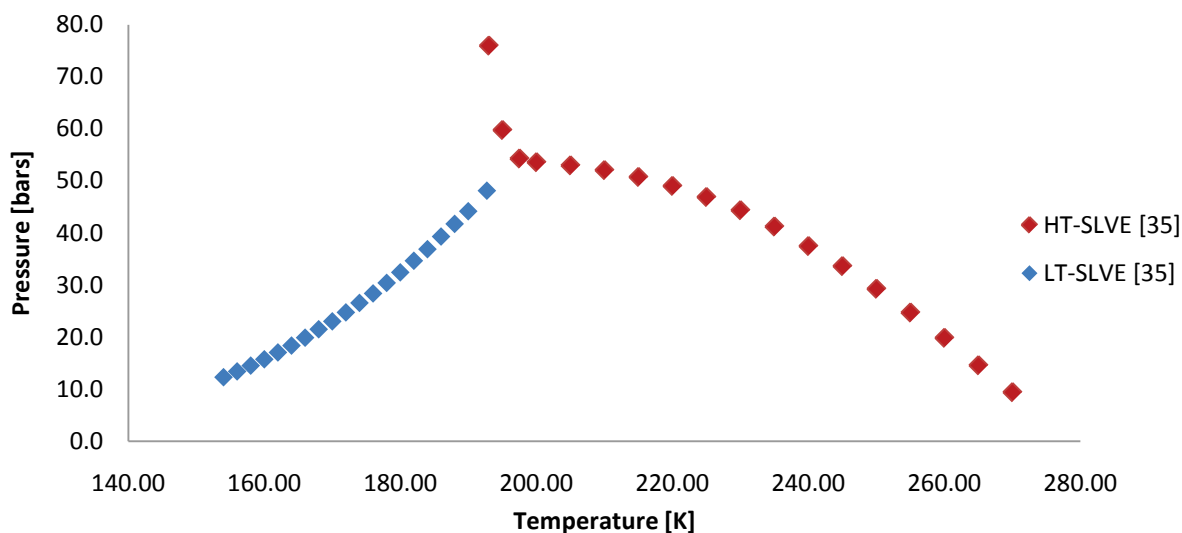


Figure 5-22 Experimental three-phase locus of binary  $C_6H_{12}$ - $CH_4$  mixture [35]

The phase behavior in the low temperature solid-liquid-vapor locus is similar to the binary system consisting of benzene and methane, but the locus of the high temperature solid-liquid-vapor locus tends to bend towards the low temperature three-phase locus. This is a behavior observed previously in methane – n-hexane and methane – n-heptane systems, in addition to the system under consideration [35]. However, for temperatures lower than 200 K the three-phase locus is rising rapidly with regards to the pressure, similar to the binary systems with methane and benzene.



### 5.3 Discussion of the simulations result and model evaluation

Generally, the understanding of solid-fluid equilibrium in hydrocarbon dominant mixtures is currently limited to a few binary and ternary systems, and a selection of the binary systems has been investigated further in the previous chapter. It is also recognized that the understanding of the phase behavior for these mixture investigated is crucial in order to be able to produce good predictions of the simulations.

For the simulations carried through with NeqSim and HYSYS is the Soave-Redlich-Kwong equation of state selected, and there is no significant difference in the accuracy compared to the Peng-Robinson equation of state. It is also recognized from previously work, that these equations of state are widely used for describing the fluid phases in solid-fluid equilibrium calculations, and the prediction of freezing point temperatures. This method is representing a more general correlation of phase equilibrium calculations in combination with the expression of the solid phase, referring to equation (3.51). In contrasts to the method based on empirical correlated activity coefficients, where the parameters have been fitted to larger amount of experimental data available.

It has been shown that the general correlation, which NeqSim represent, by applying the Soave-Redlich-Kwong equation of state and classical mixing rules with binary interaction parameter, is able to predict the freezing point temperatures as well as the activity coefficients based model, represented by the GPA simulation tool, at least for the binary mixtures consisting of carbon dioxide and methane. The need of experimental data in these models is still crucial for the accuracy of the predictions, the interaction parameters in the model have to be determined. This is done by parameter fitting to the experimental data, for the binary mixtures containing carbon dioxide and methane, the optimization have been based on the vapor-liquid binary interaction coefficient existing in the NeqSim component library. It is discovered a smaller interaction parameter dependency for solid-vapor phase equilibrium, in contrast to the solid-liquid equilibrium for the carbon dioxide-methane binary system. The optimization resulted in a solid-fluid binary coefficient of 0.12, equal to the vapor-liquid interaction parameter from the commercial simulation program PVTsim® 13, with the use of Soave-Redlich-Kwong equation of state. However, it is recognized a wide acceptance for a temperature-dependent interaction parameter, hence for further work; the dependency should be further investigated and implemented in the NeqSim source code.

For the binary mixtures including methane and heavier components, benzene and cyclohexane respectively, the experimental data are scarce, which introduces a higher uncertainty to the predictions, and especially regarding the optimization of the binary interaction parameters.

In addition, is the computation of these mixtures more challenging and this resulted in unstable calculations; for the binary mixtures consisting of methane and benzene the NeqSim simulator was not able to predict reliable freezing point temperatures for mixtures containing more than 0.001 mole % of benzene. In contrast did the GPA simulator managed to calculate mixtures containing higher concentrations of benzene. Regarding the interaction parameter used for the mixtures containing benzene a value equal to 0.0909 was recognized as an optimal value for the same system. Regarding the interaction parameter in binary methane rich systems with cyclohexane it was not possible to investigate different parameters due to the instability of the calculations, thus the simulation were carried out without interaction parameters.

However, the predictions were quite reasonable, considering the circumstances, and this represents a situation where the model was exposed to a system outside the experimental database and confirms the application qualities this model possesses.

In addition are the expressions which describe the solid phase fugacities, dependent on experimental component data, as the enthalpy of sublimation, and the triple point condition. Regarding the carbon dioxide component the experimental values are well documented, but considering the benzene and cyclohexane components, these experimental values are subject to a larger spread. Thus there is a need for further research, in order to determine these values and optimize the parameters in the model.

## Part 2 Experimental work and evaluation of the freeze out rig

### 6 Presentation of the experimental equipment - Freeze out rig

The rig is built by Sanchez Technologies and was transported to StatoilHydro's research center in the beginning of February 2008, and installed in April the same year. Later it has been made various modifications on the rig, in order to minimize the startup time and get it operating.

The main function of the freeze out rig (PVT-80/170 LT) is to measure the freezing point temperatures in hydrocarbon dominant mixtures, mainly mixtures similar to natural gas. A 3D-model of the freeze out rig where the main external components of the rig are identified is presented in figure 6-1. The rig consists of a low temperature Dewar container which holds the main components of the system used to study phase equilibriums. There is vacuum established between the two cylinders that ensure isolation of the inner system, the volume of the inner system is 140 liters.

The cooling system involve two different methods; mechanical cooling, and with liquid nitrogen. Two automatic gas pumps and an arrangement of valves, injectors, compress and circulate the mixture of interest in the system. The rig specifications involves pressures up to 500 bar and temperatures down to  $-170^{\circ}\text{C}$ . After the gas mixture is compressed and injected, it's feed into the internal system where it is cooled. The sapphire cell is directly connected with a blind cell that is used to transport the gas mixture, or isolate the different phases by aligning the pumps.

It is possible to observe freeze outs in two different ways, can be by direct observation through the sapphire cell to see if there are formed solid or through a cold finger that is connected to a fiber optic system.

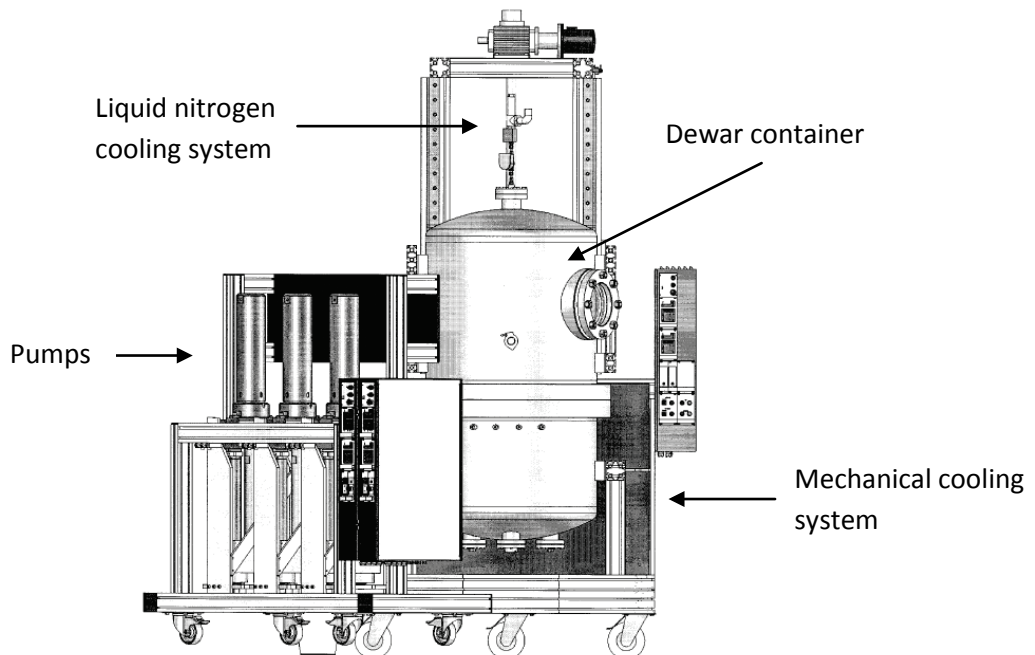


Figure 6-1 3D model of the freeze out rig

## 6.1 Modifications

As mentioned, there have been done several short-term modifications on the rig to reduce the startup time, and work is being done to develop a better sampling system. From the original configuration, the sampling valves, including filter and bypass valve, have been removed along with the corresponding piping inside the interior system. Hence, it is currently not possible to take samples of the formed crystals in the mixture. However, there are still possibilities for sampling the gas- and liquid-phase from the pipes that leads out from the sapphire and blind cell, indicated in figure 6-2.

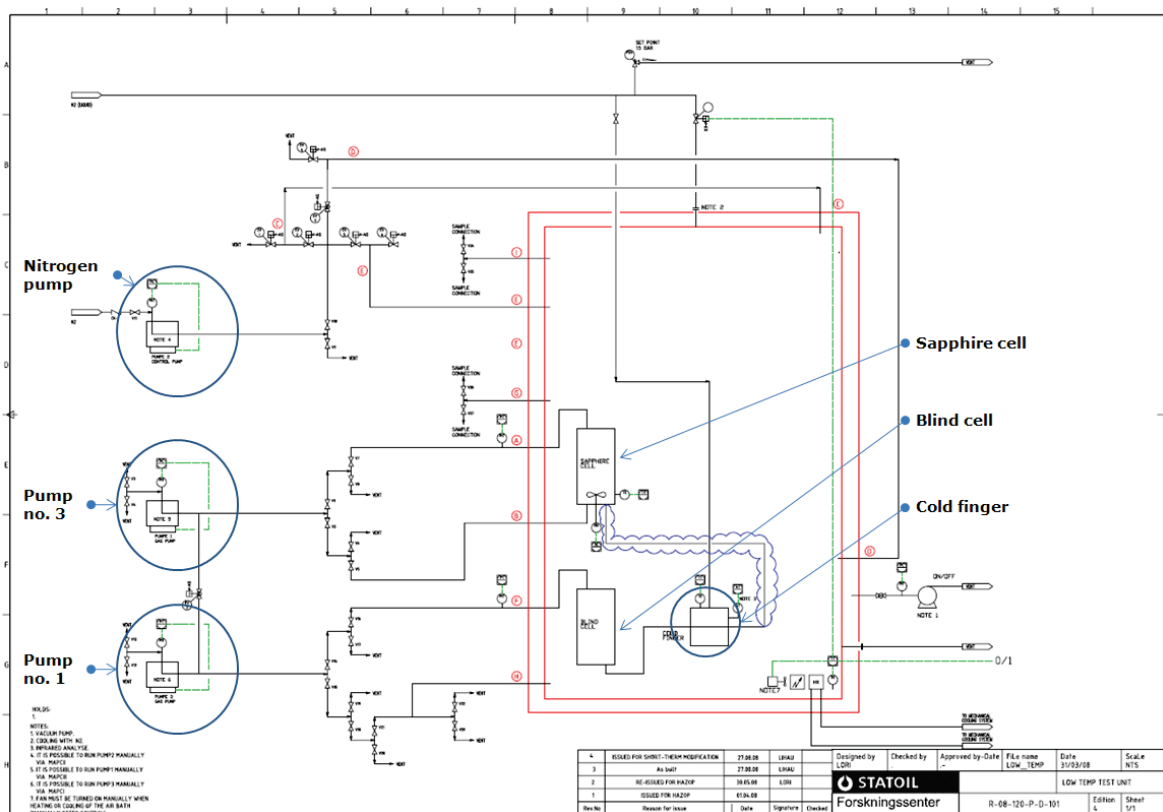


Figure 6-2 Flow sheet over freeze out rig: Short time modifications [43]

The nitrogen system involving pump number 2 and part of the pipes that was connected to the sampling valves is still present, but are not in operation, since it doesn't have any function without sampling system. From the A4 copy of the P&Id presented in appendix D2, it is possible to observe the pipelines which enter the Dewar container at the junction I, E, G and H are present outside of the container, but removed from the inner system. Except from the sampling system are the rig performing as planned, observation of phase transitions in a mixture is visually determined in sapphire cell and measured in the cold finger. [43]



Filling the system with the mixture of interest, is done through one of the valves that are connected to the pumps, thus for pump no. 1 the mixture is filled through the valve (V3) or (V4), and for pump no. 3 is (V12) or (V13) used.

### **6.2.1 Mechanical cooling**

The mechanical cooling system is design as a standard cascade process, using the refrigerants R404a and R23 as cooling medium. The R404a circuit, which have the highest temperature interval, transport heat to the cooling water through a heat exchanger. While heat are absorbed in the evaporator, that alternates with the R23 circuit. Corresponding, the R23 circuit absorbs heat from the heat exchanger inside the Dewar container in the air bath, and transport it to the R404a circuit.

Regulation of the mechanical cooling is done by a cutoff valve in the R23 circuit, before the refrigerant is compressed. The valve closes thereby the inlet of the compressor, for a limited time period. Usually when the temperature in the air bath reaches  $-70^{\circ}\text{C}$ , the mechanical cooling stops and liquid nitrogen cooling is used to cool the system further down. This switch temperature can be regulated in the control system, but the mechanical cannot operate with a lower temperature.

### **6.2.2 Liquid nitrogen cooling**

Liquid nitrogen from an external cryogenic container, with a pressure of about 4 bars, provides liquid nitrogen to the air bath, which holds a pressure of 1 bar. The liquid nitrogen enters the container on the top and flows into an open spherical surface in the top of the air bath. Fluid adds up and forms a liquid layer of nitrogen at the boiling point; nitrogen will evaporate and yield a cooling effect. The cold nitrogen gas evaporates off, and it flows down along the wall of the air bath. A fan at the bottom helps to increase circulation of cold gas. Nitrogen will evaporate at  $-196^{\circ}\text{C}$  when we have a pressure of 1 atm in the container. The mass flow of nitrogen will be adjusted using a temperature sensor inside the container, which controls a valve on the air bath inlet. The specification for the rig is as mentioned is  $-170^{\circ}\text{C}$ , in theory; liquid nitrogen could cool the system further down in temperature. The temperature constraints are liquid nitrogen mass flow, and heat loss from the containers. For reducing this heat loss the Dewar container is equipped with a radiation shield in Teflon.

## **6.3 The interior system**

The interior system consists of the fluid handling system inside the Dewar container, excluded the removed solid sampling system; the rig and the equipment are presented in presently conditions.

### **6.3.1 Sapphire cell**

The sapphire cell is a container partially made of sapphire, which are among the minerals that form rock formation and withstand significant stresses. The most important feature is that it is transparent; this makes it ideal for phase equilibrium studies, since it is possible to observe the fluid behavior inside the cell. The volume of the sapphire cell is 80 milliliter, which is in excess of 1 / 3 of total volume, including pipelines. It's also equipped with temperature and pressure sensors, in addition to a stirrer.

#### **Stirrer**

The stirrer provides circulation inside the sapphire cell, and is connected via a frequency converter for speed regulation. When the mixture is affected by a stirrer it is a known fact that the proportion of solids formed increases. It acts as a catalyst in the cell when the conditions are close to equilibrium, and makes the mixture more homogeneous.

#### **Camera**

The camera represents an additional function to the visual detection system, thus it is possible to capture images and video of interesting conditions. This can further be analyzed on the computer, and the level of details possible to detect increases. Together with control system, the camera provides the possibility to observe and operate the rig with remote control. Note that the camera is placed outside the Dewar container.

### **6.3.2 Blind cell**

The function of the blind the cell is to make it possible to transport and isolate parts of the mixture in the system; for example, you can isolate the entire liquid phase in the blind cell. Otherwise, the cell is completely identical to the sapphire cell, except that blind cell does not include a stirrer or the characteristic of being transparent. There are however a small window that makes it possible to observe a small area inside cell, but the visibility is limited. The blind cell is made of stainless steel with a volume identical to the sapphire cell, i.e. 80 millilitre.

### **6.3.3 Cold finger**

The cold finger is the coldest point in the process, it is cooled with liquid nitrogen which enters at the top of the Dewar container and runs in bypass through the cold finger, and this is shown in figure 6-2. It is placed a mirror in the channel that lead the fluid mixture through the cold finger. On the back surface of this mirror is nitrogen evaporating and cooling down the mirror. The mixture is then directed through a channel with transparent part and a mirror on the opposite side of the cross-section. Infrared light (IR) are being sent through the transparent surface in the channel and reflected in the mirror and recorded through the fiber optics which transports the light signal to a converter, in this way the digital signals can be analyzed. Thus, one can register the phase changes in the gas mixture, by continuous logging the signal from the cold finger. In addition, it placed a temperature sensor that measures the local temperature. [57-60]

#### **6.3.4 Temperature and pressure gauges**

Inside the air bath, there are four temperature sensors, placed in the sapphire cell, cold finger and in the air flow at the suction side of the circulation fan (hot side of the heat exchanger). The temperature sensors are type Pt100. The number in the name refers to the resistance of the platinum element, i.e. the resistance in this item is 100 ohms at 0 ° C. The sensors are of the simplest version, since there are no mechanical or chemical loads in the system, and have a temperature range from -200 ° C to 850 ° C. The relationship between temperature and electrical resistance is approximately linear over a small temperature interval. For example, if one assumes linearity over the temperature range from 0 ° C to 100 ° C, the deviation at 50°C is then 0.4°C. In order to take precise measurements it is necessary to linearize the resistance, to get an accurate temperature measurement. The latest definition of the relationship between resistance and temperature is the International Temperature Standard 90 (ITS-90).

There are five pressure sensors from Keller that are placed respectively in each of the fluid mixture pumps (pump no. 1 and 3), nitrogen pump, sapphire cell and blind cell. This is pressure sensors of the type 33X, which is very accurate; they have an error margin of 0.1% of full scale (700 bars). They has included a 4-20mA A / D converter, which enables the sensors to deliver a digital signal to the control system. In addition are the deviation from the temperature dependence and non-linearity's is mathematically compensated. In addition, there is a pressure sensor that registers the vacuum between the two layers of the Dewar container; this is placed at the inlet to the vacuum pump.

Since the signals are connected to the control system through a measuring unit, and the documentation on this system is limited, it is difficult to calculate the precision and the error margin of the signals received from the system. The errors stated above, refers directly to the measuring sensors.

#### **6.3.5 Circulation fan**

As mentioned earlier there is a circulation fan in the bottom of the air bath which provide circulation and thus uniform temperature in the system. The temperature regulation functions are dependent on the fan, which means that fan must be operating in order to start the temperature regulation functions.

The circulation fan is securing an efficient cooling effect and optimal temperature distribution; it is useless to regulate the temperature without the fan running. The fan is connected to a frequency converter which allowing speed control; this regulation can be done manually via a potentiometer or via PC. The fan is also equipped with an electric heating element that it should be operated in extremely low temperatures; it can be a problem that the grease in the bearings will get stiff and freeze.



## **7 Experiences and limitations of the rig which affect the experimental work**

This part will focus on the experimental work and operational study carried through related to the freeze out rig. Since the experimental work at the rig mostly have included trouble-shooting and experiments for determining the behavior of the rig, and no phase studies; the experimental part of this report will focus on what we have discovered by running these experiments. Hence, an indication of the main challenges, and where the potential areas for improvement are located.

Due to the modification work and the fact that the rig is not operating in a satisfactory manner the experimental study of binary mixtures has been postponed. The rig has so far only operated with pure fluids, mostly carbon dioxide. Since this is a non-hazardous fluid with regards to operating personal and equipment; it is non-explosive and non-poisonous gas. Ideal for performing initial testing of the possibilities and capacity limits the rig possess, due to the high triple point of carbon dioxide it is possible to detect phase transitions at a reasonable high temperature and pressure. Some tests with helium have in addition been carried through for detecting leakages; due to the low density of helium is it an optimal fluid to perform leakage tests with.

Regarding to operate the rig with methane rich binary mixtures, there have to be performed some initial safety analysis of the rig, due to the hazard risks hydrocarbon mixtures represent. At StatoilHydro they have a class of hazard system consisting of three danger levels, and the rig itself are defined in the highest class of hazard; considering the intentions of investigating hydrocarbon dominant mixtures, and the temperature and pressure specifications (-170°C and 500 bars). This implies that there have to be performed a safety analysis, HAZOP and an interdisciplinary final control, where the process and equipment get a final operational approval from the people involved in the project.

This is a quite time consuming process which involves several people on different levels, and a comprehensive study of the equipment. In addition there have been discovered several issues that needs improvement before this interdisciplinary final control can approve the rig for operating with hydrocarbon dominant mixtures. Thus it has been difficult to have the desired progress regarding the experimental work.

## 7.1 Temperature control in the interior system

The most severe issues discovered regarding the reliability of the freeze out rig and the quality of the measurements is the low temperature control experienced. There are several factors which influence this behavior; the most important are presented beneath.

### 7.1.1 Placement of the temperature sensors

A fundamental fault is the placement of the temperature sensors which is placed in the steel surrounding the fluid cells and not in the fluid itself. This applies for the sapphire cell and the blind cell (filter temperature sensor). Hence, the construction error is preventing the actual temperature of the fluid to be measured. And when there is a large temperature gradient through the steel and sapphire material it is difficult to compensate for this error since each sensor got to be calibrated for itself depending on how much material it is in contact with.

### 7.1.2 Heat leakage from the Dewar container

The cause for the relatively large temperature differences in the Dewar container is heat leakages and unstable regulation of the cooling system. The last issue will be discussed later, but the factors affecting the temperature gradients are directed to the “high” pressure in the vacuum insulation in the double sheeted Dewar container, and the radiation shield in the same volume.

#### 7.1.2.1 Radiation shield – Multilayer insulation (MLI)

To reduce the heat loss through the Dewar container, a multilayer super insulating radiation shield are a good and simple measure. In relation with the pre-project to this thesis [4], there was carried out a simple heat transfer calculation for determining a gross estimate of the insulation effect the present radiation shield presents compared to the multilayer super insulation. This calculation was affected by a typing error, this has been updated and the result is presented in figure 7-1.

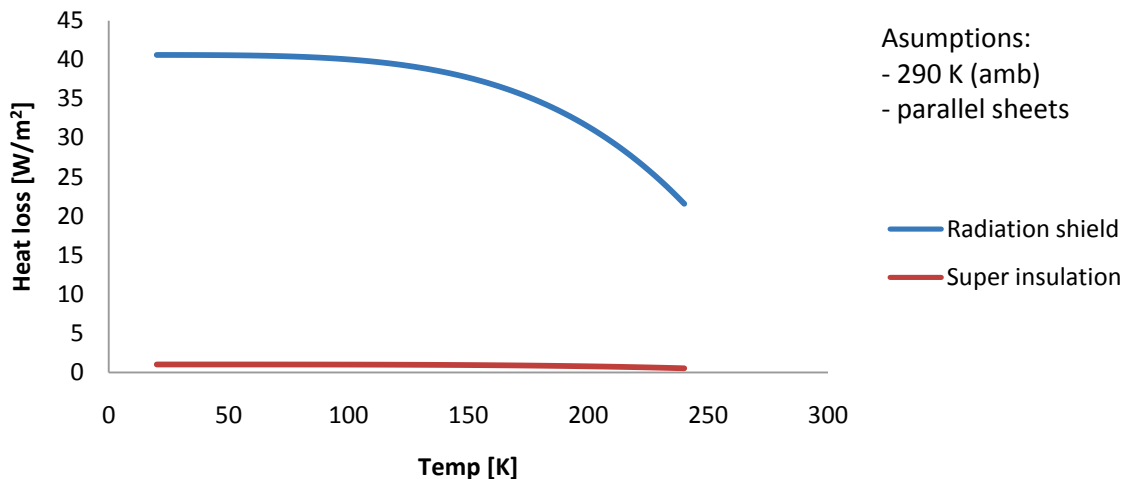


Figure 7-1 Heat loss due to radiation in the Dewar container at different temperatures

This MLI radiation shield consists of 10 layers of thin aluminum foil, compared to the current solution which are a Teflon radiation shield, the MLI will reflect the heat radiation waves from the interior system more efficiently than the current solution. The assumptions in the calculation are; treating the containers as two parallel plates; thus, the shape coefficients and the area ratio between the two containers, and between the layers in the radiation shields are simplified to a value of 1. This will not affect the result in a large extent since the decisive factor is the number of layers in the radiation

shields, and the area ratio between layers with aluminum in the MLI shield is in reality close to 1. It is also assumed an ambient temperature of 290K and a uniform temperature throughout the walls of the Dewar container.

The insulation will cause a smaller temperature gradient through the Dewar container and inside the air bath, hence a smaller temperature differences between the fluid and air bath. This will reduce the risk of getting freeze outs in the pipes and unwanted blockage of the system. Since the effect of the mechanical cooling is regulated by an on/off valve and not a level regulator on the compressor, the effect of a radiation screen would not save mechanical cooling effect. In the case where the system is cooled with liquid nitrogen, however, it will be possible in theory could reduce the mass flow in similar magnitude as the heat loss reduction due to the fact that mass flow is proportional to the cooling effect. Thus by installing a super insulating radiation shield it is possible to reduce the mass flow of liquid nitrogen, depending of the temperature interval.

### 7.1.2.2 Effect of gas pressure on thermal conductivity of MLI

Considering installing the super insulating radiation shield, the vacuum pressure in the volume between the surfaces in the double sheeted Dewar container can be optimized to reduce the heat loss. The vacuum established in the volume between the two layers of the Dewar container is presently 5 millibar (3.75 torr), which is the minimum pressure the vacuum pump can obtain. This gas pressure will not be able to limit the thermal conduction in the volume and results in a higher heat loss than necessary.

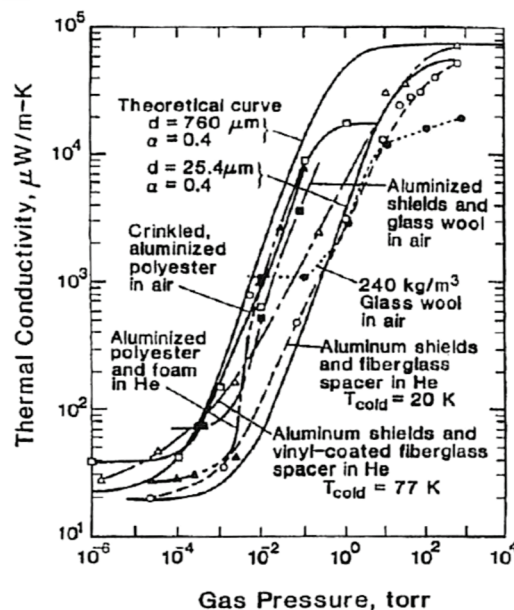


Figure 7-2 Effect of gas pressure on thermal conductivity of multilayer insulation (MLI) [45]

The coherence of the mentioned thermal conductivity and the gas pressure are described by an S-shaped curve presented in figure 7-2, which shows that below  $10^{-4}$  torr are the decrease of thermal conductivity in the gas, insignificantly affected by lowering the pressure. At the point where the pressure reaches atmospheric pressure the heat conduction component become the dominant heat transfer type, and the heat transfer from thermal radiation is only a small fraction of the total heat loss.

The present pressure obtained in the rig, which are 3.75 torr, is in the uppermost area in the figure, depending on the insulating material. The conclusion is that the pressure should be reduced to at least  $10^{-3}$  torr or below, thus the thermal conductivity will be reduced with a factor of about 100. However, the specification of the minimum pressure the Dewar container is designed for is not obtained from the producer. Hence, the limitation of the heat leakage is the minimum pressure.

#### **7.1.2.3 Heat effect produced by the circulation fan**

Since the cooling effect from the mechanical and liquid nitrogen cooling are dependent of circulation of the air in the air bath. However, in addition to increase the heat transfer from the cooling system and the fluid investigated, the fan produces heat which affects the temperature inside the air bath. By optimizing the operation of the fan, a reduction of the heat effect the fan produces can be obtained. A suggestion is operating the fan with periodic duty. However, this will also affect the heat transfer between the air bath and the fluid, thus the operation got to be optimized.

The amount of heat effect from the circulation fan is not determined, and it could be imagined that after installing the super insulating radiation shield and reducing the vacuum pressure, the temperature distribution in the interior system are satisfactory.

The main benefit of a reduced heat loss is, as mentioned, that the interior system will keep a more steady temperature, would not get the large temperature difference between air bath and the fluid, which leads to the risk of freeze outs in pipelines and areas which are not available for visual detection.

### **7.1.3 Temperature regulation**

#### **Mechanical cooling**

In addition to the placement of the temperature sensors and heat leakages are the temperature control system in the rig inadequate, and resulting in a lower accuracy of the temperature measurements. Both the mechanical and liquid nitrogen cooling systems are controlled by an automatic pulse-width regulated valve, this means that when the set point temperature in the sapphire cell are reached, for the mechanical cooling system a valve in the refrigeration circuit is closed for a period of time until there is a need for more cooling effect. This procedure itself leads to a different high and low pressure in the refrigeration circuit, thus the condensing temperature get affected and causes instabilities in the system [4]. The experienced temperature variation when running with mechanical cooling is with an amplitude of approximately 1-2 K in the air bath, at the highest accuracy. The problem is the time period before the system reaches this oscillation with an amplitude of 1-2 K, where the accuracy of the temperature variation is much lower. And the time the mechanical cooling system uses to stabilize is random and unpredictable.

#### **Liquid nitrogen cooling**

Regarding the liquid nitrogen cooling system; it is regulated by the same method, and operate with the same temperature oscillations. But the time it uses for reaching this operation mode is almost immediately. Thus for running experiments it is recommended using the liquid nitrogen cooling system. The mechanical cooling system is more useful when running experiments overnight and keeping the temperature low when the rig is in a standby mode, to avoid spending time on cooling. This is also a cheaper cooling method and involves less risk.

### **7.1.3.1 Heating control**

Another feature that is missing is the automatic control of the heater placed in the air bath, this is only manually regulated. For running experiments where it is necessary to crossing the phase transition equilibrium lines there is a need for more precise regulating. In addition to situations where the experiments are finished and the system is brought back to ambient conditions, is it convenient to using the heater. But without an automatic regulation system connected to the heater is there a risk of getting huge temperature differences between the air bath and fluid. And with regards to the equipment inside the Dewar container, this temperature differences could lead to shear stresses which eventually leads to cracks in the equipment, especially critical are the sapphire cell.

### **7.1.3.2 Cold finger regulator**

The temperature and cooling effect distributed to the cold finger is presently controlled manually, by regulating a valve on the top of the Dewar container, connected to the liquid nitrogen. The purpose with installing a cold finger was initially to be able to have a point in the process which held a lower temperature than the rest of the system; thus when the system is reaching equilibrium condition, the cold finger would be able to detect phase transitions before the rest of the system is cooled down to the given temperature. This way the cooling process can be done more efficient and the equilibrium point can be measured more precise. The problem is the regulation of this function, it would be an improvement if the valve was automatic regulated and connected with the temperature sensor placed in the cold finger. Thus it would be possible to automatic regulate the valve in the cold finger on the basis of a temperature function, or more suitable a temperature difference between the sapphire cell and cold finger.

### **7.1.4 Experimental determination by secondary detection**

These failures of the temperature control are leading to an unstable and uneven temperature distribution in the Dewar container and the interior system, thus the risk of getting freeze outs in parts of the system that are not available for visual detection are increasing. This is the main challenge related to the freeze out rig, involving several problematic factors, the most important are mentioned above. For the time being is the rig configuration suitable for performing experiments applying visual observation method (synthetic method), due to the sapphire cell and cold finger (SynVis) and secondary detection by plotting certain experimental variables in a suitable manner (SysNon). Since the experienced freeze outs starts in volumes which are not available for visual detection, thus the only possibility to determine the formation of solids is by using secondary detection; plotting the average pressure in the cell against the total volume [4]. This method is applicable on systems where it is known which component will precipitate and the amount of the solid phase are substantial. For methane rich binary systems with low concentration of the freezing component, this method is expected to be inadequate.

## **7.2 Freeze out on surfaces**

As long the system is cooled from a heat sink in the air bath, there will be a temperature gradient between the fluid, and the heat exchanger (gas evaporator). When the functionality of temperature control in the rig is operating with high inaccuracies, the result is high temperature differences between the fluid handling system and the air bath. Thus the risk of getting freeze outs on the surfaces in contact with the fluid increases.

This is also dependent of the thermal mass distribution in the system, in order to cool the system further down it is needed a temperature difference between the fluid and air bath. And since the amount of thermal mass is higher in the sapphire and blind cell compared to the pipes; the pipes are reacting more rapidly on temperature changes compared to the equilibrium cells. These pipes have recently been insulated, and together with a more steady temperature control the risk of freeze outs in these parts of the system will hopefully be decreased.

## 7.3 Sampling of different phases

The original configuration of the rig, allowed in principle to take out fluid samples from both; the sapphire cell and blind cell in addition to solid particles from the filter system. However, the solid sampling system failed early in the starting phase of the project, and was removed with the intention of getting the rig in operation sooner. Thus there are no possibilities for sampling the solid phase for the time being.

### 7.3.1 Sampling of solids

As mentioned introductorily, the only possibility to take samples of the solids from the sapphire cell and blind cell, through the filter system. Note that this is a modification project early in the design phase, for getting this system operating there are several challenges to overcome. First, the challenge is to lead the precipitated particles through the piping and to the filter.

One difficulty is that a substantial portion of the solid particles freezes on the surface of sapphire cell and not in the fluid mixture. The ratio of the solid particles precipitated in the fluid volume versus the surface area is dependent of the state of the fluid. It is experienced for pure carbon dioxide phase studies that freeze out from vapor mainly occur at the surface. Regarding freeze outs from liquid phase, are the precipitating process starting on the surface before one get crystal particles in the liquid surroundings. These particles which precipitate will slowly sink to the bottom of the sapphire cell or the blind cell, where there is an output leading to the filter system. This output constitutes a relatively small area of the bottom area in the cell, and in addition are phase studies requiring a low mass flow in the system; thus it can be imagined that it would be challenge to get enough solids to the filter. One measure to improve this condition, which requires modification of the sapphire cell, is to shape the bottom conical down to the outlet of the cell. This way the precipitated crystals will accumulate in the outlet of container.

The pumps will provide continuous flow through the sampling system. Since the pumps have a limited volume, you have to reverse the flow in cases where you have to refill one of the pumps. By running the flow through bypass valve, the particles on the filter are not disturbed by the reversed flow. Reversed flow through the filter would result in that the particles would get loose from the filter. When the filter captures particles, the pressure difference across the filter will increase, and due to the low sensitivity of the presently installed pressure sensors, it is difficult to detect the pressure difference. The sensors have an error margin of 0.1% of full scale (700 bars), something which is too high for detecting the pressure difference over the filter. To determine whether there are particles present on the filter, thus the time where there is a satisfactory quantity to sample on the filter, one must be able to measure pressure differences even as low as the Pascal (Pa) area. It had been appropriate to install a sensitive differential pressure gauge of the flow coming in and out of the pneumatic valves in sampling circuit.

Next challenge is to remove the solid particles from the filter and get it analyzed, either via a sample bottle or a directed connected gas chromatograph. In order to take samples of the particles that are caught on the filter, it is necessary to remove the surrounding fluid which is present in the filter volume between the pneumatic valves, and this without disrupting the phase equilibrium. The pneumatic sampling valves are connected with piping circuits I and G (shown in the P&Id of the original configuration in appendix D1) which exits the Dewar container and offers a possibility to connect sampling and sample analysis equipment. The most obvious method to remove the fluid

surrounding the filter is by using an inert gas at the same pressure and temperature as the mixture between the sampling valves, to avoid that the solid particles melts or evaporate. Probably it will be used helium as the flushing medium, since natural gas mixtures often contains nitrogen. A critical parameter here is the volume flow of the inert gas; this must be sufficient small to prevent the solid particles from falling off the filter. The flow direction of the inert gas should be same direction as the fluid mixture entered the filter with for the same reason, depending on circulation direction controlled by the pumps. After all the liquid has been removed solid on the filter, this mixture consisting of helium and solid particles is heated by the electric elements in the valves and filter housing and sent for analysis.

### **7.3.2 Sampling of liquid and vapor phase**

As mentioned while discussing the sapphire and blind cell, there are originally four outlets from the Dewar container including the outlets at the top and bottom of the sapphire and blind cell, the outlet in the bottom of the blind cell transport the fluid via the cold finger and further to a four-ended pipe connection where one of the pipes are leading out of the Dewar container. This last output are unfortunately been removed as part of the modification of the filter sampling system, thus the piping from the outlet of the blind cell goes directly to the bottom of the sapphire cell via the cold finger.

Presently there are possibilities to drain the vapor phase from both the top of the sapphire and blind cell, while the liquid phase is appropriate to drain from the bottom of the sapphire cell. Regarding sampling the liquid phase when there is solids present requires a measure to remove the solids particles. This can for example be done by a filter for preventing solids carrying over during sampling, ref. [33]. Another issue with the rig is as discussed earlier the temperature difference between the air bath and the fluid handling system, in sampling situation there will be a risk of getting condensation when sampling the vapor phase, and freeze outs when sampling the liquid, this applies the pipes running out of the Dewar container from the sapphire and blind cell. These pipes have been insulated as a result of the experimental work done previously. A further measure would be to install electric heating elements on the pipes lengths.



## **7.4 Detection of phase transitions**

The consequences related to the temperature control are also affecting the functionality of the different detection methods. The rig is originally equipped with two main detection systems, in form of a transparent sapphire cell and an infrared detection system in the cold finger. In addition it is possible to detect phase transitions by secondary detection. The types of mixtures available for investigation are systems where the solid forming component is known, due to the missing sampling system. Thus, the relevant systems for studying are mainly single component and binary component systems.

### **7.4.1 Visual detection in the Sapphire cell**

Since there have been detected freeze outs in other parts of the system than the sapphire cell at several instances, the reliability of the visual detection is highly uncertain. This affects the determination at which point in time the actual formation of crystals starts, thus it is difficult to determine the condition of the system at equilibrium.

In one instance, where the rig was operated with pure carbon dioxide it was experienced freeze out from the liquid phase in form of a transparent solid layer at the sapphire cell surface. This solid formation was not detected before the heating of the system took place, where it was observed a fine pattern of cracks in the solid layer as it was melting.

### **7.4.2 Infrared detector in the cold finger**

This system produces a signal expressed as a percentage of the reflected light waves in the mirror behind the fluid flow. Due to the phase transitions in the fluid this will result in a drop of the signal. From the previously completed experiments it is observed a slow drop in this signal without any phase transitions taking place, and it seems to vary with the temperature. This could be caused by density changes of the fluid, if this is true the signal is also dependent of the pressure and viscosity of the fluid. Hence, the signal will be affected by the mixture and the component properties. This is an issue necessary to investigate in more depth, and hopefully there is a way to compensate this drop in signal which would increase the reliability of the detection system.

### **7.4.3 Secondary detection**

This method is carried out by plotting the measured average pressure of the four pressure sensors against the total fluid volume, thus it is possible to detect the point in time when the freeze out starts by keeping a constant pressure in the system and compare the volume. When parts of the mixture start to form a solid phase the volume will decrease due to the change in density as long the pressure is held constant. It is experienced with pure liquid carbon dioxide that this process happens quite fast and the pumps don't have the capacity to keep a constant pressure, thus the pressure decreases and the temperature increases as the system is in equilibrium.

This method is applicable when the amount of the forming solids is relatively high, the highest possible total volume is 3620 milliliter and depending on how stable the pressure and temperature control are, it is reasonable to believe at least a few tenths of formed solid is needed to detect. This meaning in the area of parts per thousands, and it is quite optimistic to use this method in mixtures where it is expected to freeze a few parts per million (ppm) fractions.



## 8 Experimental results and model evaluation

Initially the experimental object was to validate the freeze out rig and produce new experimental data on the subject of freeze out from vapor phase, for carbon dioxide in binary methane rich mixture.

The previously experimental work has consisted of simple experiments to increase understanding of the operating characteristics and the functionality of the different system included in the rig. For this purpose it has been done several experiments for pure carbon dioxide, and it is in fact the only component which has been used in phase studies. However, by using this non-explosive, non-hazardous gas, a safe investigation of the rig is obtained. And by carry through the experimental work, presented in table 8-1, it is expected to reveal the overall capabilities of the rig. Based on this experience it should also be developed detailed and precise procedures for use of the rig. The initial experimental test matrix is presented in the table beneath, where the expected freeze out temperatures from simulations and literature are determined. The empty cells are indicating that there was no experimental data available for the specific conditions.

System	Comp. [mole %]	Pressure [bars]	Equilibrium	Expected freeze out temperatures				
				Simulations [K]		Experimental [K]		
				NeqSim	HYSYS	Temp	Pressure	Ref.
Pure CO <sub>2</sub>	-	9.25	SLE	216.49	216.18	216.68	9.25	[46]
	-	5.185	SLVE	216.58	216.58	216.58	5.185	[26, 27]
Methane - Carbon dioxide	90%	6.89	SVE	188.70	188.830	191.21	7.10	[36]
	10%	20.68	SVE	199.25	199.817	-	-	-
		41.36	SVE	-	204.036	-	-	-

Table 8-1 Experimental Test Matrix

The test matrix, table 8-1, confirms the original experimental objective of the project, where the rig are validated, through phase equilibrium experiments with pure carbon dioxide and low pressure binary mixture experiment with carbon dioxide and methane. Further it was planned to produce high pressure phase equilibrium data for same mixture. However, a safety analysis have to be carried out to make sure the rig are prepared, and the necessary safety precautions are meet for operating the rig with hydrocarbon mixtures. As described introductory in chapter 7, this is a quite time consuming process and have lead to postponements of the experimental work.

The problems related to detection of freeze outs are the main challenge in order to carry through the experiments including hydrocarbon dominant binary mixtures, thus it is natural to select a composition of 10 mole % carbon dioxide in the first binary mixture experiment. For the low concentration experiments it is necessary to improve the factors which cause the temperature difference in the vacuum insulated container, due to the expected problem of detecting small amounts of participated solids, as discussed in the previous chapter. The experience gathered from the binary carbon dioxide experiment would determine if it is possible to detect freeze outs of low concentration experiments. Hence, the binary experiments including heavier hydrocarbons are postponed.

The experiment including binary mixtures of carbon dioxide and methane was scheduled already in the 12<sup>th</sup> week in 2009 (between 16<sup>th</sup> and 20<sup>th</sup> of March). Most likely, the experiment can be accomplished in the turn of June, 2009; hence it is not relevant for this report.

## 8.1 Pure carbon dioxide experiment

The experimental objective for this investigation is to determine the freezing point temperature in liquid carbon dioxide and the triple point. The result from this experiment will indicate how accurate the rig is able to operate. The raw data from the experiment are available on the CD-ROM, attached to the report.

### 8.1.1 Experimental method

The freeze out rig (PVT 80/170) can be operated with various experimental methods and procedures. For description of the various experimental methods used in cryogenic phase studies see appendix C5. However, since the equilibrium cell is transparent there are possibilities for visually observe (SynVis) the phase transitions of the fluid.

In addition the rig is equipped with an infrared system placed in the cold finger, for investigating the phase behavior. Infrared radiation (IR) is a widely used experimental method (SynNon) for determining the freezing point of cryogenic systems. When it starts to form solids in the mixture the crystals will cause some reflection of the light rays in different directions, this leads to a change in the original signal. A critical issue is when a transparent solid formation occurs on the mirror surface, thus there will not be a change in the signal and the freeze out can't be detected. The temperature is recorded when the system detect a significant change in reflection, and this is considered to be the freezing point temperature.

#### 8.1.1.1 Procedure

The experiment should be carried out with pure carbon dioxide to observe the behavior of the fluid, by investigating the transition between liquid and solids. The experiment includes determination of freezing point temperature and the triple point at constant pressure. The detection methods used are detection with the IR detector and visual observation. The result will be analyzed and compared with relevant literature. Before the experiment, the normal procedures including flushing, connection of CO<sub>2</sub>, and isolation of the inner system carried through. The pressure is regulated first by using the pressure regulator to 9.25 bars; for securing pressure flexibility in the system, the bottle pressure are adjusted manually as close to this value as possible. The procedure is illustrated in the phase diagram beneath.

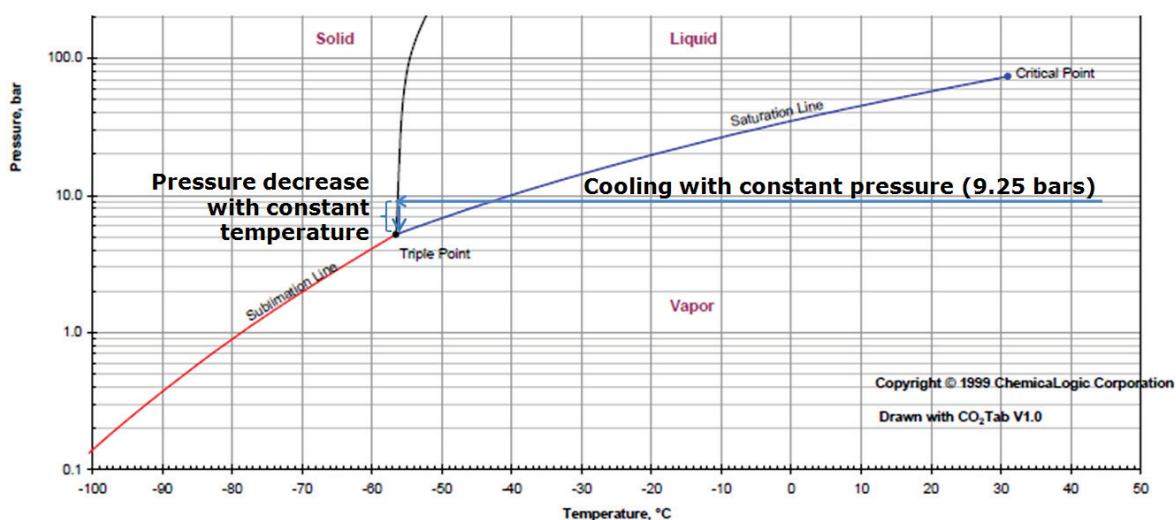


Figure 8-1 Phase diagram of pure carbon dioxide; indicating experiment procedure

Since the experiment doesn't require a lower cooling temperature than  $-70\text{ }^{\circ}\text{C}$ , the mechanical cooling system is used. The first step in the procedure is to condense the carbon dioxide, from gas to liquid phase. This is done by cooling the system with constant pressure, as indicated in figure 8-1.

#### **Vapor-Liquid phase transition**

The mechanical cooling system starts with a set point temperature of  $-40\text{ }^{\circ}\text{C}$  and is adjusted when the system temperature reaches this set point. Automatic pressure regulation is initiated at 9.25 bars in the computer, at the same time is the stirrer and circulation pump started. By the time the temperature in the sapphire cell reaches the previous set point temperature, a new set point temperature of  $-42\text{ }^{\circ}\text{C}$  with a small temperature ramp, to obtain a more precise temperature regulation and secure that the system is stable. The phase transition at this condition (a pressure of 9.25 bars) is at  $-42.22\text{ }^{\circ}\text{C}$ , calculated by REFPROP [46].

#### **Liquid-Solid phase transition**

When more and more fluid is condensing, a new temperature set point is initiated for the mechanical cooling system at  $-55\text{ }^{\circ}\text{C}$ , this is done to increase the condensation rate and get the system close to the expected liquid-solid line at  $-56.47\text{ }^{\circ}\text{C}$  (216.68K). At the point where the temperature in the sapphire cell is equal to the previous temperature set point at  $-55\text{ }^{\circ}\text{C}$  point, the circulation is stopped and a new temperature set point of  $-57\text{ }^{\circ}\text{C}$  is initiated. This procedure, by reducing the set point, is continued until the detection of a solid phase.

#### **Triple point procedure:**

At the time a solid phase is detected and freezing point temperature is determined with an acceptable temperature precision, the pressure is lowered to 5.185 bars and temperature set point are adjusted to  $-56\text{ }^{\circ}\text{C}$ . The temperature are held constant, while the pressure are reduced slowly until the environment in the cell are approaching the triple point and there are detected a gas phase.

### **8.1.2 Results**

Each step in the procedure was followed, however, the experiment lasted for two full days; due to the time needed for the mechanical cooling system to stabilize at the initiated temperature, the rig was left with liquid carbon dioxide inside over night. Thus the system is brought stable at a low temperature and the last part of the procedure can be completed efficiently. The logging rate was every ten seconds, hence the large number measurements. As mentioned, all the raw data are available on the CD-ROM attached to the report.

#### **8.1.2.1 Freezing point conditions**

After the system parameters were initiated to a temperature of  $-57\text{ }^{\circ}\text{C}$  and the pumps were automatic regulating the pressure to 9.25 bars, it was detected solid formation on the walls in the sapphire cell. The temperature and pressure in sapphire cell were at this time  $-56.64\text{ }^{\circ}\text{C}$  and 9.22 bars. However, there is a reason to believe the solid formation started someplace else than in the sapphire cell; at the same time was it detected a pressure difference between gas pump no. 1 and 3. This indicates that there was a blockage somewhere in the system between the two pumps. To confirm this theory, the automatic controlled valve EV7 (indicated in figure 6-3), which is placed outside the Dewar container and controls the bypass pipe between the pumps, was opened. This resulted in a pressure balancing between the pumps, thus a clear indication of a blockage. The valve EV7 was closed, and circulation was started to verify, and at the same time a measure for trying to remove the blockage, but instead it lead to a pressure difference between the pumps.

Figure 8-2 is presenting the system condition in the time period where the participated solid phase was detected in the sapphire cell; hence, the time period where the pressure drops occurred.

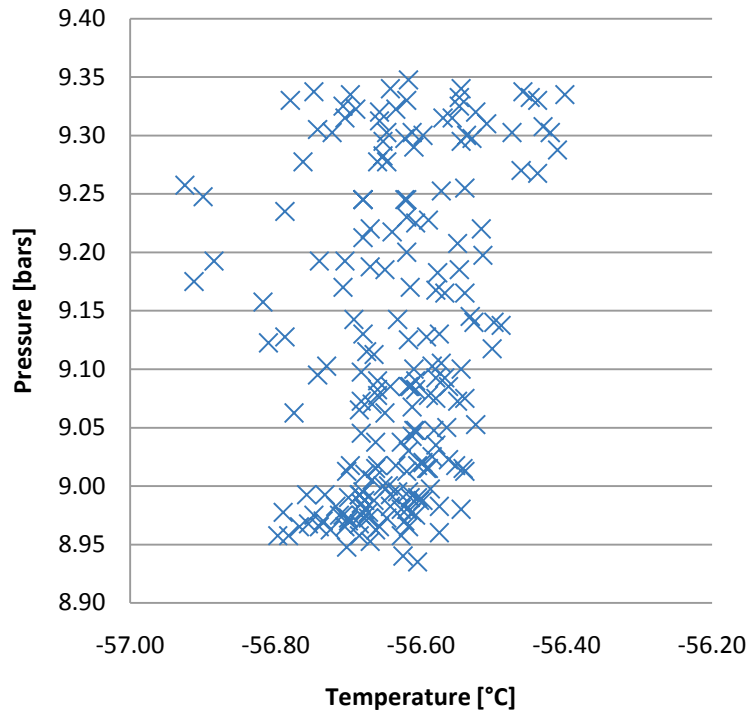


Figure 8-2 Pressure – Temperature diagram: Freezing point measurements [8632-8838]

The pressure and temperature values in the figure are average values, respectively from the pressure sensors in pump number 1, 3, sapphire cell and blind cell, and the temperature sensors placed in the air bath, sapphire cell, blind cell and in the cold finger. The system behavior corresponding to the figure is starting at a high pressure (ca. 9.35 bars) and this pressure was fluctuating upon cooling.

Further the pressure was varying close to 9.30 bars [8632-8677], until the average temperature reached a temperature of  $-56.93^{\circ}\text{C}$ , then the pressure started dropping [8678-8838] until the pumps were activated and controlled to keep a constant pressure of 9.25 bars. This pressure drop resulted in a minimum average pressure value of 8.94 bars in the system, referring to the figure 8-2. The temperature was reasonable stable in this sample interval [8678-8838], resulting in an average temperature calculated to  $-56.64^{\circ}\text{C}$ , with a standard deviation of  $0.0799^{\circ}\text{C}$ . This was the time where the pressure difference between the pumps was detected and a blockage was suspected. The pressure sensor on pump number 1 measured a pressure of 8.72 bars, while the pressure in pump number 3 was 9.2 bars, thus a difference of 0.48 bars.

Due to no visual determination, or an indication on the signal from the IR-detector it is difficult to determine precisely the time of the first formed solid particle. However, there are reasons for believing that the point where the temperature reached  $-56.93^{\circ}\text{C}$  was the initiating freezing conditions (pressure at this point was 9.26 bars, referring to sample number 8678). Since this is when the solid formation accelerated and caused a severe pressure drop, without any other interference on the system.

### 8.1.2.2 Solid-Liquid equilibrium

After this pressure drop was observed, the pumps were initiated to keep a constant pressure of 9.25 bars, as mentioned. This resulted in a stabilizing of the system, indicating by the horizontal increasing curve in figure 8-3, where the average pressure was increased from the low point at 8.94 bars to 9.15 bars. There was still a blockage of the system, thus the automatic controlled valve EV7 was opened to level out the pressure difference between the two pumps, or between the two sides of the blockage. This is indicated by the vertical line on the left hand side in figure 8-3. Note that the dynamics (volume decrease) of the system is moving from right to left in the diagram, indicated by the arrows in the figure.

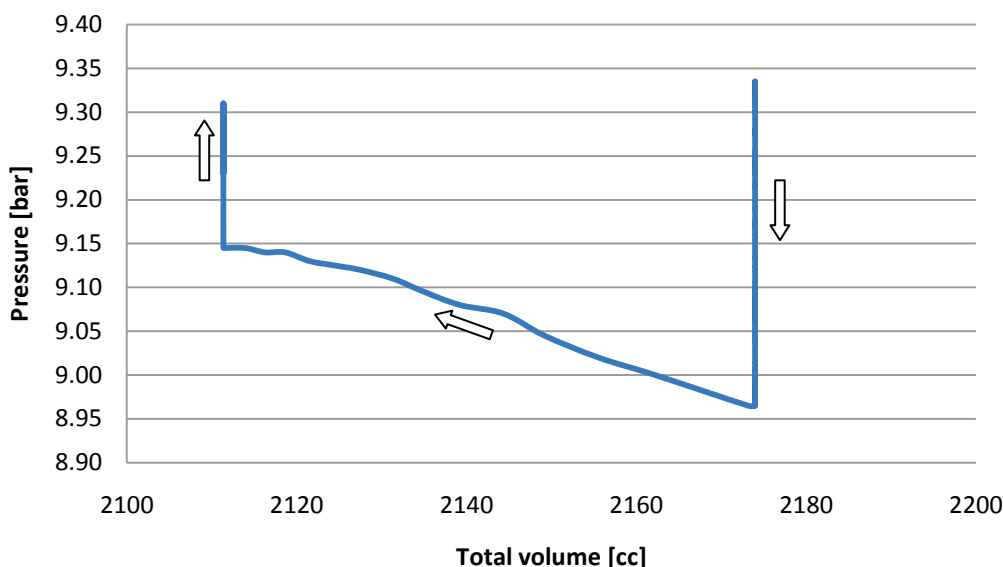


Figure 8-3 Pressure-Volume diagram: Pressure regulation measurements [8631-8969]

After this pressure regulation procedure, the pressure was trying to keep a stable pressure at 9.25 bars; however, the solid forming liquid resulted in small volume changes, which affected the pressure. Anyhow, this is as close the system got to a solid-liquid equilibrium state, and by studying the measured data the equilibrium temperature and pressures was determined, see table 8-2 beneath.

Parameter	Average	Standard deviation	Confidence interval	Number of points	Reference points	Volume changes [cc]
Temperature [°C]	-56.58	0.060	0.010	135	[8854-8988]	0.0012
Pressure [bars]	9.26	0.025	0.004			

Table 8-2 Calculated experimental sublimation conditions for pure CO<sub>2</sub>

Instead of using the standard deviation for reporting the density of the measurements, a confidence level method is used, due to the fluctuations of the system over time, which are affecting the system and resulting in non-equilibrium conditions. The calculations are based on a confidence level of 95 % (equals an  $\alpha = 0.05$ ), in which means that the temperature fluctuation over time are reduced, and the solid-liquid equilibrium temperature are determined within a interval of  $-56.58 \pm 0.010^\circ\text{C}$ , or corresponding  $216.57 \pm 0.010\text{ K}$ . Similar, the pressure measurements where within an interval of  $9.26 \pm 0.004\text{ bars}$ . This measured equilibrium temperature represent a deviation of  $0.11 \pm 0.010\text{ K}$

compared to the experimental sources reported in literature [46]. However, it is only compensated for the random errors in the measurements; the systematic (offset) errors are hard to determine due to the insufficient documentation of the measurements cards in the control system, and the temperature distribution in the Dewar container. Thus, the measurement accuracy is not determined, but the repeatability of the experiment is taken into account. The results are further discussed in chapter 8.2.

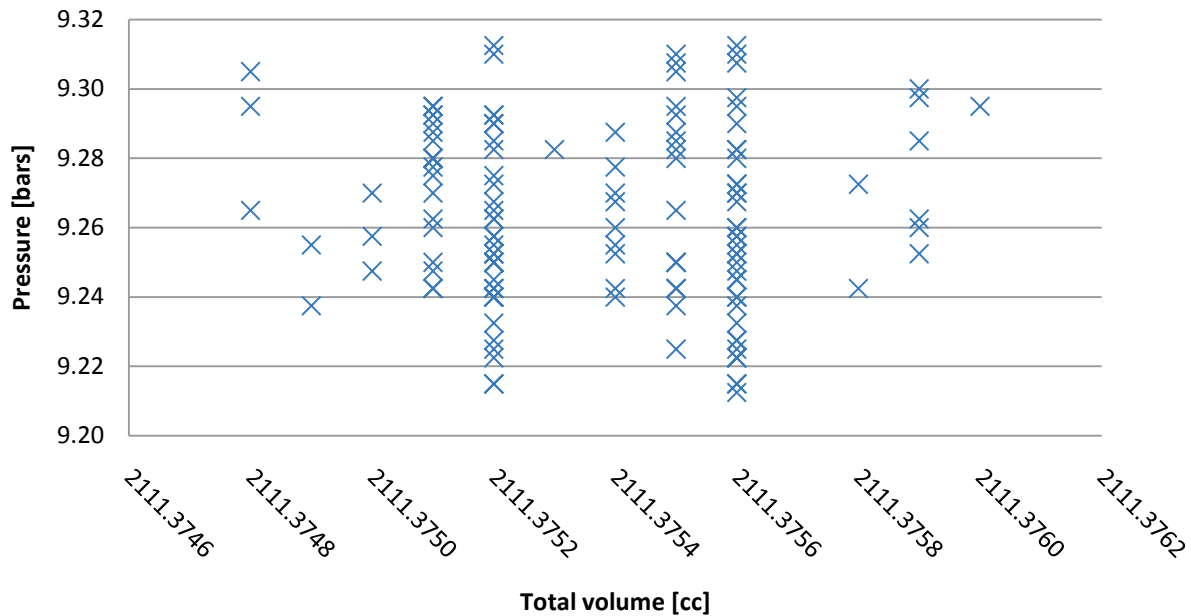


Figure 8-4 Pressure – Volume diagram: Solid-Liquid equilibrium measurements [8854-8988]

As mentioned previously, during this time period the system was quite stable, this is also confirmed by figure 8-4. Where the volume are plotted as a function of the pressure, considering the fact that the measurements are within a volume difference of 0.0012 cc, in which are close to a constant volume. Thus the conclusion of solid-liquid equilibrium is reached at the conditions stated previously.

### 8.1.2.3 Triple point

The one pump was initiated with a pressure of 6 bars to create a pressure gradient over the blockage and the valve (V3) on pump no. 3, connected to the carbon dioxide bottle was closed. This measure failed to remove the blockage, and instead the other pump was initiated to reduce the pressure to 6 bars. At this point it was observed that the solid formation on the walls of the sapphire cell had been solved in the liquid and a while later the blockage in the pipes disappeared. This was detected by a pressure drop in pump number 1. Next, the pumps were adjusted to 5.185 bars, and it was registered that the signal from the IR detector in the cold finger got reduced. In addition to adjusting the pumps, the valve (V8) was opened to rapidly reduce the pressure. And after the temperature set point in the sapphire cell was further reduced it were detected three phase conditions in the sapphire cell, with liquid in the bottom, gas between and solid formation in the top of the cell. The system was slowly brought down in pressure until there were detected a vapor phase in the sapphire cell. During this pressure letdown period the signal from the IR detector has fluctuating a lot, however, the signal went up again when entering the three-phase equilibrium conditions. Since the valve, controlling the feed from the carbon dioxide bottle, have been closed there is no fluid entering the system. Thus the condition regarded as the triple point; is where the volume changes are the



smallest, due to the pressure regulation there will always be small variation. The results of the calculations done to determine the three phase conditions are presented in table 8-3.

Parameter	Average	Standard deviation	Confidence interval	Number of points	Reference points	Volume changes [cc]
Temperature [°C]	-56.40	0.091	0.019	91	[9978-10068]	8.3381
Pressure [bars]	5.18	0.007	0.001			
Temperature [°C]	-56.44	0.074	0.019	61	[10008-10068]	0.09710
Pressure [bars]	5.18	0.006	0.001			

Table 8-3 Calculations of experimental triple point conditions for pure CO<sub>2</sub>

With this volume difference in consideration, presented in table 8-3, the most precise measurements is for the time period including the last 61 data points. This could also be seen from the difference in standard deviations between the two measuring periods. Thus the three phase point for pure carbon dioxide is experimental determined with a temperature of  $-56.44 \pm 0.019^\circ\text{C}$  ( $216.71 \pm 0.019$  K), calculated with a confidence level of 95 %. Similar are the pressure determined to  $5.18 \pm 0.001$  bars. These measurements represent a temperature deviation of  $0.13 \pm 0.019$  K, and a pressure deviation of  $0.01 \pm 0.001$  bars, compared to the experimental values in the literature [26, 27], which are 216.58 K and 5.185 bars. The results are further discussed in chapter 8.2.

The points in the second measurements interval are plotted in figure 8-5, in a pressure-temperature diagram. However, there are several points outside the core of samples, but these points are to some extent corrected for by using a confidence level of 95 %.

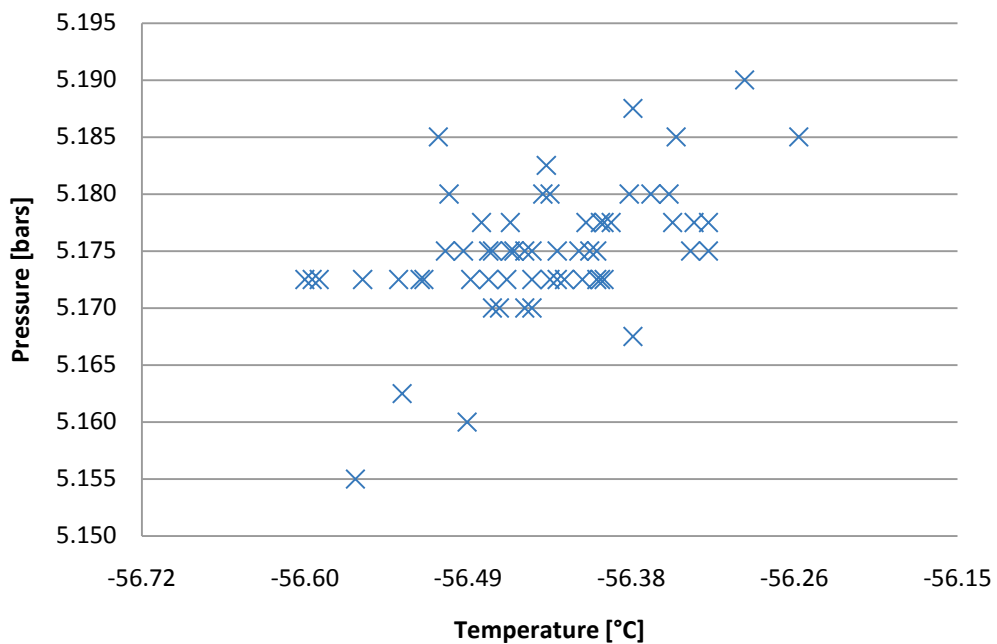


Figure 8-5 Pressure – Temperature diagram: Triple point measurements [10008-10068]

The figure may be hard to analyze since several points are on top of each other, however, there are a gathering of points in the middle, close to the conditions determined above.

#### 8.1.2.4 Detection of the phase transitions

Regarding the determination of the freeze outs and solids in the system, it was impossible to visually determine when the first crystallization occurred, due to the fact that the solids were formed at places in the system which was unavailable for visual detection. This was determined by the pressure differences in the system, indicating a blockage. From the earlier work done in relation to the rig, it is known that critical location of unwanted freeze out is in the pipes between the two equilibrium cells, since this is known to be the coldest points of the system. This experiment was carried out before the insulation of the pipes was installed. However, it is expected that the insulation will partially prevent these large temperature differences in the air bath and thus decrease the risk of blockage in the pipes.

In addition to the possibility of visually detect the phase transition, the IR-detection system in the cold finger was used to investigate the functionality of this method. However, the optimal use of this technique is by cooling the cold finger with liquid nitrogen and use the IR-signal to detect phase transitions before the temperature in the sapphire cell reaches the temperature in the cold finger, this way it is possible to detect phase transitions and freeze outs in advance. Especially useful when investigating mixtures at conditions where the freezing temperature are unknown. By applying this operational method the IR-signal would be more reliable, since the freeze outs would occur at the mirror in the cold finger. In this experiment the location of the freeze outs are unknown and the IR-signal was only able to detect if there were any solid particles in the fluid flow through the cold finger. The signals from the IR-detection system during the time period it were solids in the system are plotted in figure 8-6.

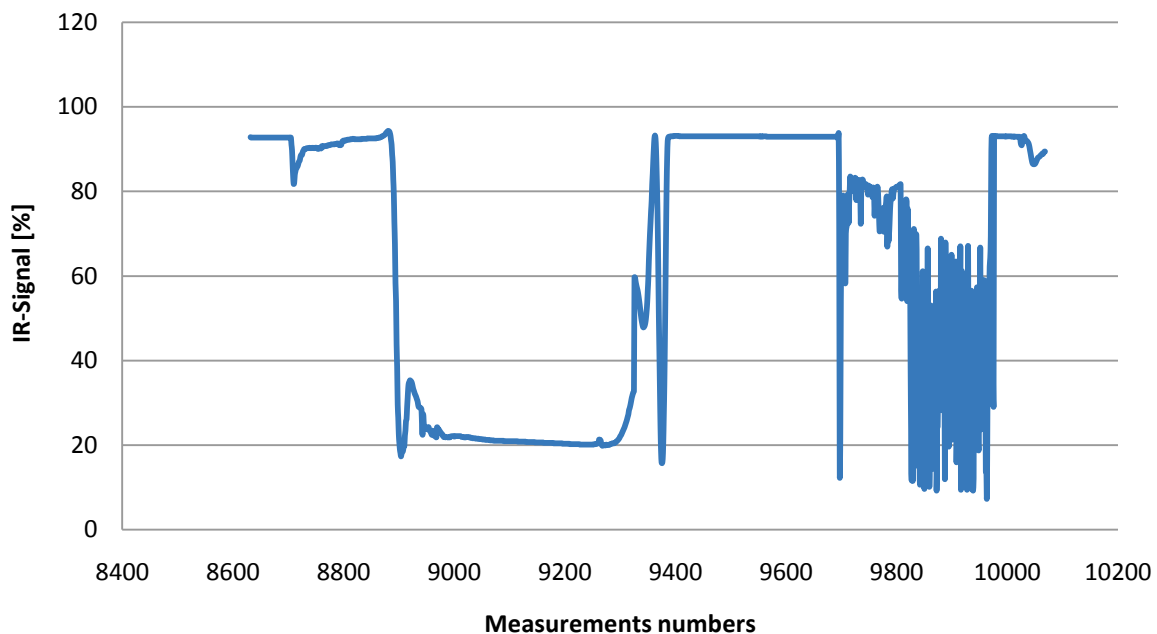


Figure 8-6 IR-signal during phase transitions [8632-10068]

By studying the measurement data, a possibly freezing point has been determined at the conditions corresponding to the measurement point 8678. However, this is only an assumption and there are circumstantial uncertainties involved. The signal at this point where stable at 92.7 %, and the signal didn't start dropping until the average pressure reached 9.14 bars (measurement point 8707). This is

indicating by the first signal drop at the left hand side in figure 8-6. Next, the signal dropped during the period between the measurement numbers 8887 and 8905, where the signal dropped from 91 % to 18 %. This is interpreted as a clear indication of solids in the system, but almost a half hour after the first indication of liquid-solid transition. Next, the signal increases again close to the initial level at 93 %, this may indicate that the solid formations which caused the blockage was dissolved in the liquid, due to the pressure reduction. The system is then stable until the pressure and temperature are reaching the triple point, where the mixture including both the liquid and solid phase start evaporating, causing an extremely varying signal. Before the system is stable at the triple point, this is the time period used in determining the triple point conditions (measuring points 10008-10068).

For this experiment the signals can only be used for interpretation of the phase behavior, and not detect any phase transitions in advance, but as mentioned previously, by using the liquid nitrogen cooling of the cold finger the functionality are expected to improve. However, there are experienced temperature drifts in earlier experiments of the signal from the IR-detector which requires further research.

## 8.2 Discussion of the results and model evaluations

The results from the experiment are presented in table 8-4, where the data selection were based on minimizing volume changes as far as possible to ensure that the system were stable. Further the number of data point's and the standard deviation was considered in order to select the most consistent dataset. However, is difficult to determine the accuracy of the measurements; some of the possible systematic and random errors are discussed beneath.

Condition	Experimental result		Data from literature			Deviations	
	Temperature [K]	Pressure [bars]	Temperature [K]	Pressure [bars]	Ref.	Temperature [K]	Pressure [bars]
<b>Solid-Liquid equilibrium</b>	216.57 ±0.018	9.26 ±0.004	216.68	9.25	[46]	0.110	0.010
<b>Triple point</b>	216.71 ±0.019	5.18 ±0.001	216.58	5.185	[26, 27]	0.130	0.005

Table 8-4 Experimental results and data from literature

The temperature sensors have previously been calibrated in order to reduce the systematic errors, the temperature sensors were calibrated with the use of liquid nitrogen and dry ice as reference temperatures. However, the documentation of the measurement system is currently insufficient in order to determine the temperature measurement accuracy of the rig. There are determined some systematic errors causing deviations in the experiment; placement of the temperature sensors and the temperature distribution in the air bath. The location of the temperature sensors in the sapphire and the current temperature sensor in the blind cell are placed in the steal bottom of the cells, while instead they should be placed in the fluid.

Regarding the temperature distribution, consider figure 8-7 which shows the temperature variations in the air bath, sapphire cell and in the cold finger. As described in chapter 7, the air bath temperature sensor is placed at the suction side of the circulation fan, which is on the hot side of the heat-exchanger, in the bottom of the air bath. Hence the temperature measured in the air bath is higher than the temperatures in sapphire cell, blind cell and cold finger. The temperature difference between the sapphire cell and cold finger is caused by the location of the cold finger; it is placed at a lower level in the air bath, in addition is it known that the cold finger has a considerable lower mass than the equilibrium cells. Thus it will more rapidly respond to temperature changes in the air bath.

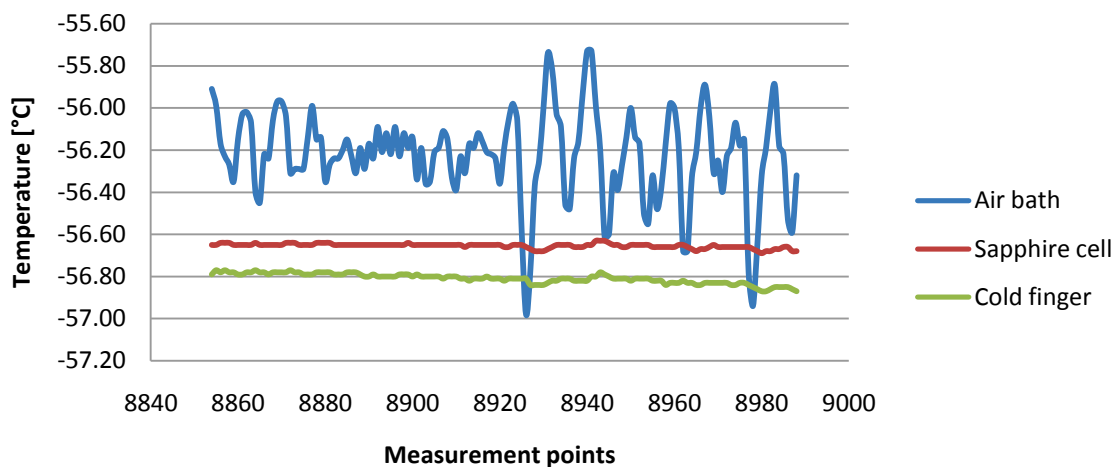


Figure 8-7 Temperature variations in the air bath: Solid-Liquid equilibrium [8854-8988]

However, if the heat loss from the air bath had been reduced it would result in smaller temperature gradients in the air bath, and a more uniform temperature distribution. Further, by using an average value of the four temperature sensors placed in the system is also a systematic error, however, selecting another method of determine the “real” temperature would not improved the calculations, since the calculations still would be based on assumptions. In order to reduce these systematic errors, the temperature sensors should be calibrated, and the measurement system sufficiently documented for determining the accuracy of the measuring process.

Regarding the random errors, the most severe is the temperature fluctuation in the air bath, due to the poor regulation of the mechanical cooling system. This error is somehow compensated for due to the calculations are based on average temperatures over time, thus the precision of the measurements are considered to be sufficient. Hence, the calculations have determined the repeatability of the experiment, which constitute a good foundation to base the future experiments on when investigating the systematic errors and the accuracy of the freeze out rig.

The experimental results gathered in this experiment are not of any value to the work with the thermodynamic models, since the carbon dioxide properties are extensively documented elsewhere [26]. However, similar single component experiments for benzene and cyclohexane would be of great value, due to the widespread in the experimental determined component properties. As presented in table 8-1, the simulated values for the triple point for pure carbon dioxide are exactly the same as the experimental determined conditions, due to the fact that these values are used in the models. The area of application is also not representative for the NeqSim model, which is intended to be used on natural gas mixtures and not pure fluids. However, the potential of using NeqSim in the further experimental work with the rig are clear, by developing thermodynamic models further in parallel with the experimental work. Thus the simulations can be used in the planning of experiments for mixtures where experimental data from the literature are absent and the experimental data obtained can further validate the proposed models. There should be a close relationship between the two research areas; this would also be advantageous in form of the total understanding of the phase behavior in multi-component mixtures including a solid phase.



## 9 Conclusion

From the literature study related to modeling and predictions of freeze out in natural gas systems, it is recognized two main methods of describing the solid-fluid equilibrium and predicting freezing point temperatures; the use of empirical correlated activity coefficients have previously been the only method to describe solid-fluid equilibrium systems, due to the difficulties of describing the solid phase in fluid mixtures. However, lately the focus has been to develop a more general correlation of the solid-fluid equilibrium, due to a scarce experimental database. And have resulted in a method based on equations of state for the description the fluid phases, in combination with an expression for the solid phase fugacity, dependent on the melting and triple point properties. This method is based on the assumption of a pure solid phase; this may be a limiting assumption in regards to natural gas systems. However, in binary mixtures this assumption represents the highest risk of solid formation at a given temperature.

### **Experimental equilibrium data and model evaluation**

For the simulations carried through in NeqSim and HYSYS is the Soave-Redlich-Kwong equation of state selected, and there is no significant difference in the accuracy compared to the Peng-Robinson equation of state. It is also recognized from previously work, that these equations of state are widely used for describing the fluid phases in solid-fluid equilibrium calculations, and the prediction of freezing point temperatures.

It has been discovered that the general correlation, which NeqSim represents, including the use of Soave-Redlich-Kwong and classical mixing rules with binary interaction parameters; is able to predict the freezing point temperatures of carbon dioxide in liquid methane binary mixtures close to the accuracy of the activity coefficients based model, represented by the GPA simulation tool. And the NeqSim model performs even better than the commercial simulation tool HYSYS. This is partially due to the fact that HYSYS are using mixing rules without binary interaction parameters for the solid-fluid systems. The optimal binary interaction parameter for the methane-carbon dioxide system is determined to be 0.12; however, the interaction parameter dependency for SVE systems is discovered to be less than in SLE systems. The binary interaction parameters are discovered to be of crucial importance to the accuracy of the predictions, both for the binary mixtures containing carbon dioxide and the heavy hydrocarbons.

The computation of binary mixtures including methane and heavier hydrocarbons is more challenging due to numerical challenges. For the binary mixtures consisting of methane and benzene the NeqSim model was not able to predict reliable freezing point temperatures for mixtures containing more than 0.001 mole % of benzene. In contrast did the GPA simulator managed to calculate mixtures containing higher benzene concentrations.

Regarding the low concentration predictions for mixtures containing benzene, a binary interaction parameter equal to 0.0909 was recognized as an optimal value. The interaction parameter for methane binary mixtures including cyclohexane was not possible to investigate, due to the numerical problems. However, in order to extensively validate the proposed models; there is discovered a need of more experimental data on the subject of solid-fluid equilibrium for heavy hydrocarbons in binary methane rich mixtures.

### **Experimental work related to the freeze out rig**

The current state of the freeze out rig makes it incapable of studying these mixtures, thus the focus of the experimental work has been to investigate the behavior and trouble-shooting of the rig. From the experience gathered it has been confirmed that the rig are not yet able to conduct useful phase studies with the binary mixtures of interest.

Hence, it has been carried out a pure carbon dioxide experiment, where solid-liquid equilibrium and the triple point were determined. The solid-liquid equilibrium was measured at a pressure of 9.26 bars and a temperature of -56.58°C, while the triple point was determined at 5.18 bars and -56.44°C. The precision of the measurements were considered to be sufficient, however the temperature fluctuation in the air bath which are leading to unstable conditions was corrected for by handling the temperature and pressure measurements as average values. Hence the repeatability of the experiment is preserved and forms a good foundation for further developing and improvements of the rig. In order to increase the accuracy of the measurements the systematic errors in the temperature measurements should be corrected; the temperature sensors in the sapphire cell and blind cell should be placed in the fluid, and the air bath temperature sensor should be placed at a location in which represent the average air bath temperature.

In order to operate the rig with binary mixtures where the component exposed to freeze outs are known, the detection system have to be capable to detect small fractions of precipitated solids. However, there is a risk of freeze outs in pipelines and areas which are not available for visual detection, due to large temperature difference between the air bath and fluid. Hence, the detection of phase transitions is limited to the use of a secondary detection method, by analyzing the measured average pressure in regards to volume changes in the system.

For mixtures containing a low concentration of the component exposed to crystallization and the amount of forming solids are low, this method is expected to be insufficient in order to determine the freezing points. However, by reducing the heat loss from the Dewar container the temperature distribution within the air bath will be more uniform. This heat loss is reduced by installing a multilayer radiation shield and lowering the vacuum pressure to  $10^{-4}$  torr between the two cylinder walls of the Dewar container. When implementing these measures it is expected to be able to visually detect freeze outs through the sapphire cell, thus the rig is capable of operating with known compositions where the component exposed to freeze outs also is known, e.g. the binary mixtures investigated in this study.



## 10 Further work

Based on the investigation of the NeqSim application, it is recognized that NeqSim represent a flexible environment which are well suited for testing and validation of different thermodynamic models, in form of the advantage by programming in the object oriented language Java. Hence, the further work regarding determination and optimization of the various binary interaction parameters with the use of Soave-Redlich-Kwong equation of state and the expression for the solid fugacity; are recommended to involve the use of NeqSim. Regarding the calculations of methane rich binary mixtures including hydrocarbons; this includes investigation of the computational problems for mixtures with higher benzene content than 0.01 mole %, and the problems experienced with cyclohexane. Further it is recognized a wide acceptance for a temperature-dependent interaction parameter, hence, the dependency should be further investigated and implemented in the NeqSim model.

It is necessary to optimize the model with regards to the component parameters used in the solid fugacity expression, including the enthalpy of sublimation and the triple point properties. This may be done by fitting the parameters to experimental data available, however, the existing database for the heavy hydrocarbons investigated are scarce. The method is based on the assumption of a pure solid phase. For investigating whether this is a limiting assumption it is necessary with more experimental data of natural gas mixtures containing more realistic compositions than the binary mixtures investigated in this study. One of the main issues concerning the developing of reliable thermodynamic models for solid-fluid systems is the lack of experimental data, which prevents extensive validation of the proposed models.

Hopefully the freeze out rig at StatoilHydro research center will provide the research environment with high quality experimental data of such mixtures. However, in order to produce solid-fluid equilibrium data including binary hydrocarbon dominant mixtures there are several challenges, related to the freeze out rig, which have to be solved. First, reducing the heat loss and make sure the temperature distribution within the air bath are uniform. This would result in a lower risk of phase transitions in locations which are unavailable for visual observation, and leads to freeze outs in the sapphire cell, where it can be detected. Secondly, the temperature sensors in the sapphire cell and blind cell have to be located where they can measure the temperature of the fluid mixtures.

Further, for studying multi-component mixtures, similar to real natural gas mixtures, where the composition of the precipitating substance is unknown; a solution for the sampling of the different phases has to be developed, including extensively testing and validation.



## References

1. Kurata, F., *Solubility of Solid Carbon Dioxide in Pure Light Hydrocarbons and Mixtures of Light Hydrocarbons*. Gas Processors Association, 1974. **Research Report RR-10**.
2. de Hemptinne, J.C., *Benzene crystallization risks in the LIQUEFIN liquefied natural gas process*. Process Safety Progress, 2005. **24**(3): p. 203-212.
3. Eggeman, T. and S. Chafin, *Beware the pitfalls of CO<sub>2</sub> freezing prediction*. Chemical Engineering Progress, 2005. **101**(3): p. 39-44.
4. Amble, S. and V.F. Lavik, *Freezing point and freeze out in natural gas systems*, in *Department of Energy and Process Engineering*. 2008, NTNU: Trondheim. p. 122.
5. Solbraa, E., *Equilibrium and Non-Equilibrium Thermodynamics of Natural Gas Processing*, in *Fakultet for ingeniørvitenskap og teknologi*. 2002, Norwegian University of Science and Technology, Faculty of Engineering Science and Technology: Trondheim. p. 332.
6. Michelsen, M.L. and J.M. Mollerup, *Thermodynamic models: fundamentals & computational aspects*. 2004, Holte: Tie-Line Publications. XIV, 330 s.
7. Løkken, T.V., et al., *Water content of high pressure natural gas: Data, prediction and experience from field*, in *IGRC (International Gas Union Research Conference)*. 2008: Paris, France.
8. Folas, G.K., et al., *Data and prediction of water content of high pressure nitrogen, methane and natural gas*. Fluid Phase Equilibria, 2007. **252**(1-2): p. 162-174.
9. Knapp, H., M. Teller, and R. Langhorst, *Solid liquid equilibrium data collection: Binary systems* DECHEMA Chem. Data Ser, 1987. **VIII**.
10. ZareNezhad, B., *Prediction of CO<sub>2</sub> freezing points for the mixtures of CO<sub>2</sub>-CH<sub>4</sub> at cryogenic conditions of NGL extraction plants*. Korean Journal of Chemical Engineering, 2006. **23**(5): p. 827-831.
11. *GPSA Engineering Data Book*. Vol. Eleventh Edition. 1998, Gas Processors Suppliers Association: Tulsa
12. Hlavinka, M.W. and V.N. Hernandez, *Proper Interpretation of Freezing and Hydrate Prediction Results from Process Simulation*.
13. Davis, J.A., N. Rodewald, and F. Kurata, *Solid-Liquid-Vapor Phase Behavior of the Methane-Carbon Dioxide System*. Aiche Journal, 1962. **8**(4): p. 537-539.
14. Kohn, J.P. and K.D. Luks, *Solubility of Hydrocarbons in Cryogenic LNG and NGL Mixtures*. Gas Processors Association, 1976. **Research Report RR-22**.
15. Luks, K.D., et al., *Measurement and Prediction of the Solubility of Hydrocarbons in Cryogenic LGN and NGL.*, in *Proceedings, Annual Convention - Gas Processors Association*. 1978. p. 25-29.
16. Carter, K. and K.D. Luks, *Extending a classical EOS correlation to represent solid-fluid phase equilibria*. Fluid Phase Equilibria, 2006. **243**(1-2): p. 151-155.
17. Luks, K.D., J.D. Hottovy, and J.P. Kohn, *3-Phase Solid-Liquid-Vapor Equilibria in the Binary Hydrocarbon Systems Methane-Normal-Hexane and Methane-Benzene*. Journal of Chemical and Engineering Data, 1981. **26**(4): p. 402-403.
18. Rijkers, M.P.W.M., et al., *Experimental-Determination of the Phase-Behavior of Binary-Mixtures of Methane+Benzene*. Fluid Phase Equilibria, 1992. **77**: p. 327-342.
19. Neumann, A., R. Mann, and W.D. von Szalghary, *Solubility of solid benzene in liquid hydrocarbons*. Kaeltetech Klim, 1972. **24**: p. 145-149.
20. Solbraa, E., *NeqSim USERS GUIDE*. 2002, Norwegian University of Technology and Science.
21. Perry, R.H. and D.W. Green, *Perrys's Chemical Engineers' Handbook*. 1999: McGraw-Hill.
22. Wei, Y.S. and R.J. Sadus, *Equations of state for the calculation of fluid-phase equilibria*. Aiche Journal, 2000. **46**(1): p. 169-196.

23. Poling, B.E., J.P. O'Connell, and J.M. Prausnitz, *The properties of gases and liquids*. 2001, New York: McGraw-Hill. 1 b. (various pagings).
24. Elliott, J.R., *Introductory chemical engineering thermodynamics*. 1999.
25. Rydberg, T., *Freezing in hydrocarbon mixtures and CO<sub>2</sub>*, in *Energi og prosessteknikk*. 2003, NTNU: Trondheim. p. 69.
26. Angus, S., B. Armstrong, and K.M. de Reuck, *International Thermodynamic Tables of the Fluid State - 3 Carbon Dioxide*, Pergamon, New York. 1976.
27. Linstrom, P.J. and W.G. Mallard, *NIST Chemistry WebBook - NIST Standard Reference Database Number 69*
28. *BYU edition of DIPPR database, Brigham Young University, Provo, UT*, in *Design Institute of Physical Properties (DIPPR)*. 2003, BYU.
29. Kohn, J.P. and K.D. Luks, *Solubility of Hydrocarbons in Cryogenic LNG and NGL Mixtures (An Update of Research Report RR-22)*. Gas Processors Association, 1977. **Research Report RR-27**.
30. Kohn, J.P. and K.D. Luks, *Solubility of Hydrocarbons in Cryogenic LNG and NGL Mixtures*. Gas Processors Association, 1978. **Research Report RR-33**.
31. Keeler, R.M., *User's Guide for Predicting Solid-Liquid-Vapor Equilibrium in LNG and NGL Systems* Gas Processors Association: Tulsa, Oklahoma.
32. *Aspen Plus 11.1 User Guide*. 2001, Aspen Technology, Inc.: Cambridge, MA.
33. Cheung, H. and E.H. Zander, *Solubility of Carbon Dioxide and Hydrogen Sulfide in Liquid Hydrocarbons at Cryogenic Temperatures*. Chem. Eng. Progress Symposium Series, 1968. **64**: p. 34-43.
34. Kurata, F., *Solubility of Heavier Hydrocarbons in Liquid Methane*. Gas Processors Association, 1975. **Research Report RR-14**.
35. Kohn, J.P., et al., *Three-Phase Solid-Liquid-Vapor Equilibria of the Binary Hydrocarbon Systems Methane-n-Octane and Methane-Cyclohexane*. Journal of Chemical & Engineering Data, 1977. **22**(4): p. 419-421.
36. Agrawal, G.M. and R.J. Laverman, *Phase behavior of the methane carbondioxide system in the solid-vapor region*. Adv. Cryog. Eng., 1974. **19**: p. 317-338.
37. Le, T.T. and M.A. Trebble, *Measurement of carbon dioxide freezing in mixtures of methane, ethane, and nitrogen in the solid-vapor equilibrium region*. Journal of Chemical and Engineering Data, 2007. **52**(3): p. 683-686.
38. Brewer, J. and F. Kurata, *Freezing Points of Binary Mixtures of Methane*. Aiche Journal, 1958. **4**(3): p. 317-318.
39. Donnelly, H.G. and D.L. Katz, *Phase Equilibria in the Carbon Dioxide & Methane System*. Industrial & Engineering Chemistry, 1954. **46**(3): p. 511-517.
40. Pikaar, M.J., *A Study of Phase Equilibria in Hydrocarbon-CO<sub>2</sub> System*. 1959, University of London: London.
41. Kohn, J.P. and K.D. Luks, *L-L-V equilibria in cryogenic mixtures*. Gas Processors Association, 1981(Technical Paper RR-49).
42. Kuebler, G.P. and C. McKinley, *Solubility of solid benzene, toluene, n-hexane, and n-heptane in liquid methane*. Journal Name: Adv. Cryog. Eng.; (United States); Journal Volume: 19, 1974: p. Medium: X; Size: Pages: 320-6.
43. *P&Id - PVT 80/170 Low Temperature: Short Term Modifications*, L.T.R.S.T. MODIFICATIONS.pdf, Editor. 2008, StatoilHydro.
44. *Drawing pumps and tubing*. 2007, Sanchez Technologies.
45. Flynn, T., *Cryogenic Engineering, Second Edition, Revised and Expanded*: Routledge, USA. 895.
46. Lemmon, E.W., M.L. Huber, and M.O. McLinden, *REFPROP*, National Institute of Standards and Technology (NIST) Boulder, CO 80305.
47. Prausnitz, J.M., R.N. Lichtenthaler, and E.G.d. Azevedo, *Molecular thermodynamics of fluid-phase equilibria*. 1999, Upper Saddle River, N.J.: Prentice-Hall PTR. XXIII, 860 s.

48. Fornari, R.E., P. Alessi, and I. Kikic, *High-Pressure Fluid Phase-Equilibria - Experimental Methods and Systems Investigated (1978-1987)*. Fluid Phase Equilibria, 1990. **57**(1-2): p. 1-33.
49. Dohrn, R. and G. Brunner, *High-Pressure Fluid-Phase Equilibria - Experimental Methods and Systems Investigated (1988-1993)*. Fluid Phase Equilibria, 1995. **106**(1-2): p. 213-282.
50. Christov, M. and R. Dohrn, *High-pressure fluid phase equilibria - Experimental methods and systems investigated (1994-1999)*. Fluid Phase Equilibria, 2002. **202**(1): p. 153-218.
51. Sterner, C.J., *Phase Equilibria in CO<sub>2</sub>-Methane Systems*. Adv. Cryog. Eng., 1961. **6**: p. 467-474.
52. Mraw, S.C., S.-C. Hwang, and R. Kobayashi, *Vapor-liquid equilibrium of the methane-carbon dioxide system at low temperatures*. Journal of Chemical & Engineering Data, 1978. **23**(2): p. 135-139.



## Appendix

Appendix .....	97
Appendix A1 - Mixing rules: Combining rules .....	99
Appendix A2 - Two phase TP-flash .....	101
A2.1 Deduction of the stability criterion .....	101
A2.2 Stationary point.....	101
Appendix A3 - Phase envelope calculations.....	103
Appendix B1 - NeqSim.....	105
B1.1 The Thermodynamic Module .....	105
B1.2 Thermodynamic Library .....	106
Appendix B2 - GPA: The Thermodynamic description of the problem.....	107
Appendix C1 - Thermodynamic models used in simulations .....	111
C1.1 NeqSim predictions with PR and SRK EOS compared to Agrawal [36] .....	111
C1.2 HYSYS predictions with PR and SRK EOS compared to Agrawal [36] .....	112
Appendix C2 - Experimental data from literature and simulated data: Binary CO <sub>2</sub> -CH <sub>4</sub> system ....	114
C2.1 Solubility of CO <sub>2</sub> in liquid CH <sub>4</sub> : Predictions and experimental data from Kurata [1].....	114
C2.2 Solubility of CO <sub>2</sub> in liquid CH <sub>4</sub> : Predictions and experimental data from Davis [13].....	115
C2.3 Solubility of CO <sub>2</sub> in liquid CH <sub>4</sub> : Predictions and experimental data from Cheung [33] .....	116
C2.4 Solubility of CO <sub>2</sub> in CH <sub>4</sub> : Predictions and experimental data from Agrawal [36] .....	117
C2.5 Solubility of CO <sub>2</sub> in CH <sub>4</sub> : Predictions and experimental data from Le [37] .....	118
C2.6 Solubility of CO <sub>2</sub> in CH <sub>4</sub> : Predictions and experimental data from Davis [13].....	119
C2.7 Binary interaction parameter dependency in NeqSim model: Predictions and experimental SLE data from Kurata [1] .....	120
C2.8 Binary interaction parameter dependency in NeqSim model: Predictions and experimental SLE data from Davis [13] .....	121
C2.9 Binary interaction parameter dependency in NeqSim model: Predictions and experimental SVE data from Davis [13].....	122
C2.10 Binary interaction parameter dependency in NeqSim model: Predictions and experimental SVE data from Agrawal [36] .....	124
C2.11 Accuracy of different simulation tools compared with experimental data from Kurata [1] .....	126
Appendix C3 - Experimental data from literature and simulated data: Binary C <sub>6</sub> H <sub>6</sub> -CH <sub>4</sub> system ....	127
C3.1 Solubility of C <sub>6</sub> H <sub>6</sub> in CH <sub>4</sub> : Predictions and experimental data from Kurata [34] .....	127
C3.2 Solubility of C <sub>6</sub> H <sub>6</sub> in CH <sub>4</sub> : Predictions and experimental data from Neumann [19] .....	128

C3.3 Solubility of C <sub>6</sub> H <sub>6</sub> in CH <sub>4</sub> : Predictions and experimental data from Luks [17] .....	129
C3.4 Solubility of C <sub>6</sub> H <sub>6</sub> in CH <sub>4</sub> : Experimental data from Rijkers [18].....	130
C3.5 Binary interaction parameter dependency in NeqSim model: Predictions and experimental data from Kurata [34] .....	132
C3.6 Binary interaction parameter dependency in NeqSim model: Predictions and experimental data from Neumann [19].....	134
Appendix C4 - Experimental data from literature and simulated data: Binary C <sub>6</sub> H <sub>12</sub> -CH <sub>4</sub> system ..	135
C4.1 Solubility of C <sub>6</sub> H <sub>12</sub> in CH <sub>4</sub> : Experimental data from Kohn [35].....	135
Appendix C5 - Experimental methods used in literature .....	137
C5.1 Analytical method.....	137
C5.2 Synthetic method .....	138
C5.3 Literature review of experimental methods .....	139
Appendix C6 - Unavailable experimental work .....	141
Appendix D1 - P&Id: Freeze out rig, as built.....	142
Appendix D2 - P&Id: Freeze out rig, short term modifications .....	143



## Appendix A1 - Mixing rules: Combining rules

This chapter will give an introduction of the different combining rules based on the review article of Wei and Sadus [22].

“As noted above, any mixing rule will invariably contain a contribution from interactions between unlike molecules. In other words, the cross terms  $a_{ij}$  and  $b_{ij}$  ( $i \neq j$ ) must be evaluated. They can be determined by an appropriate combining rule. The contribution from unlike interaction to the intermolecular parameters representing energy ( $\varepsilon$ ) and hard-sphere diameter ( $\sigma$ ) can be obtained from

$$\begin{aligned} \varepsilon_{ij} &= \xi_{ij} \sqrt{\varepsilon_{ii} \varepsilon_{jj}} \\ \sigma_{ij} &= \zeta_{ij} \frac{(\sigma_{ii} + \sigma_{jj})}{2} \end{aligned} \quad (\text{A1.1})$$

In equation (A1.1), the  $\xi_{ij}$  (also commonly defined  $1 - k_{ij}$ ) and  $\zeta_{ij}$  (also commonly defined as  $1 - l_{ij}$ ) terms are adjustable parameters which are used to optimize agreement between theory and experiment. The  $\zeta_{ij}$  term does not significantly improve the analysis of high-pressure equilibria, and it can be usually omitted ( $\zeta_{ij} = 1$ ). The  $\xi_{ij}$  term is required, because it can be interpreted as reflecting the strength of unlike interaction except the simple mixtures of molecules of similar size. This interpretation is supported by the fact that values of  $\xi_{ij}$  obtained from the analysis of the critical properties of many binary mixtures consistently decline with increasing size difference between the component molecules as detailed elsewhere (Sadus, 1992a, 1994).

In terms of the equation of state parameters, the equivalent combining rules to equations (A1.1) are

$$\begin{aligned} a_{ij} &= \xi_{ij} b_{ij} \sqrt{\frac{a_{ii} a_{jj}}{b_{ii} b_{jj}}} \\ b_{ij} &= \zeta_{ij} \frac{(b_{ii}^{1/3} + b_{jj}^{1/3})^3}{8} \end{aligned} \quad (\text{A1.2})$$

where the rule for  $b_{ij}$  is referred to as the Lorentz rule (Hicks and Young, 1975; Sadus, 1992a). More commonly, the equation of state parameters are obtained from

$$\begin{aligned}
 a_{ij} &= \xi_{ij} \sqrt{a_{ii} a_{jj}} \\
 b_{ij} &= \zeta_{ij} \frac{(b_{ii} + b_{jj})}{2}
 \end{aligned}
 \tag{A1.3}$$

where the combining rule for  $a_{ij}$  is referred to as the van der Waals combining rule. At this point, it should be noted that there is a common misconception in the literature that equation (A1.3) and not equation (A1.2) is the equivalent of equation (A1.1). This error is understandable in view of the functional similarity of equation (A1.3) and (A1.1). However, it should also be observed that the  $a$  and  $b$  parameters have dimensions of *energy*  $\times$  *volume* and *volume*, respectively, compared with a dimension of energy *energy* for  $\varepsilon$  and a dimension of *distance* for  $\sigma$ . Another combining rule for  $b_{ij}$  is the geometric mean rule proposed by Good and Hope (1970)

$$b_{ij} = \zeta_{ij} \sqrt{b_{ii} b_{jj}}
 \tag{A1.4}$$

Sadus (1993) compared the accuracy of the Lorentz (A1.2), arithmetic (A1.3), and geometric (A1.4) rules for  $b_{ij}$  when used in the prediction of Type III phenomena. For molecules of similar size, all three combining rules give almost identical results, but the discrepancy increases substantially for mixtures of molecules of very dissimilar size. Sadus (1993) proposed an alternative combining rule by taking a 2:1 geometric average of the Lorentz and arithmetic rules without the  $\zeta_{ij}$  parameter, that is,

$$b_{ij} = \left\{ \frac{1}{4} (2^{1/3}) \right\} (b_{ii}^{1/3} + b_{jj}^{1/3})^2 (b_{ii} + b_{jj})^{1/3}
 \tag{A1.5}$$

Sadus (1993) reported that the new combining rule (A1.5) is generally more accurate than either the Lorentz, arithmetic, or geometric combining rules.”[22]

## Appendix A2 - Two phase TP-flash

### A2.1 Deduction of the stability criterion

"The change in the Gibbs energy due to the phase split is hence:

$$\Delta G = G_I + G_{II} - G_0 = \sum_{i=1}^N \varepsilon_i \left( (\mu_i)_{II} - (\mu_i)_0 \right) = \varepsilon \sum_{i=1}^N y_i \left( (\mu_i)_{II} - (\mu_i)_0 \right) \quad (\text{A2.1})$$

where  $\varepsilon = \sum_{i=1}^N \varepsilon_i$ ,  $y_i$  is the mole fraction of component  $i$  in phase  $II$  and the subscript 0 and  $II$  refer to the single phase and to phase  $II$ , respectively. Only one phase exists of  $\Delta G$  is greater than or equal to zero for all possible trial compositions of phase  $II$ . The chemical potential,  $\mu_i$ , may be expressed in terms of the fugacity,  $f_i$ , as follows:

$$\mu_i = \mu_i^0 + RT \ln f_i = \mu_i^0 + RT (\ln z_i + \ln \phi_i + \ln P) \quad (\text{A2.2})$$

Where  $\mu_i$  is a standard state chemical potential,  $\phi$  a fugacity coefficient,  $z$  a mole fraction,  $P$  the pressure, and the subindex  $i$  stands for component  $i$ . The standard state in this case the pure component  $i$  at the temperature and pressure of the system. Equation (A2.1) may then be rewritten:

$$\frac{\Delta G}{\varepsilon RT} = \sum_{i=1}^N y_i \left( \ln y_i + \ln (\phi_i)_{II} - \ln z_i - \ln (\phi_i)_0 \right) \quad (\text{A2.3})$$

where  $z_i$  is the mole fraction of component  $i$  in the total mixture." [23]

### A2.2 Stationary point

"It can now be shown that a stationary point must satisfy the equation:

$$\ln y_i + \ln (\phi_i)_{II} - \ln z_i - \ln (\phi_i)_0 = k \quad (\text{A2.4})$$

where  $k$  is independent of the component index. Introducing new variables,  $Y_i = \ln y_i - k$

Equation (A2.4) may be rewritten:

$$\ln Y_i = \ln z_i + \ln (\phi_i)_0 - \ln (\phi_i)_{II} \quad (\text{A2.5})$$

Michelsen suggests using the following initial estimate for the ratio  $K_i$  between the mole fraction of component  $i$  in the vapor phase, and in the liquid phase:

$$\frac{y_i}{x_i} = K_i = \frac{P_{ci}}{P} \exp \left( 5.42 \left( 1 - \frac{T_{ci}}{T} \right) \right) \quad (\text{A2.6})$$

Where  $T_{ci}$  is the critical temperature, and  $P_{ci}$  is the critical pressure of component  $i$ . As initial estimates for  $Y_i$ , use  $K_i z_i$ , if phase 0 is a liquid, and  $z_i/K_i$ , if phase 0 is a vapor. The fugacity coefficient,  $(\phi_i)_{II}$ , corresponding to the initial estimates for  $Y_i$ , are determined. Based on these fugacity coefficients, new  $Y_i$ -values are determined, and so on. For a single phase mixture this direct substitution calculation converges to either the trivial solution (i. e., to two identical phases) or to  $Y_i$ -values fulfilling the criterion:

$$\sum_{i=1}^N Y_i \leq 1 \quad (\text{A2.7})$$

Which corresponds to a non-negative value of the constant  $k$  of equation (A2.4). A negative  $k$ -value would be an indication of the presence of two or more phases. The molar composition of phase  $II$  obtained by solving equation (A2.5) is then usually a good starting point in the calculation of the phase compositions.”[23]

### Appendix A3 - Phase envelope calculations

A phase envelope calculation are performed by calculating the pressure and temperature for a mixture with a given vapor mole fraction  $\beta$ . The calculation is initiated by using equation a simple  $K$ -factor model, presented beneath, for calculating the various  $K$ -values:

$$\frac{y_i}{x_i} = K_i = \frac{P_{ci}}{P} \left[ 5,42 \left( 1 - \frac{T_{ci}}{T} \right) \right] \quad (\text{A3.1})$$

This is the same model used to initiate the TP-flash calculation, see Appendix A2.2. By using this model for initial estimates of the  $K$ -values, equation (3.45) can be solved for the temperature.

Next, an equation of state is used to estimate the  $K$ -values, and equations (3.44) and (3.45) are solved simultaneous with regards to  $T$  and  $\ln K_i$ .

For estimating the next point at the phase envelope, at a slightly higher pressure, the derivatives of  $T$  and  $\ln K_i$  with respect to  $P$ , can be used. When the two first points are calculated an extrapolating method can be used based on the two previously calculations, to find the next points.



## Appendix B1 - NeqSim

### B1.1 The Thermodynamic Module

The thermodynamic system object, defines the thermodynamic model that is used for a specific system (for example one of the equations of state), in addition to the composition of the system. The thermodynamic system object consists of a vector of phase objects; and the phase object contains a vector of component objects; phase object contains an object consisting of physical properties, mixing rule object and the chemical reaction object. This structure is presented in figure 4-1.

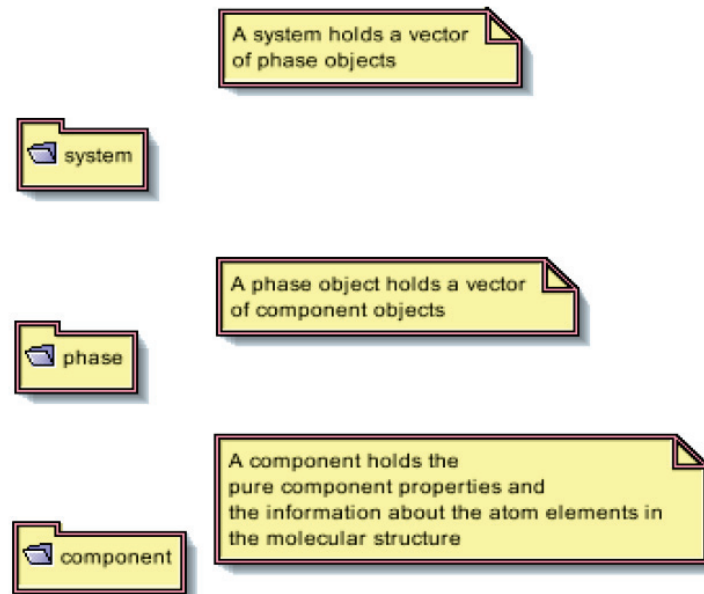


Figure B1-1 Main packages in the thermodynamic library [5]

“The main packages are system, phase and component. When you create a thermodynamic system object – you would typically create an instance of an object that implements the methods defined in the SystemInterface class. All models that implement/inherit from this base class – can perform the same operations – independent of which models they are based on. Active use of polymorphism creates an easy extendable and maintainable code.”[5]

The thermodynamic system requires a set of input data to calculate the parameters of interest, an equation of state have to be chosen, in addition to specify temperature, pressure and composition mixing rule. Next the system will be resolved, and there are created a thermodynamic operational object for the specified system. The component object includes all the variables to each component in the mixture, the data are taken from the thermodynamic library. In addition, the methodology used to reflect the specific variables or combinations of variables that are calculated for example from a flash calculation procedure or similar procedures. [20, 25]

## **B1.2 Thermodynamic Library**

The library contains all data that is being used in the calculations, e. g., component properties, EOS parameters and coefficients, and the data is stored in Microsoft Access format.

### **Phase object**

“A phase object holds a vector of components. The phase object can hold any number of components. A phase object also holds the mixing rule object. All mixing rules are defined in a single object as inner classes. The mixing rules currently implemented in the mixing rule class are: ”[5]

- Classic mixing rule with and without binary interaction parameters
- Huron-Vidal mixing rule
- Wong-Sandler mixing rule
- Electrolyte mixing rule
- CPA combining rules (own object)

### **The component object**

This object holds all the data which are in relation to a specific component and the properties are read from the thermodynamic library (the access-database).

The structure of the source code makes it simple to add new types of systems, phases and components. “Normally few lines of code have to be typed into new objects when you add new models. You will typically inherit from objects already defined in the hierarchy – and the most of the code is already written.”[5]



## Appendix B2 - GPA: The Thermodynamic description of the problem

This description are based on outtakes from the GPA User's Guide [31] and research report RR 22 by GPA [14].

"For a system of  $n$  solutes and  $m$  solvents, the equilibria restrictions are:

$$\begin{aligned}\mu_{is}(T, P) &= \mu_{il}(T, P, x_k) \\ i &= 1, 2, \dots, n\end{aligned}\quad (\text{B2.1})$$

$$\begin{aligned}\mu_{kl}(T, P, x_k) &= \mu_{kg}(T, P, y_k) \\ k &= 1, 2, \dots, m+n\end{aligned}\quad (\text{B2.2})$$

Where  $i = 1, 2, \dots, n$  refers to solutes,  $k = 1, 2, \dots, m+n$  refers to solutes and solvents in a group. Each component in the solid state is assumed to form its own pure solid phase. If one fixes the solute-free solvent composition of the liquid phase and also the temperatures (a total of  $m+1$  restrictions), then equations (B2.1) and (B2.2), will have  $m+2n$  unknowns and thus constitute a completely defined problem. From here on,  $j = 1, 2, \dots, \pi$  will refer to the set of solvents.

If one suppresses the pressure dependence in equation (B2.1), equation (B2.1) can be solved as a subset of the total problem, independently from equation (B2.2). Once binary systems ( 1 solute + 1 solvent) demonstrated a readily correlatable solubility behavior in the terms of temperature only in the Henry's regime (i.e., w solubility regime), the multi-component problem was cast the same way, starting with the binary data information as the base input. The effect of adopting this viewpoint is that equation (B2.1) are uncoupled from equation (B2.2). After equation (B2.1) have been solved as subset, yielding  $x_k$ , equation (B2.2) are solved in the spirit of a bubble point calculations, yielding  $y_k$  and  $P$ .

Equation (B2.1) are rewritten in the form of equations from Research Report RR-22 [14], but in a restricted form, the restrictions being dictated by the lack of extensive ternary and higher data. Equation (B2.1) are described as:

$$\ln y_i^* x_i = -\frac{\Delta h_i^\infty}{RT_{m,i}} \left[ \left( \frac{T_{m,i}}{T} \right) - 1 \right] - c_i \quad (\text{B2.3})$$

Where

$$\begin{aligned}\Delta h_i^\infty &= \sum_{k \neq i}^{m+n} x_k \Delta h_i^{(k)\infty} / (1-x_i) \\ &+ \tilde{x}_1 \sum_{j=2}^5 x_j \bar{H}_{i,j} / (1-x_i)^2 \\ &+ (\tilde{x}_1 \tilde{x}_6 \bar{H}_{i,6} + x_2 x_3 \bar{H}_{2,3}) / (1-x_i)^2\end{aligned}\quad (\text{B2.4})$$

And

$$\begin{aligned}
c_i &= \sum_{k \neq 1}^{m+n} x_k c_i^{(k)} / (1 - x_1) \\
&+ x_1 \sum_{j=2}^5 x_j c_{i,j} / (1 - x_i)^2 \\
&+ (\tilde{x}_1 \tilde{x}_6 \bar{c}_{1,6} + x_2 x_3 \bar{c}_{2,3}) / (1 - x_i)^2
\end{aligned} \tag{B2.5}$$

$\tilde{x}_1$  is the sum of fractions of CH<sub>4</sub> and N<sub>2</sub>.  $\tilde{x}_6$  is the sum of fractions of hexane and all other solutes except solute  $i$ .  $x_1$  through  $x_5$  are fractions of ethane, propane, n-butane and n-pentane respectively. As an approximation, it is assumed that all solutes enhance the solubility of other solutes at low concentrations to the same degree as hexane, and thus the pseudo fraction  $\tilde{x}_6$  is used. In a similar spirit, CH<sub>4</sub> and N<sub>2</sub> were lumped together as a pseudo-solvent as  $\tilde{x}_1$ , mainly due to the lack of data on liquid N<sub>2</sub> systems. " [31]

The next equations are gathered from the research report RR 16 [14], and represents general expressions in contrast of the User's Guide.

$$b_{ii'}^j = (b_{ii'}^j b_{i'i'}^j)^{1/2} \tag{B2.6}$$

$$b_{ii'i''}^j = (b_{ii'}^j b_{i'i'}^j b_{i'i''}^j)^{1/3} \tag{B2.7}$$

$$b_{ii'}^j = (b_{ii'}^j b_{i'i'}^j)^{1/2} \cdot (1 - a_{ii'}^j) \tag{B2.8}$$

$$\begin{aligned}
\ln y_i^* &= \sum_l \sum_{l'}^n b_{ll'} x_l x_{l'} - 2 \sum_l \sum_{l'}^n b_{ll'} x_l \delta_{l'i} \\
&+ 2 \sum_l \sum_{l'}^n \sum_{l''}^n b_{ll'l''} x_l x_{l'} x_{l''} \\
&- 3 \sum_l \sum_{l'}^n \sum_{l''}^n b_{ll'l''} x_l x_{l'} \delta_{l''i}
\end{aligned} \tag{B2.9}$$

"Equation (B2.9) is used for  $y_i^*$  where

$$b_{ii'} = \sum_{j=1}^m x_j b_{ii'}^{(j)} / \sum_{j=1}^m x_j \tag{B2.10}$$

$$b_{ii'i''} = \sum_{j=1}^m x_j b_{ii'i''}^{(j)} / \sum_{j=1}^m x_j \tag{B2.11}$$

And equations (B2.6) and (B2.7) are used but not equation (B2.8). Solvent-solvent effects are not well enough understood at this time to make corrections to  $H_i$  and  $\bar{c}_i$  in equation (B2.4) and (B2.5). All parameters used in this description of the solid-liquid equilibria are listed in Section VII.

The primary goal is the prediction of  $x_k$ . The solution of equation (B2.2) provides additional phase equilibria information but can be carried out as a separate computation once  $x_k$  are obtained. Given this information, the Chueh-Prausnitz version of the Redlich-Kwong equation was chosen for the gas phase description while a version of the Scatchard-Hildebrand description was used for the liquid-phase activity coefficients. Briefly, let

$$f_{kg} = f_{kl} \quad (\text{B2.12})$$

or

$$Py_k \phi_k = f_{kl}^{\circ} y_k x_k \quad (\text{B2.13})$$

Where  $\phi_k$  is given by equation (5.13-16) to (5.13-21) of Prausnitz's "Molecular Thermodynamics of Fluid-Phase Equilibria"[47].

$$\begin{aligned} \ln \phi_k = & \ln \left( \frac{v}{v-b} \right) + b_k / (v-b) - 2 \left[ \left( \sum_l^{m+n} y_l a_{lk} \right) / RT^{3/2} b \right] \ln \left( \frac{v+b}{v} \right) \\ & + \frac{ab_k}{RT^{3/2} b^2} \left[ \ln \frac{v+b}{v} - \frac{b}{v+b} \right] - \ln (Pv/RT) \end{aligned} \quad (\text{B2.14})$$

Where

$$b = \sum_l y_l b_l = \sum_l y_l \Omega_{bl} RT_{cl} / P_{cl} \quad (\text{B2.15})$$

$$a_{ij} = (\Omega_{ai} + \Omega_{aj}) R^2 T_{c_{ij}}^{2.5} / 2 P_{c_{ij}} \quad (\text{B2.16})$$

$$P_{c_{ij}} = z_{c_{ij}} RT_{c_{ij}} / v_{c_{ij}} \quad (\text{B2.17})$$

$$v_{c_{ij}} = \left[ \frac{1}{2} (v_{c_i}^{1/3} + v_{c_j}^{1/3}) \right]^3 \quad (\text{B2.18})$$

$$z_{c_{ij}} = 0.291 - 0.08 (\omega_i + \omega_j) / 2 \quad (\text{B2.19})$$

$$T_{c_{ij}} = (T_{c_i} T_{c_j})^{1/2} (1 - k_{ij}) \quad (\text{B2.20})$$

$y_k$  is represented by equations (7-94) to (7-97) of Reid and Sherwood's "The Properties of Gases and Liquids":

$$\ln y_k = V_k^* (\delta_k - \bar{\delta})^2 / RT \quad (\text{B2.21})$$

Where  $\delta_k$  is the solubility parameter of component  $k$ , and

$$\bar{\delta} = \frac{\sum_l^{m+n} x_l V_l^* \delta_l}{\sum_l^{m+n} x_l V_l^*} \quad (\text{B2.22})$$

$$V_k^* = V_{\omega k} (5.7 + 3.0Tr_k) \quad (\text{B2.23})$$

The pure liquid fugacity  $f_{kl}^\circ$

$$f_{kl}^\circ = f_{ksat}^\circ \exp\left[\frac{V_k^* (P - P_{sat})}{RT}\right] \quad (\text{B2.24})$$

Where

$$f_{ksat}^\circ = \phi_{ksat} P_{sat} \quad (\text{B2.25})$$

And  $P_{sat}$  is determined from the Antoine equation:

$$\log_{10} P_{sat} = A - B/(C - t) \quad (\text{B2.26})$$

Where  $P_{sat}$  is in mmHg and  $t$  is in °C.

It should be noted that the solution to equation (B2.13) is included in the program for the user's convenience, if he wishes  $P$  and  $y_k$  information. It is recognized that the user may wish to employ an alternative vapor-liquid equilibria description. Such a modification could be substituted for (or run separately from) the above description, as equation (B2.1) and (B2.2) are uncoupled and yield  $x_k$  at some  $T$  prior to one's carrying out the vapor-liquid computation. The vapor-liquid description included in this program provides a reasonable estimate of the values  $P$  and  $y_k$  if they are desired, but certainly could be quantitatively improved on, without altering the solid-liquid equilibria description. " [31]

## Appendix C1 - Thermodynamic models used in simulations

### C1.1 NeqSim predictions with PR and SRK EOS compared to Agrawal [36]

Point No.	Composition, mole %			Pressure [bars]	Temperature [K]	NeqSim kij=0 (PR)			NeqSim kij=0 (SRK)		
	CH <sub>4</sub>	N <sub>2</sub>	CO <sub>2</sub>			Temp [K]	(T <sub>calc</sub> -T <sub>exp</sub> )	ABS	Temp [K]	(T <sub>calc</sub> -T <sub>exp</sub> )	ABS
1	99.88	-	0.12	1.79	137.54	140.41	2.87	2.87	140.42	2.88	2.88
2				3.45	143.21	144.24	1.04	1.04	144.26	1.05	1.05
3				5.17	144.32	146.53	2.21	2.21	146.56	2.24	2.24
4				6.83	147.82	148.02	0.20	0.20	148.06	0.24	0.24
5				8.55	149.76	149.13	-0.64	0.64	149.18	-0.58	0.58
6	99.03	-	0.97	1.79	155.15	155.01	-0.14	0.14	155.02	-0.13	0.13
7				3.79	158.21	160.50	2.29	2.29	160.53	2.32	2.32
8				5.24	161.26	162.86	1.60	1.60	162.90	1.64	1.64
9				6.96	163.98	164.88	0.90	0.90	164.93	0.95	0.95
10				10.82	166.48	167.81	1.33	1.33	167.90	1.42	1.42
11				13.79	168.37	169.21	0.84	0.84	169.33	0.96	0.96
12				17.86	170.59	170.40	-0.19	0.19	170.55	-0.04	0.04
13				20.68	172.04	170.83	-1.21	1.21	171.01	-1.03	1.03
14	98.2	-	1.8	1.72	158.21	159.62	1.41	1.41	159.63	1.42	1.42
15				1.86	159.32	160.22	0.91	0.91	160.24	0.92	0.92
16				3.45	163.98	165.08	1.09	1.09	165.10	1.12	1.12
17				3.52	164.54	165.24	0.70	0.70	165.26	0.72	0.72
18				5.24	168.37	168.38	0.00	0.00	168.42	0.05	0.05
19				6.96	170.32	170.58	0.26	0.26	170.64	0.32	0.32
20				8.62	174.15	172.19	-1.96	1.96	172.26	-1.89	1.89
21				12.13	174.26	174.60	0.34	0.34	174.71	0.45	0.45
22				15.72	176.04	176.21	0.17	0.17	176.35	0.31	0.31
23				22.61	176.76	177.77	1.01	1.01	177.99	1.23	1.23
24	96.93	-	3.07	1.72	159.59	164.10	4.51	4.51	164.12	4.52	4.52
25				1.79	160.43	164.43	4.00	4.00	164.44	4.02	4.02
26				3.52	166.21	170.08	3.88	3.88	170.11	3.91	3.91
27				3.55	166.43	170.16	3.73	3.73	170.18	3.76	3.76
28				5.24	170.82	173.45	2.63	2.63	173.49	2.68	2.68
29				6.96	174.98	175.82	0.84	0.84	175.88	0.90	0.90
30				14.00	179.37	181.26	1.89	1.89	181.40	2.02	2.02
31				20.62	181.59	183.61	2.01	2.01	183.81	2.22	2.22
32				20.82	183.21	183.65	0.45	0.45	183.86	0.65	0.65
33				21.44	182.15	183.79	1.64	1.64	184.00	1.85	1.85
34				27.85	184.04	184.52	0.48	0.48	184.82	0.78	0.78
35	89.33	-	10.67	1.72	177.71	175.66	-2.05	2.05	175.67	-2.04	2.04
36				3.52	184.32	182.63	-1.69	1.69	182.66	-1.66	1.66
37				5.24	187.65	186.61	-1.04	1.04	186.66	-0.99	0.99
38				7.10	191.21	189.66	-1.54	1.54	189.73	-1.48	1.48
39				8.69	193.98	191.68	-2.31	2.31	191.76	-2.22	2.22
40				10.34	196.65	193.39	-3.26	3.26	193.49	-3.16	3.16
41				12.07	197.71	194.88	-2.83	2.83	195.00	-2.71	2.71
42				14.13	198.09	196.35	-1.75	1.75	196.49	-1.60	1.60
						<b>BIAS/AAD</b>	<b>0.59</b>	<b>1.57</b>	<b>BIAS/AAD</b>	<b>0.67</b>	<b>1.60</b>
						Min	-3.26	0.00	Min	-3.16	0.04
						Max	4.51	4.51	Max	4.52	4.52

### C1.2 HYSYS predictions with PR and SRK EOS compared to Agrawal [36]

Point No.	Composition, mole %			Pressure [bars]	Temperature [K]	HYSYS (SRK)		HYSYS (PR)		
	CH <sub>4</sub>	N <sub>2</sub>	CO <sub>2</sub>			Temp [K]	(T <sub>calc</sub> -T <sub>exp</sub> )	Temp [K]	(T <sub>calc</sub> -T <sub>exp</sub> )	ABS
1	99.88	-	0.12	1.79	137.54	140.11	2.57	140.10	2.56	2.56
2				3.45	143.21	144.06	0.85	144.04	0.84	0.84
3				5.17	144.32	146.44	2.12	146.42	2.11	2.11
4				6.83	147.82	148.03	0.21	148.01	0.19	0.19
5				8.55	149.76	149.24	-0.52	149.21	-0.55	0.55
6	99.03	-	0.97	1.79	155.15	154.78	-0.37	154.77	-0.38	0.38
7				3.79	158.21	160.41	2.21	160.39	2.19	2.19
8				5.24	161.26	162.86	1.60	162.84	1.58	1.58
9				6.96	163.98	164.99	1.01	164.96	0.98	0.98
10				10.82	166.48	168.17	1.69	168.12	1.63	1.63
11				13.79	168.37	169.78	1.41	169.71	1.34	1.34
12				17.86	170.59	171.28	0.69	171.19	0.59	0.59
13				20.68	172.04	171.97	-0.07	171.86	-0.18	0.18
14	98.20	-	1.80	1.72	158.21	159.42	1.21	159.41	1.20	1.20
15				1.86	159.32	160.03	0.72	160.03	0.71	0.71
16				3.45	163.98	165.00	1.02	164.98	1.00	1.00
17				3.52	164.54	165.16	0.62	165.15	0.61	0.61
18				5.24	168.37	168.42	0.04	168.39	0.02	0.02
19				6.96	170.32	170.73	0.41	170.69	0.37	0.37
20				8.62	174.15	172.45	-1.70	172.40	-1.75	1.75
21				12.13	174.26	175.09	0.83	175.02	0.76	0.76
22				15.72	176.04	176.94	0.91	176.85	0.81	0.81
23				22.61	176.76	179.08	2.32	178.95	2.19	2.19
24	96.93	-	3.07	1.72	159.59	163.93	4.34	163.92	4.33	4.33
25				1.79	160.43	164.26	3.84	164.26	3.83	3.83
26				3.52	166.21	170.04	3.84	170.02	3.82	3.82
27				3.55	166.43	170.12	3.69	170.10	3.67	3.67
28				5.24	170.82	173.52	2.70	173.49	2.67	2.67
29				6.96	174.98	176.01	1.02	175.97	0.98	0.98

Point No.	Composition, mole %		Pressure [bars]	Temperature [K]	HYSYS (SRK)		HYSYS (PR)		
	CH <sub>4</sub>	N <sub>2</sub>			CO <sub>2</sub>	Temp [K]	(T <sub>calc</sub> -T <sub>exp</sub> )	Temp [K]	(T <sub>calc</sub> -T <sub>exp</sub> )
30			14.00	179.37	181.91	2.54	181.82	2.45	2.45
31			20.62	181.59	184.74	3.15	184.61	3.02	3.02
32			20.82	183.21	184.81	1.60	184.67	1.47	1.47
33			21.44	182.15	184.99	2.84	184.85	2.70	2.70
34			27.85	184.04	186.35	2.31	186.17	2.13	2.13
35	89.33	-	1.72	177.71	175.53	-2.17	175.52	-2.18	2.18
36		10.67	3.52	184.32	182.64	-1.68	182.62	-1.70	1.70
37			5.24	187.65	186.74	-0.91	186.70	-0.95	0.95
38			7.10	191.21	189.91	-1.30	189.86	-1.34	1.34
39			8.69	193.98	192.03	-1.96	191.97	-2.02	2.02
40			10.34	196.65	193.84	-2.81	193.77	-2.88	2.88
41			12.07	197.71	195.44	-2.27	195.35	-2.35	2.35
42			14.13	198.09	197.04	-1.05	196.94	-1.16	1.16
					<b>BIAS/AAD</b>	<b>0.89</b>	<b>BIAS/AAD</b>	<b>0.84</b>	<b>1.67</b>
					Min	-2.81	Min	-2.88	0.02
					Max	4.34	Max	4.33	4.33





### C2.2 Solubility of CO<sub>2</sub> in liquid CH<sub>4</sub>: Predictions and experimental data from Davis [13]

Sample no.	Mol % CO <sub>2</sub>	Mol % CH <sub>4</sub>	Temp [K]	Pressure [bars]	NeqSim			GPA			HYSYS						
					Temp [K]	Pressure [bar]	(T <sub>calc</sub> -T <sub>exp</sub> ) ABS	Temp [K]	Pressure [bar]	(T <sub>calc</sub> -T <sub>exp</sub> ) ABS	Temp [K]	Pressure [bar]	(T <sub>calc</sub> -T <sub>exp</sub> ) ABS				
1	0.16	99.84	129.65	3.62	128.20	13.00	-1.45	1.45	129.93	3.63	0.28	0.28	121.15	10.00	-8.50	8.50	
2	0.25	99.75	135.21	5.12	133.45	15.00	-1.75	1.75	134.85	4.81	-0.36	0.36	127.24	13.00	-7.97	7.97	
3	0.37	99.63	139.43	6.36	138.34	18.00	-1.09	1.09	139.23	6.06	-0.20	0.20	132.47	15.00	-6.95	6.95	
4	0.58	99.42	144.54	8.18	144.31	21.00	-0.23	0.23	144.97	8.03	0.43	0.43	138.85	18.00	-5.69	5.69	
5	0.93	99.07	150.37	10.48	150.99	25.00	0.62	0.62	151.26	10.61	0.89	0.89	145.76	22.00	-4.61	4.61	
6	1.83	98.17	162.04	15.92	161.35	32.00	-0.69	0.69	161.10	15.60	-0.94	0.94	156.60	30.00	-5.44	5.44	
7	2.94	97.06	169.87	22.41	169.17	37.00	-0.71	0.71	168.76	20.19	-1.11	1.11	164.83	34.00	-5.04	5.04	
8	5.85	94.15	182.15	33.06	181.22	45.00	-0.93	0.93	180.52	27.88	-1.63	1.63	177.49	43.00	-4.66	4.66	
9	10.08	89.92	189.26	39.70	190.66	50.00	1.40	1.40	189.81	33.39	0.55	0.55	187.84	48.00	-1.43	1.43	
10	15.39	84.61	196.93	45.45	198.65	52.00	1.72	1.72	194.74	34.29	-2.19	2.19	195.71	48.00	-1.22	1.22	
11	20.50	79.50	201.26	48.18	203.08	51.00	1.82	1.82	197.74	33.68	-3.52	3.52	199.96	48.00	-1.30	1.30	
					<b>BIAS/AAD</b>	<b>-0.12</b>	<b>1.13</b>	<b>-0.12</b>	<b>1.13</b>	<b>BIAS/AAD</b>	<b>-0.71</b>	<b>1.10</b>	<b>BIAS/AAD</b>	<b>-4.80</b>	<b>4.80</b>		
					Min	-1.75	0.23	-1.75	0.23	Min	-3.52	0.20	Min	-8.50	1.22		
					Max	1.82	1.82	1.82	1.82	Max	0.89	3.52	Max	-1.22	8.50		



## C2.4 Solubility of CO<sub>2</sub> in CH<sub>4</sub>: Predictions and experimental data from Agrawal [36]

Sample no.	Composition, mole %			Pressure [bars]	Temp [K]	NeqSim			HYSYS		
	CH <sub>4</sub>	N <sub>2</sub>	CO <sub>2</sub>			Temp [K]	(T <sub>calc</sub> -T <sub>exp</sub> )	ABS	Temp [K]	(T <sub>calc</sub> -T <sub>exp</sub> )	ABS
1	99.88	-	0.12	1.79	137.54	140.50	2.96	2.96	140.11	2.57	2.57
2				3.45	143.21	144.42	1.21	1.21	144.06	0.85	0.85
3				5.17	144.32	146.81	2.49	2.49	146.44	2.12	2.12
4				6.83	147.82	148.40	0.58	0.58	148.03	0.21	0.21
5				8.55	149.76	149.62	-0.14	0.14	149.24	-0.52	0.52
6	99.03	-	0.97	1.79	155.15	155.09	-0.06	0.06	154.78	-0.37	0.37
7				3.79	158.21	160.69	2.48	2.48	160.41	2.21	2.21
8				5.24	161.26	163.13	1.87	1.87	162.86	1.60	1.60
9				6.96	163.98	165.25	1.26	1.26	164.99	1.01	1.01
10				10.82	166.48	168.41	1.92	1.92	168.17	1.69	1.69
11				13.79	168.37	170.01	1.64	1.64	169.78	1.41	1.41
12				17.86	170.59	171.51	0.92	0.92	171.28	0.69	0.69
13				20.68	172.04	172.21	0.17	0.17	171.97	-0.07	0.07
14	98.20	-	1.80	1.72	158.21	159.70	1.49	1.49	159.42	1.21	1.21
15				1.86	159.32	160.31	1.00	1.00	160.03	0.72	0.72
16				3.45	163.98	165.25	1.26	1.26	165.00	1.02	1.02
17				3.52	164.54	165.41	0.87	0.87	165.16	0.62	0.62
18				5.24	168.37	168.64	0.27	0.27	168.42	0.04	0.04
19				6.96	170.32	170.93	0.62	0.62	170.73	0.41	0.41
20				8.62	174.15	172.64	-1.51	1.51	172.45	-1.70	1.70
21				12.13	174.26	175.26	1.00	1.00	175.09	0.83	0.83
22				15.72	176.04	177.11	1.07	1.07	176.94	0.91	0.91
23				22.61	176.76	179.25	2.48	2.48	179.08	2.32	2.32
24	96.93	-	3.07	1.72	159.59	164.18	4.59	4.59	163.93	4.34	4.34
25				1.79	160.43	164.51	4.09	4.09	164.26	3.84	3.84
26				3.52	166.21	170.25	4.05	4.05	170.04	3.84	3.84
27				3.55	166.43	170.33	3.90	3.90	170.12	3.69	3.69
28				5.24	170.82	173.70	2.89	2.89	173.52	2.70	2.70
29				6.96	174.98	176.17	1.19	1.19	176.01	1.02	1.02
30				14.00	179.37	182.02	2.65	2.65	181.91	2.54	2.54
31				20.62	181.59	184.83	3.23	3.23	184.74	3.15	3.15
32				20.82	183.21	184.89	1.68	1.68	184.81	1.60	1.60
33				21.44	182.15	185.07	2.92	2.92	184.99	2.84	2.84
34				27.85	184.04	186.44	2.40	2.40	186.35	2.31	2.31
35	89.33	-	10.67	1.72	177.71	175.70	-2.00	2.00	175.53	-2.17	2.17
36				3.52	184.32	182.75	-1.57	1.57	182.64	-1.68	1.68
37				5.24	187.65	186.80	-0.85	0.85	186.74	-0.91	0.91
38				7.10	191.21	189.94	-1.27	1.27	189.91	-1.30	1.30
39				8.69	193.98	192.03	-1.96	1.96	192.03	-1.96	1.96
40				10.34	196.65	193.82	-2.83	2.83	193.84	-2.81	2.81
41				12.07	197.71	195.39	-2.31	2.31	195.44	-2.27	2.27
42				14.13	198.09	196.97	-1.12	1.12	197.04	-1.05	1.05
						<b>BIAS/ADD</b>	<b>1.08</b>	<b>1.83</b>	<b>BIAS/ADD</b>	<b>0.89</b>	<b>1.69</b>
						Min	-2.83	0.06	Min	-2.81	0.04
						Max	4.59	4.59	Max	4.34	4.34

## C2.5 Solubility of CO<sub>2</sub> in CH<sub>4</sub>: Predictions and experimental data from Le [37]

Point No.	Composition, mole %		Temp [K]	Pressure [bars]	NeqSim			HYSYS		
	CH <sub>4</sub>	CO <sub>2</sub>			Temp [K]	(T <sub>calc</sub> -T <sub>exp</sub> )	ABS	Temp [K]	(T <sub>calc</sub> -T <sub>exp</sub> )	ABS
1	99.00	1.00	168.60	9.62	168.13	-0.47	0.47	167.64	-0.96	0.96
2			170.50	11.10	169.18	-1.32	1.32	168.64	-1.86	1.86
3			170.70	11.41	169.37	-1.33	1.33	168.83	-1.87	1.87
4			171.00	11.04	169.14	-1.86	1.86	168.60	-2.40	2.40
5			171.10	11.49	169.42	-1.68	1.68	168.88	-2.22	2.22
6			173.40	13.19	170.39	-3.01	3.01	169.79	-3.61	3.61
7			173.60	14.35	170.96	-2.64	2.64	170.33	-3.27	3.27
8			173.70	14.26	170.92	-2.78	2.78	170.29	-3.41	3.41
9			175.10	16.94	172.02	-3.08	3.08	171.31	-3.79	3.79
10			175.20	17.08	172.07	-3.13	3.13	171.38	-3.82	3.82
11			175.50	18.09	172.42	-3.08	3.08	171.66	-3.84	3.84
12			175.60	19.52	172.84	-2.76	2.76	172.03	-3.57	3.57
13			175.90	20.13	173.01	-2.89	2.89	172.17	-3.73	3.73
14			176.20	20.09	173.00	-3.20	3.20	172.16	-4.04	4.04
15			176.30	19.31	172.78	-3.52	3.52	171.98	-4.32	4.32
16			176.90	20.99	173.22	-3.68	3.68	172.35	-4.55	4.55
17			177.00	21.29	173.29	-3.71	3.71	172.40	-4.60	4.60
18			177.60	21.94	173.42	-4.18	4.18			
19			177.70	22.99	173.63	-4.07	4.07		Liquid	
20			177.80	24.64	173.88	-3.92	3.92			
21	98.09	1.91	173.70	13.14	176.82	3.12	3.12	176.30	2.60	2.60
22			173.80	13.76	177.17	3.37	3.37	176.64	2.84	2.84
23			174.50	13.99	177.30	2.80	2.80	176.76	2.26	2.26
24			176.40	17.16	178.80	2.40	2.40	178.17	1.77	1.77
25			176.70	18.03	179.15	2.45	2.45	178.48	1.78	1.78
26			176.90	17.05	178.76	1.86	1.86	178.12	1.22	1.22
27			178.90	19.44	179.65	0.75	0.75	178.94	0.04	0.04
28			178.90	19.55	179.69	0.79	0.79	178.98	0.08	0.08
29			179.00	19.30	179.61	0.61	0.61	178.90	-0.10	0.10
30			181.00	21.35	180.25	-0.75	0.75	179.47	-1.53	1.53
31			181.10	22.07	180.45	-0.65	0.65	179.64	-1.46	1.46
32			181.90	22.35	180.52	-1.38	1.38	179.70	-2.20	2.20
33			182.20	23.45	180.79	-1.41	1.41	179.93	-2.27	2.27
34			182.30	24.97	181.11	-1.19	1.19	180.19	-2.11	2.11
35			182.40	26.51	181.39	-1.01	1.01	180.39	-2.01	2.01
36	97.07	2.93	176.50	11.99	180.58	4.08	4.08	180.15	3.65	3.65
37			176.70	12.13	180.67	3.97	3.97	180.24	3.54	3.54
38			176.90	12.53	180.95	4.05	4.05	180.51	3.61	3.61
39			179.10	14.21	181.99	2.89	2.89	181.51	2.41	2.41
40			179.60	14.77	182.31	2.71	2.71	181.81	2.21	2.21
41			179.60	14.70	182.27	2.67	2.67	181.77	2.17	2.17
42			181.80	16.44	183.16	1.36	1.36	182.62	0.82	0.82
43			181.90	16.84	183.35	1.45	1.45	182.80	0.90	0.90
44			182.10	17.58	183.68	1.58	1.58	183.11	1.01	1.01
45			182.80	19.58	184.49	1.69	1.69	183.86	1.06	1.06
46			182.80	19.71	184.54	1.74	1.74	183.90	1.10	1.10
47			183.00	19.82	184.58	1.58	1.58	183.94	0.94	0.94
48			184.60	22.92	185.58	0.98	0.98	184.83	0.23	0.23
49			184.60	22.74	185.53	0.93	0.93	184.79	0.19	0.19
50			185.30	24.28	185.95	0.65	0.65	185.15	-0.15	0.15
51			186.30	26.52	186.46	0.16	0.16	185.57	-0.73	0.73
52			186.50	25.77	186.30	-0.20	0.20	185.44	-1.06	1.06
53			187.50	29.98	187.03	-0.47	0.47	185.98	-1.52	1.52
54			187.60	30.00	187.04	-0.56	0.56	185.99	-1.61	1.61
55			187.70	30.08	187.05	-0.65	0.65	185.99	-1.71	1.71
					<b>BIAS/AAD</b>	<b>-0.25</b>	<b>2.10</b>	<b>BIAS/AAD</b>	<b>-0.73</b>	<b>2.13</b>
					Min	-4.18	0.16	Min	-4.60	0.04
					Max	4.08	4.18	Max	3.65	4.60

### C2.6 Solubility of CO<sub>2</sub> in CH<sub>4</sub>: Predictions and experimental data from Davis [13]

Sample no.	Mole % CO <sub>2</sub>	Mole % CH <sub>4</sub>	Temp [K]	Pressure [bar]	NeqSim			GPA			HYSYS				
					Temp [K]	Press [bars]	(T <sub>calc</sub> -T <sub>exp</sub> ) ABS	Temp [K]	Press [bars]	(T <sub>calc</sub> -T <sub>exp</sub> ) ABS	Temp [K]	Pressure [bar]	(T <sub>calc</sub> -T <sub>exp</sub> ) ABS		
1	0.12	99.88	140.93	6.85	148.41	6.85	7.48	173.95	23.56	33.02	33.02	148.05	6.85	7.12	7.12
2	0.63	99.37	165.59	19.59	167.66	19.59	2.06	187.90	32.37	22.31	22.31	166.77	17.00	1.17	1.17
3	1.08	98.92	175.87	27.51	174.01	25.51	-1.87	192.00	34.08	16.13	16.13	173.71	25.00	-2.17	2.17
4	1.72	98.28	177.59	28.80	179.50	28.80	1.90	195.83	34.21	18.24	18.24	179.29	29.00	1.69	1.69
5	2.79	97.21	183.98	34.62	185.52	34.62	1.53	199.11	33.21	15.13	15.13	185.43	33.00	1.45	1.45
6	3.67	96.33	188.71	39.09	188.73	39.09	0.03	200.75	32.27	12.04	12.04	188.98	37.00	0.27	0.27
7	5.65	94.35	193.65	43.22	194.58	43.22	0.93	204.31	29.51	10.66	10.66	194.82	42.00	1.17	1.17
8	11.73	88.27	205.71	48.40	205.91	48.40	0.20	209.23	22.73	3.52	3.52	205.35	47.00	-0.35	0.35
					<b>BIAS/AAD</b>		<b>1.54</b>	<b>BIAS/AAD</b>		<b>16.38</b>	<b>16.38</b>	<b>BIAS/AAD</b>		<b>1.29</b>	<b>1.92</b>
					Min		-1.87	Min		3.52	3.52	Min		-2.17	0.27
					Max		7.48	Max		33.02	33.02	Max		7.12	7.12

### C2.7 Binary interaction parameter dependency in NeqSim model: Predictions and experimental SLE data from Kurata [1]

Sample no.	Temp [K]	X [mol % CO <sub>2</sub> ]	Press. [bar]	k <sub>ij</sub> =0.09			k <sub>ij</sub> =0.11			k <sub>ij</sub> =0.12			k <sub>ij</sub> =0.13			
				Temp [K]	Press. [bars]	(T <sub>calc</sub> -T <sub>exp</sub> )	Temp [K]	Press. [bars]	(T <sub>calc</sub> -T <sub>exp</sub> )	Temp [K]	Press. [bars]	(T <sub>calc</sub> -T <sub>exp</sub> )	Temp [K]	Press. [bars]	(T <sub>calc</sub> -T <sub>exp</sub> )	ABS
1	214.30	90.00	20.79	212.33	23.00	-1.97	212.38	25.79	-1.92	212.40	27.00	-1.90	212.43	28.00	-1.87	1.87
2	213.70	86.50	24.31	211.16	27.00	-2.54	211.25	30.31	-2.45	211.30	32.00	-2.40	211.35	34.00	-2.35	2.35
3	212.60	80.00	30.14	209.31	34.00	-3.29	209.54	38.14	-3.06	209.67	40.00	-2.93	209.77	43.00	-2.83	2.83
4	211.20	76.80	36.39	208.55	37.00	-2.65	208.89	40.39	-2.31	209.04	43.00	-2.16	209.19	46.00	-2.01	2.01
5	210.40	70.00	39.37	207.26	40.00	-3.14	207.79	45.37	-2.61	208.07	47.00	-2.33	208.33	50.00	-2.07	2.07
6	209.00	60.00	43.57	205.89	44.00	-3.11	206.85	47.57	-2.15	207.32	50.00	-1.68	207.77	53.00	-1.23	1.23
7	207.60	54.30	46.47	205.33	45.00	-2.27	206.54	48.47	-1.06	207.13	51.00	-0.47	207.70	54.00	0.10	0.10
8	207.30	50.00	46.93	204.96	45.00	-2.34	206.36	48.93	-0.94	207.06	50.00	-0.24	207.75	53.00	0.45	0.45
9	206.20	42.60	48.18	204.27	46.00	-1.93	206.05	49.18	-0.15	206.92	51.00	0.72	207.46	60.00	1.26	1.26
10	201.30	20.50	48.18	198.78	46.00	-2.52	201.67	49.18	0.37	203.08	51.00	1.78	204.11	54.00	2.81	2.81
11	196.90	15.39	45.18	194.61	46.00	-2.29	197.80	48.18	0.90	198.65	52.00	1.75	199.66	55.00	2.76	2.76
12	189.30	10.08	39.54	186.96	45.90	-2.34	190.47	44.54	1.17	191.16	50.10	1.86	202.23	51.00	12.93	12.93
13	182.20	5.85	32.91	176.81	43.00	-5.39	179.75	44.91	-2.45	181.22	45.00	-0.98	194.77	45.00	12.57	12.57
14	169.90	2.94	22.35	164.55	36.00	-5.35	167.61	38.25	-2.29	169.17	37.00	-0.73	170.56	38.50	0.66	0.66
15	162.00	1.83	16.70	156.61	31.00	-5.39	159.76	33.25	-2.24	161.35	32.00	-0.65	162.84	32.00	0.84	0.84
16	150.40	0.93	10.53	146.10	24.00	-4.30	149.26	30.35	-1.14	150.99	25.00	0.59	152.54	25.00	2.14	2.14
17	144.50	0.58	8.08	139.30	21.00	-5.20	142.61	24.53	-1.89	144.31	21.00	-0.19	145.88	21.00	1.38	1.38
18	139.40	0.37	6.29	133.30	17.00	-6.10	136.57	24.29	-2.83	138.34	18.00	-1.06	139.94	18.00	0.54	0.54
19	135.20	0.25	5.07	128.34	15.00	-6.86	131.70	20.29	-3.50	133.45	15.00	-1.75	135.06	15.00	-0.14	0.14
20	129.60	0.16	3.57	123.07	12.00	-6.53	126.43	18.57	-3.17	128.20	13.00	-1.40	129.82	13.00	0.22	0.22
				<b>BIAS/AAD</b>		<b>-3.78</b>	<b>BIAS/AAD</b>		<b>-1.69</b>	<b>BIAS/AAD</b>		<b>-0.71</b>	<b>BIAS/AAD</b>		<b>1.31</b>	<b>2.56</b>
				Min		-6.86	Min		-3.50	Min		-2.93	Min		-2.83	0.10
				Max		-1.93	Max		1.17	Max		1.86	Max		12.93	12.93

**C2.8 Binary interaction parameter dependency in NeqSim model: Predictions and experimental SLE data from Davis [13]**

Sample no	Mol % CO <sub>2</sub>	Temp [K]	Press [bar]	k <sub>ij</sub> =0.09			k <sub>ij</sub> =0.11			k <sub>ij</sub> =0.12			k <sub>ij</sub> =0.15						
				Temp [K]	Press [bars]	(T <sub>calc</sub> -T <sub>exp</sub> ) ABS	Temp [K]	Press [bars]	(T <sub>calc</sub> -T <sub>exp</sub> ) ABS	Temp [K]	Press [bars]	(T <sub>calc</sub> -T <sub>exp</sub> ) ABS	Temp [K]	Press [bars]	(T <sub>calc</sub> -T <sub>exp</sub> ) ABS				
1	0.16	129.65	3.62	123.07	12.00	-6.58	6.58	126.43	18.57	-3.22	3.22	128.20	13.00	-1.45	1.45	132.92	15.00	3.27	3.27
2	0.25	135.21	5.12	128.34	15.00	-6.86	6.86	131.70	20.29	-3.51	3.51	133.45	15.00	-1.75	1.75	138.16	15.00	2.96	2.96
3	0.37	139.43	6.36	133.30	17.00	-6.13	6.13	136.57	24.29	-2.86	2.86	138.34	18.00	-1.09	1.09	143.00	18.00	3.58	3.58
4	0.58	144.54	8.18	139.30	21.00	-5.24	5.24	142.61	24.53	-1.93	1.93	144.31	21.00	-0.23	0.23	148.89	22.00	4.35	4.35
5	0.93	150.37	10.48	146.10	24.00	-4.27	4.27	149.26	30.35	-1.11	1.11	150.99	25.00	0.62	0.62	155.48	26.00	5.11	5.11
6	1.83	162.04	15.92	156.61	31.00	-5.43	5.43	159.76	33.25	-2.28	2.28	161.35	32.00	-0.69	0.69	165.68	33.00	3.64	3.64
7	2.94	169.87	22.41	164.55	36.00	-5.32	5.32	167.61	38.25	-2.27	2.27	169.17	37.00	-0.71	0.71	173.38	38.00	3.51	3.51
8	5.85	182.15	33.06	176.81	43.00	-5.34	5.34	179.75	44.91	-2.40	2.40	181.22	45.00	-0.93	0.93	195.24	46.00	13.09	13.09
9	10.08	189.26	39.70	186.72	48.00	-2.54	2.54	190.47	44.54	1.21	1.21	190.66	50.00	1.40	1.40	203.66	51.00	14.39	14.39
10	15.39	196.93	45.45	194.61	46.00	-2.32	2.32	197.80	48.18	0.87	0.87	198.65	52.00	1.72	1.72	209.27	54.00	12.34	12.34
11	20.50	201.26	48.18	198.78	46.00	-2.48	2.48	201.67	49.18	0.41	0.41	203.08	51.00	1.82	1.82	209.27	54.00	8.01	8.01
				BIAS/AAD		-4.77	4.77	BIAS/AAD		-1.55	2.01	BIAS/AAD		-0.12	1.13	BIAS/AAD		6.75	6.75
				Min		-6.86	2.32	Min		-3.51	0.41	Min		-1.75	0.23	Min		2.96	2.96
				Max		-2.32	6.86	Max		1.21	3.51	Max		1.82	1.82	Max		14.39	14.39

### C2.9 Binary interaction parameter dependency in NeqSim model: Predictions and experimental SVE data from Davis [13]

Sample no.	Mole % CO <sub>2</sub>	Temp [K]	Press [bar]	k <sub>ij</sub> =0		k <sub>ij</sub> =0.09		k <sub>ij</sub> =0.12		k <sub>ij</sub> =0.15	
				Temp [K]	(T <sub>calc</sub> -T <sub>exp</sub> )	Temp [K]	(T <sub>calc</sub> -T <sub>exp</sub> )	Temp [K]	(T <sub>calc</sub> -T <sub>exp</sub> )	Temp [K]	(T <sub>calc</sub> -T <sub>exp</sub> )
1	0.12	140.93	6.85	148.08	7.15	148.33	7.40	148.41	7.48	148.50	7.57
2	0.63	165.59	19.59	166.38	0.78	167.37	1.78	167.66	2.06	167.94	2.35
3	1.08	175.87	27.51	172.24	-3.64	173.54	-2.34	174.01	-1.87	174.50	-1.38
4	1.72	177.59	28.80	177.67	0.08	179.02	1.42	179.50	1.90	179.97	2.37
5	2.79	183.98	34.62	183.60	-0.38	184.96	0.98	185.52	1.53	186.15	2.17
6	3.67	188.71	39.09	187.14	-1.57	188.35	-0.35	188.73	0.03	189.63	0.92
7	5.65	193.65	43.22	193.09	-0.56	194.15	0.50	194.58	0.93	195.62	1.97
8	11.73	205.71	48.40	203.09	-2.61	205.69	-0.01	205.91	0.20	206.89	1.18
<b>BIAS/AAD</b>				<b>BIAS/AAD</b>	<b>-0.09</b>	<b>BIAS/AAD</b>	<b>1.17</b>	<b>BIAS/AAD</b>	<b>1.54</b>	<b>BIAS/AAD</b>	<b>2.14</b>
				Min	-3.64	Min	-2.34	Min	-1.87	Min	-1.38
				Max	7.15	Max	7.40	Max	7.48	Max	7.57
				ABS	7.15	ABS	7.40	ABS	7.48	ABS	7.57





### C2.10 Binary interaction parameter dependency in NeqSim model: Predictions and experimental SVE data from Agrawal [36]

Point No.	Composition, mole %			Press [bar]	Temp [K]	$k_{ij}=0$		$k_{ij}=0.09$		$k_{ij}=0.12$		$k_{ij}=0.15$				
	CH <sub>4</sub>	N <sub>2</sub>	CO <sub>2</sub>			Temp [K]	(T <sub>calc</sub> -T <sub>exp</sub> )	ABS	Temp [K]	(T <sub>calc</sub> -T <sub>exp</sub> )	ABS	Temp [K]	(T <sub>calc</sub> -T <sub>exp</sub> )	ABS	Temp [K]	(T <sub>calc</sub> -T <sub>exp</sub> )
1	99.88	-	0.12	1.79	137.54	140.42	2.88	2.88	2.94	2.94	140.50	2.96	2.96	140.52	2.98	2.98
2				3.45	143.21	144.26	1.05	1.05	1.18	1.18	144.42	1.21	1.21	144.46	1.25	1.25
3				5.17	144.32	146.56	2.24	2.24	2.43	2.43	146.74	2.49	2.49	146.87	2.55	2.55
4				6.83	147.82	148.06	0.24	0.24	0.50	0.50	148.31	0.58	0.58	148.48	0.66	0.66
5				8.55	149.76	149.18	-0.58	0.58	-0.25	0.25	149.51	-0.14	0.14	149.72	-0.04	0.04
6	99.03	-	0.97	1.79	155.15	155.02	-0.13	0.13	-0.07	0.07	155.09	-0.06	0.06	155.11	-0.04	0.04
7				3.79	158.21	160.53	2.32	2.32	2.44	2.44	160.65	2.48	2.48	160.73	2.52	2.52
8				5.24	161.26	162.90	1.64	1.64	1.81	1.81	163.07	1.87	1.87	163.19	1.92	1.92
9				6.96	163.98	164.93	0.95	0.95	1.18	1.18	165.17	1.26	1.26	165.32	1.34	1.34
10				10.82	166.48	167.90	1.42	1.42	1.80	1.80	168.28	1.92	1.92	168.53	2.05	2.05
11				13.79	168.37	169.33	0.96	0.96	1.47	1.47	170.01	1.64	1.64	170.18	1.81	1.81
12				17.86	170.59	170.55	-0.04	0.04	0.68	0.68	171.28	0.92	0.92	171.75	1.15	1.15
13				20.68	172.04	171.01	-1.03	1.03	-0.13	0.13	171.91	0.17	0.17	172.50	0.46	0.46
14	98.20	-	1.80	1.72	158.21	159.63	1.42	1.42	1.48	1.48	159.70	1.49	1.49	159.72	1.51	1.51
15				1.86	159.32	160.24	0.92	0.92	0.98	0.98	160.31	1.00	1.00	160.33	1.01	1.01
16				3.45	163.98	165.10	1.12	1.12	1.23	1.23	165.25	1.26	1.26	165.28	1.30	1.30
17				3.52	164.54	165.26	0.72	0.72	0.83	0.83	165.37	0.87	0.87	165.45	0.91	0.91
18				5.24	168.37	168.42	0.05	0.05	0.21	0.21	168.58	0.27	0.27	168.69	0.32	0.32
19				6.96	170.32	170.64	0.32	0.32	0.54	0.54	170.86	0.62	0.62	171.01	0.69	0.69
20				8.62	174.15	172.26	-1.89	1.89	-1.60	1.60	172.55	-1.51	1.51	172.73	-1.42	1.42
21				12.13	174.26	174.71	0.45	0.45	0.86	0.86	175.13	1.00	1.00	175.40	1.14	1.14
22				15.72	176.04	176.35	0.31	0.31	0.88	0.88	177.11	1.07	1.07	177.29	1.25	1.25
23				22.61	176.76	177.99	1.23	1.23	2.18	2.18	178.94	2.48	2.48	179.55	2.79	2.79
24	96.93	-	3.07	1.72	159.59	164.12	4.52	4.52	4.57	4.57	164.18	4.59	4.59	164.20	4.61	4.61

Point No.	Composition, mole %			Press [bar]	Temp [K]	$k_{ij}=0$			$k_{ij}=0.09$			$k_{ij}=0.12$			$k_{ij}=0.15$			
	CH <sub>4</sub>	N <sub>2</sub>	CO <sub>2</sub>			Temp [K]	(T <sub>calc</sub> -T <sub>exp</sub> )	ABS	Temp [K]	(T <sub>calc</sub> -T <sub>exp</sub> )	ABS	Temp [K]	(T <sub>calc</sub> -T <sub>exp</sub> )	ABS	Temp [K]	(T <sub>calc</sub> -T <sub>exp</sub> )	ABS	
25				1.79	160.43	164.44	4.02	4.02	4.02	164.50	4.07	4.07	164.51	4.09	4.09	164.53	4.10	4.10
26	96.93	-	3.07	3.52	166.21	170.11	3.91	3.91	4.01	170.22	4.01	4.01	170.25	4.05	4.05	170.29	4.08	4.08
27				3.55	166.43	170.18	3.76	3.76	3.86	170.29	3.86	3.86	170.33	3.90	3.90	170.36	3.93	3.93
28				5.24	170.82	173.49	2.68	2.68	2.83	173.65	2.83	2.83	173.70	2.89	2.89	173.76	2.94	2.94
29				6.96	174.98	175.88	0.90	0.90	1.11	176.10	1.11	1.11	176.17	1.19	1.19	176.24	1.26	1.26
30				14.00	179.37	181.40	2.02	2.02	2.49	181.86	2.49	2.49	182.02	2.65	2.65	182.17	2.80	2.80
31				20.62	181.59	183.81	2.22	2.22	2.98	184.58	2.98	2.98	184.83	3.23	3.23	185.07	3.48	3.48
32				20.82	183.21	183.86	0.65	0.65	1.43	184.63	1.43	1.43	184.89	1.68	1.68	185.14	1.93	1.93
33				21.44	182.15	184.00	1.85	1.85	2.66	184.81	2.66	2.66	185.07	2.92	2.92	185.33	3.18	3.18
34				27.85	184.04	184.82	0.78	0.78	2.00	186.04	2.00	2.00	186.44	2.40	2.40	186.82	2.78	2.78
35	89.33	-	10.67	1.72	177.71	175.67	-2.04	2.04	-2.02	175.69	-2.02	2.02	175.70	-2.00	2.00	175.71	-1.99	1.99
36				3.52	184.32	182.66	-1.66	1.66	-1.60	182.72	-1.60	1.60	182.75	-1.57	1.57	182.77	-1.54	1.54
37				5.24	187.65	186.66	-0.99	0.99	-0.89	186.76	-0.89	0.89	186.80	-0.85	0.85	186.84	-0.81	0.81
38				7.10	191.21	189.73	-1.48	1.48	-1.33	189.88	-1.33	1.33	189.94	-1.27	1.27	190.00	-1.21	1.21
39				8.69	193.98	191.76	-2.22	2.22	-2.03	191.95	-2.03	2.03	192.03	-1.96	1.96	192.10	-1.88	1.88
40				10.34	196.65	193.49	-3.16	3.16	-2.92	193.73	-2.92	2.92	193.82	-2.83	2.83	193.91	-2.74	2.74
41				12.07	197.71	195.00	-2.71	2.71	-2.42	195.29	-2.42	2.42	195.39	-2.31	2.31	195.50	-2.21	2.21
42				14.13	198.09	196.49	-1.60	1.60	-1.25	196.85	-1.25	1.25	196.97	-1.12	1.12	197.10	-1.00	1.00
						BIAS/AAD	0.67	1.60	0.98	BIAS/AAD	0.98	1.77	BIAS/AAD	1.08	1.83	BIAS/AAD	1.19	1.90
						Min	-3.16	0.04	-2.92	Min	-2.92	0.07	Min	-2.83	0.06	Min	-2.74	0.04
						Max	4.52	4.52	4.57	Max	4.57	4.57	Max	4.59	4.59	Max	4.61	4.61

## C2.11 Accuracy of different simulation tools compared with experimental data from Kurata [1]

Sample no.	Temp [K]	X <sub>CO<sub>2</sub></sub> [mol % CO <sub>2</sub> ]	Press [bar]	NeqSim		Eggeman [3]		ZareNezhad [10]		ProMax [12]		PROSIM [12]			
				Temp [K]	(T <sub>calc</sub> -T <sub>exp</sub> ) ABS	Temp [K]	(T <sub>calc</sub> -T <sub>exp</sub> ) ABS	Temp [K]	(T <sub>calc</sub> -T <sub>exp</sub> ) ABS	Temp [K]	(T <sub>calc</sub> -T <sub>exp</sub> ) ABS	Temp [K]	(T <sub>calc</sub> -T <sub>exp</sub> ) ABS		
1	214.30	90.00	20.79	212.40	-1.90	1.90				213.15	-1.15	1.15	213.21	-1.09	1.09
2	213.70	86.50	24.31	211.30	-2.40	2.40				212.21	-1.49	1.49	212.65	-1.05	1.05
3	212.60	80.00	30.14	209.67	-2.93	2.93				210.65	-1.95	1.95	211.65	-0.95	0.95
4	211.20	76.80	36.39	209.04	-2.16	2.16				209.98	-1.22	1.22	211.21	0.01	0.01
5	210.40	70.00	39.37	208.07	-2.33	2.33				208.87	-1.53	1.53	210.37	-0.03	0.03
6	209.00	60.00	43.57	207.32	-1.68	1.68				207.65	-1.35	1.35	209.43	0.43	0.43
7	207.60	54.30	46.47	207.13	-0.47	0.47				207.15	-0.45	0.45	208.98	1.38	1.38
8	207.30	50.00	46.93	207.06	-0.24	0.24				206.76	-0.54	0.54	208.65	1.35	1.35
9	206.20	42.60	48.18	206.92	0.72	0.72				206.15	-0.05	0.05	208.04	1.84	1.84
10	201.30	20.50	48.18	203.08	1.78	1.78	200.09	-1.21	1.21	201.20	-0.10	0.10	203.04	1.74	1.74
11	196.90	15.39	45.18	198.65	1.75	1.75	196.76	-0.14	0.14	197.51	0.61	0.61	198.87	1.97	1.97
12	189.30	10.08	39.54	191.16	1.86	1.86	190.71	1.41	1.41	190.17	0.87	0.87	191.76	2.46	2.46
13	182.20	5.85	32.91	181.22	-0.98	0.98	181.43	-0.77	0.77	180.50	-1.70	1.70	180.32	-1.88	1.88
14	169.90	2.94	22.35	169.17	-0.73	0.73	169.32	-0.58	0.58	169.00	-0.90	0.90	166.54	-3.36	3.36
15	162.00	1.83	16.70	161.35	-0.65	0.65	161.54	-0.46	0.46	161.58	-0.42	0.42	157.87	-4.13	4.13
16	150.40	0.93	10.53	150.99	0.59	0.59	151.37	0.97	0.97	151.70	1.30	1.30	146.54	-3.86	3.86
17	144.50	0.58	8.08	144.31	-0.19	0.19	144.98	0.48	0.48	145.26	0.76	0.76	139.37	-5.13	5.13
18	139.40	0.37	6.29	138.34	-1.06	1.06	139.26	-0.14	0.14	139.45	0.05	0.05	133.09	-6.31	6.31
19	135.20	0.25	5.07	133.45	-1.75	1.75	134.65	-0.55	0.55	134.61	-0.59	0.59	127.98	-7.22	7.22
20	129.60	0.16	3.57	128.20	-1.40	1.40	129.71	0.11	0.11	129.34	-0.26	0.26	122.48	-7.12	7.12
				<b>BIAS/AAD</b>	<b>-0.71</b>	<b>1.38</b>	<b>BIAS/AAD</b>	<b>-0.08</b>	<b>0.62</b>	<b>BIAS/AAD</b>	<b>-0.03</b>	<b>0.69</b>	<b>BIAS/AAD</b>	<b>-1.55</b>	<b>2.67</b>
				Min	-2.93	0.19	Min	-1.21	0.11	Min	-1.70	0.05	Min	-7.22	1.74
				Max	1.86	2.93	Max	1.41	1.41	Max	1.30	1.70	Max	2.46	7.22

## Appendix C3 - Experimental data from literature and simulated data: Binary C<sub>6</sub>H<sub>6</sub>-CH<sub>4</sub> system

### C3.1 Solubility of C<sub>6</sub>H<sub>6</sub> in CH<sub>4</sub>: Predictions and experimental data from Kurata [34]

Sample no.	Mole % C <sub>6</sub> H <sub>6</sub>	Mole % CH <sub>4</sub>	Temp [K]	NeqSim				GPA			
				Temp [K]	Press [bar]	(T <sub>calc</sub> -T <sub>exp</sub> )	ABS	Temp [K]	Press [bar]	(T <sub>calc</sub> -T <sub>exp</sub> )	ABS
1*	0.0	1.0	90.72								
2	0.000039	99.999961	99.40	90.93	11.00	-8.47	8.47	100.13	0.35	0.73	0.73
3	0.00009	99.99991	105.00	97.01	11.00	-7.99	7.99	100.13	0.35	-4.87	4.87
4	0.00020	99.99980	110.60	103.54	11.00	-7.06	7.06	105.32	0.58	-5.28	5.28
5	0.00036	99.99964	116.20	108.89	11.00	-7.31	7.31	111.34	0.99	-4.86	4.86
6	0.00071	99.99929	121.80	115.76	11.00	-6.04	6.04	118.99	1.78	-2.81	2.81
7	0.00076	99.99924	121.80	116.49	11.00	-5.31	5.31	119.81	1.89	-1.99	1.99
8	0.00097	99.99903	125.10	119.21	11.00	-5.89	5.89	122.82	2.32	-2.28	2.28
9	0.00125	99.99875	127.40	122.18	11.00	-5.22	5.22	126.10	2.88	-1.30	1.30
10	0.00206	99.99794	133.00	128.54	11.00	-4.46	4.46	133.49	4.47	0.49	0.49
11	0.00349	99.99651	138.60	136.19	11.00	-2.41	2.41	141.96	6.99	3.36	3.36
12	0.00547	99.99453	144.20	143.89	11.00	-0.31	0.31	150.17	10.24	5.97	5.97
13	0.00550	99.99450	144.20	143.99	11.00	-0.21	0.21	150.17	10.24	5.97	5.97
14	0.00545	99.99455	144.20	143.82	11.00	-0.38	0.38	150.17	10.24	5.97	5.97
15	0.00565	99.99435	144.20	144.50	11.00	0.30	0.30	150.71	10.49	6.51	6.51
16	0.00589	99.99411	144.20	145.31	11.00	1.11	1.11	151.53	10.86	7.33	7.33
17	0.00614	99.99386	144.20	146.13	11.00	1.93	1.93	152.35	11.25	8.15	8.15
18	0.00621	99.99379	144.20	146.36	11.00	2.16	2.16	152.63	11.38	8.43	8.43
19	0.00819	99.99181	149.80	152.43	11.00	2.63	2.63	158.37	14.39	8.57	8.57
20	0.0122	99.9878	155.30					167.39	20.10	12.09	12.09
21	0.0167	99.9833	160.90					175.32	26.18	14.42	14.42
22	0.0226	99.9774	166.40					181.61	31.73	15.21	15.21
23	0.0252	99.9748	166.40					182.43	32.50	16.03	16.03
24	0.0270	99.9730	166.40					182.98	33.02	16.58	16.58
25	0.0295	99.9705	166.40					183.80	33.81	17.40	17.40
26	0.0293	99.9707	172.00					183.80	33.81	11.80	11.80
27	0.0363	99.9637	177.60					185.44	35.43	7.84	7.84
28	0.0419	99.9581	183.10					186.53	36.53	3.43	3.43
29	0.0440	99.9560	183.10					186.81	36.80	3.71	3.71
30	0.0537	99.9463	183.10					188.45	38.50	5.35	5.35
31	0.0614	99.9386	183.10					189.54	39.65	6.44	6.44
32	0.0711	99.9289	183.10					190.91	41.12	7.81	7.81
33	0.0779	99.9221	188.70					191.73	42.02	3.03	3.03
34	0.0868	99.9132	188.70					192.55	42.92	3.85	3.85
35	0.0916	99.9084	188.70					193.10	43.53	4.40	4.40
36	0.1080	99.8920	199.80					194.46	45.07	-5.34	5.34
37	0.1290	99.8710	199.80					196.10	46.96	-3.70	3.70
38	0.1400	99.8600	199.80					196.65	47.60	-3.15	3.15
				<b>BIAS/AAD</b>		<b>-2.94</b>	<b>3.84</b>	<b>BIAS/AAD</b>		<b>4.74</b>	<b>6.66</b>
				Min		-8.47	0.21	Min		-5.34	0.49
				Max		2.63	8.47	Max		17.40	17.40

\*GPA

### C3.2 Solubility of C<sub>6</sub>H<sub>6</sub> in CH<sub>4</sub>: Predictions and experimental data from Neumann [19]

Sample no.	Temp [K]	x [mole % C <sub>6</sub> H <sub>6</sub> ]	x [mole % CH <sub>4</sub> ]	NeqSim				GPA			
				Temp [K]	Press [bar]	(T <sub>calc</sub> -T <sub>exp</sub> )	ABS	Temp [K]	Press [bar]	(T <sub>calc</sub> -T <sub>exp</sub> )	ABS
1	103.80	0.0006	99.9994	113.98	11.00	10.18	10.18	116.81	1.52	13.01	13.01
2	113.20	0.0007	99.9993	115.61	11.00	2.41	2.41	118.72	1.75	5.52	5.52
3	123.00	0.0014	99.9986	123.56	11.00	0.56	0.56	127.74	3.19	4.74	4.74
4	133.00	0.0021	99.9979	128.80	11.00	-4.20	4.20	133.76	4.54	0.76	0.76
5	143.20	0.0042	99.9958	139.20	11.00	-4.00	4.00	145.24	8.19	2.04	2.04
6	150.00	0.0066	99.9934	147.62	11.00	-2.38	2.38	153.99	12.06	3.99	3.99
7	153.10	0.0081	99.9919	152.15	11.00	-0.95	0.95	158.10	14.24	5.00	5.00
8	162.80	0.0118	99.9882					166.57	19.53	3.77	3.77
9	175.00	0.0202	99.9798					180.52	30.72	5.52	5.52
10	177.90	0.0470	99.9530					187.35	37.36	9.45	9.45
11	180.10	0.0403	99.9597					186.26	36.25	6.16	6.16
12	185.40	0.0483	99.9517					187.63	37.65	2.23	2.23
				<b>BIAS/ADD</b>		<b>0.23</b>	<b>3.52</b>	<b>BIAS/AAD</b>		<b>5.18</b>	<b>5.18</b>
				Min		-4.20	0.56	Min		0.76	0.76
				Max		10.18	10.18	Max		13.01	13.01

### C3.3 Solubility of C<sub>6</sub>H<sub>6</sub> in CH<sub>4</sub>: Predictions and experimental data from Luks [17]

Sample no.	Temp [K]	Mole % C <sub>6</sub> H <sub>6</sub>	Mole % CH <sub>4</sub>	molar vol. [mL/g mol]	Pressure [bar]	GPA			
						Temp [K]	Press [bar]	(T <sub>calc</sub> -T <sub>exp</sub> )	ABS
<b>Upper Branch</b>									
1	277.7	98.15	1.85	86.8	10.13				
2	276.8	96.35	3.65	86.1	20.27				
3	275.8	94.33	5.67	85.1	30.40				
4	274.9	92.47	7.53	84.2	40.53				
5	273.9	90.19	9.81	83.1	50.66				
6	273.1	88.24	11.76	82.2	60.80				
7	272.2	85.98	14.02	81.0	70.93				
8	271.6	84.44	15.56	80.1	81.06				
9	270.9	82.49	17.51	78.9	91.19				
10	270.4	80.92	19.08	78.0	101.33				
11	269.9	79.31	20.69	77.0	111.46				
12	269.4	77.75	22.25	76.1	121.59				
13	269.0	76.42	23.58	75.3	131.72				
14	268.7	75.37	24.63	74.7	141.86				
15	268.4	74.09	25.91	74.0	151.99				
16	268.2	73.08	26.92	73.4	162.12				
17	268.1	72.46	27.54	73.0	172.25				
<b>Lower Branch</b>									
18a	190.5	0.015	99.985	70.2	46.26				
19	185	0.017	99.983	63.5	38.91	175.87	26.635	-9.13	9.13
20	180	0.0165	99.9835	58.7	33.23	175.05	25.952	-4.95	4.95
21	175	0.015	99.985	54.8	30.09	172.59	23.968	-2.41	2.41
22	170	0.0135	99.9865	52.1	23.61	169.85	21.88	-0.15	0.15
23	165	0.011	99.989	49.8	19.76	164.93	18.421	-0.07	0.07
						<b>BIAS/AAD</b>		<b>-3.342</b>	<b>3.342</b>
						Min		-9.13	0.07
						Max		-0.07	9.13

### C3.4 Solubility of C<sub>6</sub>H<sub>6</sub> in CH<sub>4</sub>: Experimental data from Rijkers [18]

Sample no.	Temp [K]	Pressure [bar]	Mole % C <sub>6</sub> H <sub>6</sub>	Mole % CH <sub>4</sub>
<u>Vapor phase comp</u>				
1*	264.95	4.2064	8.04	91.96
2*	266.15	4.7256	12.67	87.33
3*	266.3	5.2398	18.82	81.18
4*	266.08	5.3981	23.59	76.41
<u>Liquid phase comp</u>				
1	265.87	5.3981	26.78	73.22
2	265.84	5.3397	29.9	70.1
3	266.37	5.2428	37.28	62.72
4	266.22	5.1875	39.11	60.89
5	266.59	4.7192	44.38	55.62
6	265.68	4.4438	47.15	52.85
7	266.43	4.1413	51.76	48.24
8	266.19	4.0068	51.9	48.1
9	265.89	3.3384	57.36	42.64
10	265.5	3.2752	58.79	41.21
11	266.26	2.3986	65.53	34.47
12	267.48	1.814	71.13	28.87
13	269.54	1.1058	79.91	20.09
14	272.93	0.509	89.83	10.17
15**	278.45	0.0005	100	0







Sample no.	Mole % C <sub>6</sub> H <sub>6</sub>	Mole % CH <sub>4</sub>	Temp [K]	k <sub>ij</sub> =0.0209		k <sub>ij</sub> =0.0509		k <sub>ij</sub> =0.0809		k <sub>ij</sub> =0.1109								
				Temp [K]	(T <sub>calc</sub> -T <sub>exp</sub> )	Temp [K]	(T <sub>calc</sub> -T <sub>exp</sub> )	Temp [K]	(T <sub>calc</sub> -T <sub>exp</sub> )	Temp [K]	(T <sub>calc</sub> -T <sub>exp</sub> )	Temp [K]	(T <sub>calc</sub> -T <sub>exp</sub> )					
27	0.0363	99.9637	177.6															
28	0.0419	99.9581	183.1															
29	0.0440	99.9560	183.1															
30	0.0537	99.9463	183.1															
31	0.0614	99.9386	183.1															
32	0.0711	99.9289	183.1															
33	0.0779	99.9221	188.7															
34	0.0868	99.9132	188.7															
35	0.0916	99.9084	188.7															
36	0.1080	99.8920	199.8															
37	0.1290	99.8710	199.8															
38	0.1400	99.8600	199.8															
				BIAS/AAD	-45.60	45.60	BIAS/AAD	-24.69	24.69	BIAS/AAD	-8.01	8.01	BIAS/AAD	-2.94	3.84	BIAS/AAD	6.68	6.73
				Min	-48.10	42.55	Min	-27.81	21.17	Min	-12.84	3.39	Min	-8.47	0.21	Min	-0.41	0.24
				Max	-42.55	48.10	Max	-21.17	27.81	Max	-3.39	12.84	Max	2.63	8.47	Max	14.44	14.44

\*GPA

### C3.6 Binary interaction parameter dependency in NeqSim model: Predictions and experimental data from Neumann [19]

Sampl e no.	Tem p [K]	x [mole % C <sub>6</sub> H <sub>6</sub> ]	x [mole % CH <sub>4</sub> ]	k <sub>ij</sub> =0.0209			k <sub>ij</sub> =0.0509			k <sub>ij</sub> =0.0809			k <sub>ij</sub> =0.0909			k <sub>ij</sub> =0.1109		
				Temp [K]	(T <sub>calc</sub> -T <sub>exp</sub> )	ABS	Temp [K]	(T <sub>calc</sub> -T <sub>exp</sub> )	ABS	Temp [K]	(T <sub>calc</sub> -T <sub>exp</sub> )	ABS	Temp [K]	(T <sub>calc</sub> -T <sub>exp</sub> )	ABS	Temp [K]	(T <sub>calc</sub> -T <sub>exp</sub> )	ABS
1	103.8	0.0006	99.9994	72.99	-30.81	30.81	93.49	-10.31	10.31	109.32	5.52	5.52	113.98	10.18	10.18	122.62	18.82	18.82
2	113.2	0.0007	99.9993	74.51	-38.69	38.69	95.03	-18.17	18.17	110.92	-2.28	2.28	115.61	2.41	2.41	124.29	11.09	11.09
3	123.0	0.0014	99.9986	81.90	-41.10	41.10	102.55	-20.45	20.45	118.76	-4.24	4.24	123.56	0.56	0.56	132.51	9.51	9.51
4	133.0	0.0021	99.9979	86.68	-46.32	46.32	107.45	-25.55	25.55	123.89	-9.11	9.11	128.80	-4.20	4.20	137.99	4.99	4.99
5	143.2	0.0042	99.9958	95.83	-47.37	47.37	116.90	-26.30	26.30	134.00	-9.20	9.20	139.20	-4.00	4.00	149.22	6.02	6.02
6	150.0	0.0066	99.9934	102.60	-47.40	47.40	124.05	-25.95	25.95	141.95	-8.05	8.05	147.62	-2.38	2.38	158.51	8.51	8.51
7	153.1	0.0081	99.9919	105.94	-47.16	47.16	127.63	-25.47	25.47	146.16	-6.94	6.94	152.15	-0.95	0.95	164.18	11.08	11.08
8	162.8	0.0118	99.9882															
9	175.0	0.0202	99.9798															
10	177.9	0.0470	99.9530															
11	180.1	0.0403	99.9597															
12	185.4	0.0483	99.9517															
				BIAS/ ADD	-42.69	42.69	BIAS/ ADD	-21.74	21.74	BIAS/ ADD	-4.90	6.48	BIAS/ ADD	0.23	3.52	BIAS/ ADD	10.00	10.00
				Min	-47.40	30.81	Min	-26.30	10.31	Min	-9.20	2.28	Min	-4.20	0.56	Min	4.99	4.99
				Max	-30.81	47.40	Max	-10.31	26.30	Max	5.52	9.20	Max	10.18	10.18	Max	18.82	18.82

## Appendix C4 - Experimental data from literature and simulated data: Binary C<sub>6</sub>H<sub>12</sub>-CH<sub>4</sub> system

### C4.1 Solubility of C<sub>6</sub>H<sub>12</sub> in CH<sub>4</sub>: Experimental data from Kohn [35]

Sample no.	Temp [K]	Press [bar]	x [mole % C <sub>6</sub> H <sub>12</sub> ]	X [mole % CH <sub>4</sub> ]	vol. [mL/g -mol]	NeqSim				GPA			
						Temp [K]	Press [bar]	(T <sub>calc</sub> -T <sub>exp</sub> )	ABS	Temp [K]	Press [bar]	(T <sub>calc</sub> -T <sub>exp</sub> )	ABS
1	279.83	-	100.00	0.00	-								
2	270.00	9.42	96.32	3.68	102.2								
3	265.00	14.59	94.41	5.59	100.4								
4	260.00	19.86	92.43	7.57	98.6								
5	255.00	24.72	90.40	9.60	96.7								
6	250.00	29.28	88.34	11.66	94.8								
7	245.00	33.64	86.29	13.71	93.1								
8	240.00	37.49	84.11	15.89	91.3								
9	235.00	41.24	81.83	18.17	89.6								
10	230.00	44.38	79.44	20.56	87.8								
11	225.00	46.91	76.93	23.07	86.1								
12	220.00	49.04	74.36	25.64	84.4								
13	215.00	50.76	71.69	28.31	82.5								
14	210.00	52.08	68.90	31.10	80.5								
15	205.00	52.99	65.44	34.56	78.1								
16	200.00	53.60	61.93	38.07	75.4								
17	197.50	54.31	59.98	40.02	73.6								
18	195.00	59.78	57.90	42.10	71.1								
19	193.00	75.99	56.22	43.78	68.0								
20a	192.74	48.13	0.41	99.59	-	193.65	48.13	0.91	0.91				
21	190.00	44.18	0.518	99.482	69.5	192.71	44.18	2.71	2.71				
22	188.00	41.75	0.588	99.412	64.6	191.85	41.75	3.85	3.85				
23	186.00	39.31	0.629	99.371	61.8	190.87	39.31	4.87	4.87				
24	184.00	36.88	0.651	99.349	59.5	189.75	36.88	5.75	5.75				
25	182.00	34.65	0.661	99.339	57.8	188.60	34.65	6.60	6.60	179.97	29.89	-2.03	2.03
26	180.00	32.42	0.652	99.348	56.1	187.27	32.42	7.27	7.27	179.15	29.16	-0.85	0.85
27	178.00	30.40	0.635	99.365	54.8	186.00	30.40	8.00	8.00	178.06	28.22	0.06	0.06
28	176.00	28.37	0.617	99.383	53.7	184.62	28.37	8.62	8.62	176.69	27.06	0.69	0.69
29	174.00	26.55	0.591	99.409	52.7	183.21	26.55	9.21	9.21	174.50	25.27	0.50	0.50
30	172.00	24.72	0.572	99.428	52.0	181.77	24.72	9.77	9.77	173.13	24.19	1.13	1.13
31	170.00	23.00	0.540	99.460	51.1	180.31	23.00	10.31	10.31	170.40	22.11	0.40	0.40
32	168.00	21.48	0.511	99.489	50.4	178.93	21.48	10.93	10.93	168.21	20.53	0.21	0.21
33	166.00	19.86	0.483	99.517	49.6	177.37	19.86	11.37	11.37	165.75	18.84	-0.25	0.25
34	164.00	18.34	0.453	99.547	48.9	175.70	18.34	11.70	11.70	163.02	17.07	-0.98	0.98
35	162.00	17.02	0.420	99.580	48.3	174.26	17.02	12.26	12.26	160.01	15.25	-1.99	1.99
36	160.00	15.71	0.391	99.609	47.5	172.72	15.71	12.72	12.72	157.28	13.71	-2.72	2.72
37	158.00	14.49	0.358	99.642	47.0	171.22	14.49	13.22	13.22	153.99	12.00	-4.01	4.01
38	156.00	13.37	0.334	99.666	46.5	169.77	13.37	13.77	13.77	151.53	10.82	-4.47	4.47
39	154.00	12.26	0.310	99.690	46.0	168.23	12.26	14.23	14.23	149.07	9.72	-4.93	4.93
						<b>BIAS/AAD</b>	<b>10.76</b>	<b>10.67</b>	<b>BIAS/AAD</b>	<b>-1.28</b>	<b>1.68</b>		
						Min	6.60	6.60	Min	-4.93	0.06		
						Max	14.23	14.23	Max	1.13	4.93		

a) K point (V-L critical point in presence of solid)



## Appendix C5 - Experimental methods used in literature

In relation with investigating the different experimental results, it is important to consider the various experimental methods and procedures that are used to generate the experimental data.

The compilation by Fornari, Alessi and Kikic [48] is a review article where all publications published between 1978 and 1987 are gathered. Similar Dohrn and Brunner reviewed a collection of publications published between 1988 and 1993 [49]. Christov and Dohrn have continued gathered and reviewed the publications between 1994 and 1999 [50]. All these review articles divide the experimental methods in two different sub categories, analytical methods (direct sampling methods) and synthetic methods (indirect methods).

The structure of the different analytic and synthetic methods, in the work by Dohrn, Brunner and Christov, are divided in a more logical way than the work by Fornari, Alessi and Kikic. Thus the arrangement to Dohrn, Brunner, and Christov, see Figure 4, will be used as a reference.

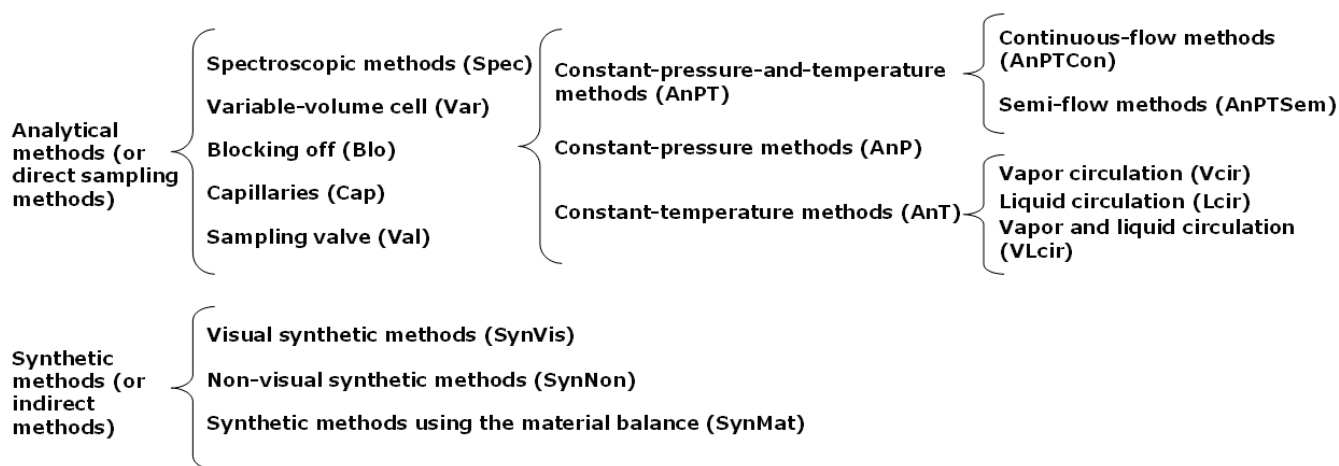


Figure C5-1 Overview of experimental methods cf. Dohrn, Brunner and Christov [49, 50]

### C5.1 Analytical method

The analytical method involves sampling and determination of the composition of phases that exist when the mixture has reached equilibrium. Extracting a sample from a cell can lead to pressure and large disturbances in the equilibria. When using a stirrer to achieve faster equilibrium is called the static-analytical method. Different methods are used to extract the sample from the cell without interrupting the equilibria, as spectroscopic, variable-volume cell, blocking off, capillaries, and sampling valve. The most common methods for investigating solid in cryogenic systems are spectroscopic analysis and sampling valve connected to a gas chromatograph.

Spectroscopic analysis is the most important tool of modern chemistry to determine different elements or components using electromagnetic radiation. Spectroscopic methods are used to identify and confirm the molecular structures, monitor reactions and to control the purity of the compounds. For cryogenic systems is infrared spectroscopy the most widely used method among the spectroscopic techniques. The technique exploits the fact that each connection has its unique infrared spectrum, as a fingerprint. By sending many infrared light waves against the sample at the same time, a change in the light waves are recorded and analyzed. Cells that are commonly used are classified either as transmission or reflection cell, depending on whether the light wave shall penetrate or be reflected from the sample.

Variable-volume cell, blocking off and capillaries are all methods to prevent significant pressure and temperature interference in phase equilibrium when a sample is extracted from the cell.

One of the sampling valve methods are chromatographic analysis which is used for separation and detection of chemical components in gases and volatile components in solutions, mainly organic solutions. Components with different physical and chemical properties such as molecular weight, boiling point etc. will diffuse with different speed through the chromatographic system. The components will be detected at different times at a given point, or at different points at a given time. It is important that the measuring equipment is reliable, the measurement procedure and the amount of the samples not interfere with the equilibrium state, and that the measurement is representative of the phase which is investigated.

All the analytical methods mentioned in Figure C5-1 can be classified either as a constant-temperature method, constant-pressure and -temperature method or as a constant-pressure method; depending of the how the equilibria is achieved. The intention with constant temperature method is to adjust the pressure above or below the phase equilibrium. Measurements of the different phases are achieved by extracting gas-(V<sub>cir</sub>), liquid-(L<sub>cir</sub>) or gas-liquid samples (VL<sub>cir</sub>) continuously by using of capillaries or sampling valve and then to be sent back (recycled) to the equilibrium cell. For the constant pressure method have the same options, except now the temperature is regulated. Considering the constant-pressure and -temperature method, often called the dynamic method, both the pressure and temperature is held constant. This method is general divided into continuous-flow and semi-flow methods, depending on the flow.

## **C5.2 Synthetic method**

Synthetic method involves observing the phase change in an equilibrium cell, by using a mixture of known composition in the cell. It is not necessary with sampling, and the experimental procedure is often simple and quick, thus the equipment is often quite reasonable in price. The temperature and pressure in the equilibrium cell is adjusted until the mixture is homogeneous. Next, vary either the pressure or temperature until a new phase is observed. The pressure and temperature where this phase separation starts, in addition to mole fraction, define a point at the phase envelope. Synthetic methods may be used where the analytical methods fail. For multi-component systems, experiments with synthetic methods provide less information than with the analytical methods and thus there is a need for further experiments. Different analyzing methods are visual observation, non-visual observation and by using material balance, see figure C5-1.

A new phase is usually detected by visual observation, where a blurred area or point is observed in the cell. Visual synthetic method can be used both to determine the simple vapor-liquid equilibrium and to study more complex phase behavior, such as solid-liquid equilibrium.

As an alternative to visual observation, other physical properties can be observed to detect phase transitions, so-called non-visual observation. If the total volume of a variable-volume cell can be measured accurately, a new phase is observed when there is a sudden change in pressure-volume relationship.



### **C5.3 Literature review of experimental methods**

When reviewing the different methods for solubility studies at low temperatures, the two main methods are recognized in the studies of light hydrocarbon systems; visual observation and spectroscopy. In general have phase equilibrium studies employed experimental techniques in which the coexisting phases are sampled and analyzed after equilibrium conditions have been established in a phase equilibrium cell. However there is a simpler non-sampling visual technique available for mixtures where the precipitate is a pure substance, this technique is employed in the later studies of solids in light hydrocarbons. [36]

#### ***C5.3.1 Spectroscopy – analytical method***

The traditional experimental methods in studies of phase equilibrium have been conducted mostly using sampling techniques in which a saturated solution containing the solid is created and then sampled using an analytical device such as a gas chromatograph or a mass spectroscopy device. These methods are classified as isothermal since constant temperature and pressure are required before the solution is sampled. Sampling methods allow for all types of equilibria to be measured but are more difficult to operate and have potential problems during the sampling of a solution in equilibrium.[36]

The studies of Kurata, Davis and Cheung were all conducted with spectroscopy methods, either gas chromatography or mass spectroscopy, or both. In general the experimental equipment consists of an equilibrium cell inside a Dewar flask, with or without possibilities to observe the cell content visually. The air bath between the equilibrium cell and the walls in the Dewar flask is chilled by a cascade refrigerator or liquid nitrogen or both. In addition is the cell equipped with pressure and temperature gauges, and a precise temperature control, e.g. Kurata used a system which provided temperature control within approximately  $\pm 0.15\text{K}$  from 90 to 325K [1]. Thus the errors in the measurements were not caused by inadequacies of the control system but rather temperature gradients in the air bath.

For sampling the vapor- and liquid-phase a method involving capillary tubes is widely used. The tubes could be mounted inside the equilibrium cell, allowing samples to be removed for analysis. To prevent disturbance of the equilibrium state in the cell, the cell could be agitated by a stirrer or a magnetic ball, and sampled withdrawn slowly.

The vapor and liquid sampling system could be in direct contact with the spectroscopy equipment or filled into sample containers and analyzed later. For the liquid phase, which is hardest to sample, it could be an option to have a filter for preventing solids carrying over during sampling (e. g. a fritted pyrex disk with maximum 5- $\mu$  pore size), before the liquid is warmed and flash vaporized. This way the liquid composition don't get contaminated.[33]

Another way to handle the issue with sampling the liquid phase in presence of a solid is for example the way Davis handled the problem. In his study which conducted three-phase experiments of a methane-carbon dioxide mixture, he selected two different spectroscopy methods for vapor samples containing more/less than 1% of carbon dioxide. For the samples where the carbon dioxide composition were less than 1%, he selected gas density measurements, and samples containing more than 1% were analyzed by mass spectrometer.

By reversing the procedure for determining the vapor phase composition the difficulties of sampling a liquid in the presence of a solid were eliminated. Thus the composition is fixed, and the bubble temperature experimentally determined where solid appeared and disappeared.[13] This last procedural is described in more details in the next section, called visual observation.

### ***C5.3.2 Visual observation – synthetic method***

In three-phase experiments where the method of visual observation (SynVis) are being used, all have a very similar procedure where a known mixture is brought into the equilibrium cell with a given amount and the bath temperature is lowered to form crystals. This is a non-sampling visual technique where the pressure and temperature at which the solid phase begins to form is determined. This solid equilibrium state can also be determined from a discontinuity which occurs at the phase boundary when certain experimental variables are plotted in a suitable manner (SysNon).

After a given amount of the mixture of investigation is injected to the equilibrium cell and cooled until a solid phase is visually detected, the bath is slowly warmed to the crystal formation disappears. These temperatures are noted and when the temperature difference is sufficient low, the freezing point has been determined with the desired accuracy (e. g. 0.2K from the study of methane-benzene by Kurata [34]).

## Appendix C6 - Unavailable experimental work

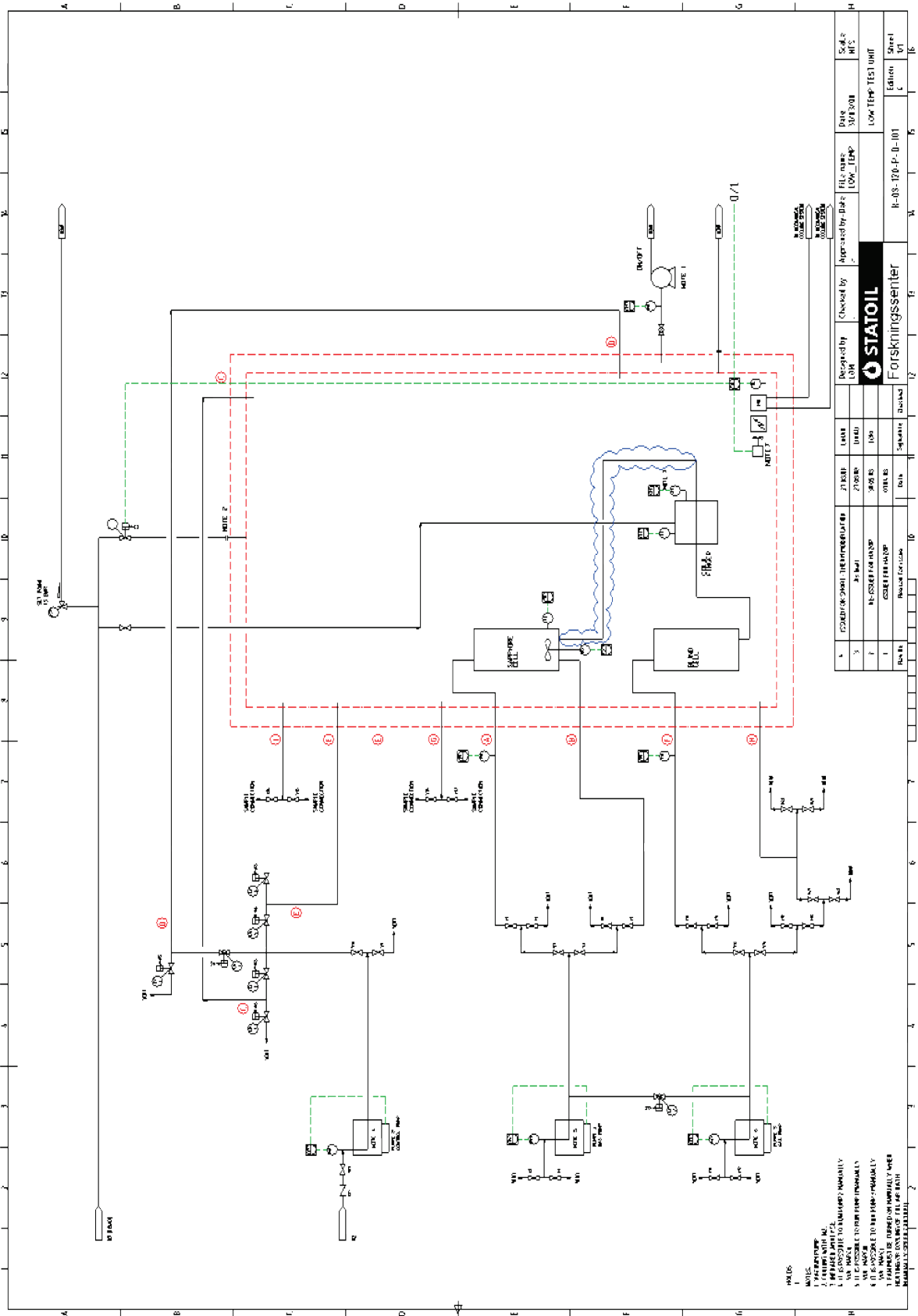
<b>Component</b>	<b>Ref</b>	<b>Author</b>	<b>Systems</b>
Carbon dioxide	[9]	Boyle	SLE
Carbon dioxide	[9]	Voss	SLE
Carbon dioxide	[51]	Sterner	SLE, SVE
Carbon dioxide	[52]	Mraw	SLE
Carbon dioxide	[40]	Pikaar	SLE, SVE
Carbon dioxide	[11]	GPSA	SVE
Benzene <sup>(1)</sup>	[42]	Kuebler	SLE

Table C5-1 Unavailable experimental work

<sup>(1)</sup>The experimental data are gathered in the compilation from GPA, the research report RR 14.



# Appendix D2 - P&Id: Freeze out rig, short term modifications



NO.	REVISION	DESCRIPTION	DATE	BY	CHKD BY
1	1	ISSUED FOR SHORT TERM MODIFICATION	27/08/16	AK	AK
2	2	ISSUED FOR HANDBOOK	30/08/16	AK	AK
3	3	ISSUED FOR HANDBOOK	01/11/16	AK	AK

Designed by	LOM	Checked by	AK	Approved by	AK
Date	30/08/16	File name	LOW_TEMP	Scale	MKS
				Date	LOW TEMP TEST UNIT
				Revision	1
R-03-120-P-0-101				Sheet	01

- TANKS  
 1. RECTANGULAR  
 2. CIRCULAR  
 3. SPHERICAL  
 4. U.S. POSSIBLE TO DIMENSION NORMALLY  
 5. U.S. POSSIBLE TO DIMENSION NORMALLY  
 6. U.S. POSSIBLE TO DIMENSION NORMALLY  
 7. U.S. POSSIBLE TO DIMENSION NORMALLY  
 8. U.S. POSSIBLE TO DIMENSION NORMALLY  
 9. U.S. POSSIBLE TO DIMENSION NORMALLY  
 10. U.S. POSSIBLE TO DIMENSION NORMALLY  
 11. U.S. POSSIBLE TO DIMENSION NORMALLY  
 12. U.S. POSSIBLE TO DIMENSION NORMALLY  
 13. U.S. POSSIBLE TO DIMENSION NORMALLY  
 14. U.S. POSSIBLE TO DIMENSION NORMALLY  
 15. U.S. POSSIBLE TO DIMENSION NORMALLY  
 16. U.S. POSSIBLE TO DIMENSION NORMALLY  
 17. U.S. POSSIBLE TO DIMENSION NORMALLY  
 18. U.S. POSSIBLE TO DIMENSION NORMALLY  
 19. U.S. POSSIBLE TO DIMENSION NORMALLY  
 20. U.S. POSSIBLE TO DIMENSION NORMALLY  
 21. U.S. POSSIBLE TO DIMENSION NORMALLY  
 22. U.S. POSSIBLE TO DIMENSION NORMALLY  
 23. U.S. POSSIBLE TO DIMENSION NORMALLY  
 24. U.S. POSSIBLE TO DIMENSION NORMALLY  
 25. U.S. POSSIBLE TO DIMENSION NORMALLY  
 26. U.S. POSSIBLE TO DIMENSION NORMALLY  
 27. U.S. POSSIBLE TO DIMENSION NORMALLY  
 28. U.S. POSSIBLE TO DIMENSION NORMALLY  
 29. U.S. POSSIBLE TO DIMENSION NORMALLY  
 30. U.S. POSSIBLE TO DIMENSION NORMALLY  
 31. U.S. POSSIBLE TO DIMENSION NORMALLY  
 32. U.S. POSSIBLE TO DIMENSION NORMALLY  
 33. U.S. POSSIBLE TO DIMENSION NORMALLY  
 34. U.S. POSSIBLE TO DIMENSION NORMALLY  
 35. U.S. POSSIBLE TO DIMENSION NORMALLY  
 36. U.S. POSSIBLE TO DIMENSION NORMALLY  
 37. U.S. POSSIBLE TO DIMENSION NORMALLY  
 38. U.S. POSSIBLE TO DIMENSION NORMALLY  
 39. U.S. POSSIBLE TO DIMENSION NORMALLY  
 40. U.S. POSSIBLE TO DIMENSION NORMALLY  
 41. U.S. POSSIBLE TO DIMENSION NORMALLY  
 42. U.S. POSSIBLE TO DIMENSION NORMALLY  
 43. U.S. POSSIBLE TO DIMENSION NORMALLY  
 44. U.S. POSSIBLE TO DIMENSION NORMALLY  
 45. U.S. POSSIBLE TO DIMENSION NORMALLY  
 46. U.S. POSSIBLE TO DIMENSION NORMALLY  
 47. U.S. POSSIBLE TO DIMENSION NORMALLY  
 48. U.S. POSSIBLE TO DIMENSION NORMALLY  
 49. U.S. POSSIBLE TO DIMENSION NORMALLY  
 50. U.S. POSSIBLE TO DIMENSION NORMALLY  
 51. U.S. POSSIBLE TO DIMENSION NORMALLY  
 52. U.S. POSSIBLE TO DIMENSION NORMALLY  
 53. U.S. POSSIBLE TO DIMENSION NORMALLY  
 54. U.S. POSSIBLE TO DIMENSION NORMALLY  
 55. U.S. POSSIBLE TO DIMENSION NORMALLY  
 56. U.S. POSSIBLE TO DIMENSION NORMALLY  
 57. U.S. POSSIBLE TO DIMENSION NORMALLY  
 58. U.S. POSSIBLE TO DIMENSION NORMALLY  
 59. U.S. POSSIBLE TO DIMENSION NORMALLY  
 60. U.S. POSSIBLE TO DIMENSION NORMALLY  
 61. U.S. POSSIBLE TO DIMENSION NORMALLY  
 62. U.S. POSSIBLE TO DIMENSION NORMALLY  
 63. U.S. POSSIBLE TO DIMENSION NORMALLY  
 64. U.S. POSSIBLE TO DIMENSION NORMALLY  
 65. U.S. POSSIBLE TO DIMENSION NORMALLY  
 66. U.S. POSSIBLE TO DIMENSION NORMALLY  
 67. U.S. POSSIBLE TO DIMENSION NORMALLY  
 68. U.S. POSSIBLE TO DIMENSION NORMALLY  
 69. U.S. POSSIBLE TO DIMENSION NORMALLY  
 70. U.S. POSSIBLE TO DIMENSION NORMALLY  
 71. U.S. POSSIBLE TO DIMENSION NORMALLY  
 72. U.S. POSSIBLE TO DIMENSION NORMALLY  
 73. U.S. POSSIBLE TO DIMENSION NORMALLY  
 74. U.S. POSSIBLE TO DIMENSION NORMALLY  
 75. U.S. POSSIBLE TO DIMENSION NORMALLY  
 76. U.S. POSSIBLE TO DIMENSION NORMALLY  
 77. U.S. POSSIBLE TO DIMENSION NORMALLY  
 78. U.S. POSSIBLE TO DIMENSION NORMALLY  
 79. U.S. POSSIBLE TO DIMENSION NORMALLY  
 80. U.S. POSSIBLE TO DIMENSION NORMALLY  
 81. U.S. POSSIBLE TO DIMENSION NORMALLY  
 82. U.S. POSSIBLE TO DIMENSION NORMALLY  
 83. U.S. POSSIBLE TO DIMENSION NORMALLY  
 84. U.S. POSSIBLE TO DIMENSION NORMALLY  
 85. U.S. POSSIBLE TO DIMENSION NORMALLY  
 86. U.S. POSSIBLE TO DIMENSION NORMALLY  
 87. U.S. POSSIBLE TO DIMENSION NORMALLY  
 88. U.S. POSSIBLE TO DIMENSION NORMALLY  
 89. U.S. POSSIBLE TO DIMENSION NORMALLY  
 90. U.S. POSSIBLE TO DIMENSION NORMALLY  
 91. U.S. POSSIBLE TO DIMENSION NORMALLY  
 92. U.S. POSSIBLE TO DIMENSION NORMALLY  
 93. U.S. POSSIBLE TO DIMENSION NORMALLY  
 94. U.S. POSSIBLE TO DIMENSION NORMALLY  
 95. U.S. POSSIBLE TO DIMENSION NORMALLY  
 96. U.S. POSSIBLE TO DIMENSION NORMALLY  
 97. U.S. POSSIBLE TO DIMENSION NORMALLY  
 98. U.S. POSSIBLE TO DIMENSION NORMALLY  
 99. U.S. POSSIBLE TO DIMENSION NORMALLY  
 100. U.S. POSSIBLE TO DIMENSION NORMALLY